Inaugural dissertation

for

obtaining the doctoral degree

of the

Combined Faculty of Mathematics, Engineering and Natural Sciences

of the

Ruprecht – Karls – University

Heidelberg

Presented by

M.Sc. Edoardo Ratto

Born in: Alba, Italy

Oral examination: 28.06.2023

mTORC1 regulates lysosomal catabolic activity by preventing V-ATPase assembly

Referees:

Prof. Dr. Marius Lemberg

Dr. Wilhelm Palm

I. Summary

Lysosomes are acidic cellular organelles specialised in digesting macromolecules derived from extracellular and intracellular sources. Digestion of macromolecules is carried out in the lysosome by hydrolases that are catalytically active at acidic pH. The acidic pH of lysosomes is generated by the vacuolar ATPase (V-ATPase). The V-ATPase is constituted of a membrane-integral domain (V_o) and a cytoplasmic domain (V_1). The interaction of the two domains at the lysosome forms a functional proton pump that acidifies the lysosomal lumen by transporting protons across the membrane. Lysosomal catabolic pathways are suppressed by the cellular amino acid sensor mTORC1. Previous data from our laboratory showed that mTORC1 inhibition results in the upregulation of lysosomal catabolism of endocytosed proteins through an unknown mechanism. The resulting products from the digestion of those macromolecules can be used as nutrients, supporting cell survival and proliferation during starvation. Lysosomal acidification by the V-ATPase increases lysosomal hydrolase activity thus increasing the degradation of extracellular and intracellular proteins. The aim of my PhD was to understand the molecular mechanisms through which mTORC1 inhibition promotes lysosomal degradation of extracellular proteins. I discovered that mTORC1 controls lysosomal catabolism of extracellular protein by regulating lysosomal pH. The acidification of the lysosomal lumen increases lysosomal cathepsin activity promoting protein catabolism. My data suggest that mTORC1 controls lysosomal pH by regulating V-ATPase assembly at the lysosomal surface. During nutrient abundance, mTORC1 is active and the V-ATPase V_1 domain is mainly in the cytoplasm where it is stabilised by the chaperonin TRiC. mTORC1 inhibition triggers V-ATPase assembly at the lysosomal membrane, increasing acidification of the lysosomal lumen. Through mTORC1-dependent regulation of V-ATPase assembly, cells can increase the catabolic activity throughout the cellular lysosomal population and degrade extracellular proteins accumulated in lysosomes. This suggests that mammalian cells that experience a decrease in extracellular nutrients can rapidly adapt by activating latent lysosomal catabolic capacity.

II. Zusammenfassung

Lysosomen sind Zellorganelle, welche auf die Verdauung von Makromolekülen aus extra- und intrazellulären Quellen spezialisiert sind. Eine Reihe von Hydrolasen sind im Lysosom für die Verdauung von Makromolekülen zuständig und im sauren Lumen des Organells aktiv. Der saure pH-Wert des Lysosomes wird durch die vakuoläre ATPase (V-ATPase) erzeugt, welche aus einer membranintegralen Domäne (V_o) und einer zytoplasmatischen Domäne (V_1) besteht. Durch Assemblierung der beiden Domänen bildet sich eine funktionelle Protonenpumpe, die Protonen durch die lysosomale Membran in das Organelllumen transportiert. Frühere Studien unserer Arbeitsgruppe zeigten, dass die Inhibierung von mTORC1, einem zellulären Aminosäuresensor, durch einen unbekannten Mechanismus zur erhöhten lysosomalen Verdauung endozytierter Proteinen führt. Die hierbei freigesetzten Aminosäuren können als Nährstoffe verwendet werden, die Überleben und Wachstum von Zellen unter Nährstoffmangel fördern. Ziel meiner Dissertation war die Aufklärung des molekularen Mechanismus, durch welchen mTORC1 den lysosomalen Abbau extrazellulärer Proteine reguliert. Dabei stellte sich heraus, dass mTORC1-Inhibierung zur Ansäuerung des lysosomalen Lumens und einer erhöhten Aktivität lysosomaler Proteasen führt. Meine Daten zeigen des Weiteren, dass die pH-Regulation durch mTORC1 über Steuerung der V-ATPase-Assemblierung an der lysosomalen Membran erfolgt. Sind Nährstoffe reichlich forhanden und mTORC1 ist folglich aktiv, dann ist die V-ATPase-V_1-Domäne hauptsächlich im Zytoplasma lokalisiert, wo sie durch das Chaperonin TRiC stabilisiert wird. Durch mTORC1-Inhibierung assemblieren die V-ATPase V_1- und V_o-Domänen in eine aktive Protonenpumpe. Als Folge sinkt der pH-Wert des lysosomalen Lumens und es kommt zum vermehrten Abbau von endozytierten Proteinen im Lysosom. Meine Daten deuten darauf hin, dass Säugerzellen sich schnell an Nährstoffmangel anpassen können, indem sie die katabole Kapazität von Lysosomen aktivieren.

Table of contents

III. Acknowledgements

This work would not have been possible without the help of many friends and colleagues. First of all, I would like to thank my supervisor Wilhelm. Thanks for the opportunity to join the lab and for being my mentor for the past 4.5 years. Thanks for all the long and fruitful discussions about experiments and science, and for keeping your door open for any problems or questions I had in the past years. I would also like to thank my TAC members, Marius Lemberg and Claudia Scholl, for their valuable input during our meetings throughout the years. I also want to thank Berdt Bukau and Ana Banito for accepting to be part of my PhD defence committee. I would like to thank Dominic Helm and Martin Schneider from the DKFZ proteomic core facility for their help in experimental set-up and the many statistical analyses for our paper. I would like to thank Fabricio Loayza-Puch and his entire lab for constructive discussion during lab meetings and for sharing their reagents and lab space with me during the revision.

Next, I would like to thank all the members of the Palm lab, past and present, for contributing to an amazing environment in the lab. A special thanks to Cata(rina) our senior PhD student in the lab, Julia, and Rafael for all your amazing scientific (and non) support, for the laugh, for the lunches, and all the coffee and chocolate that we shared in the last years, and to be good friends. Without their infinite support and help it would have been much harder. To thank Sven and Leon for all the help in the lab, experiments discussion and cakes. I want to thank Roy for all the laughs and fun for the first two years of my PhD and for exploring the lysosome together. I want to thank also Nora and Marten, who helped me a lot in my PhD project. I want to thank all my former students for driving me crazy but also for all the laughs and help, especially with Aslıhan.

This experience would not have been possible without unconditional support, in all shapes and forms, from all my friends and family. I would like to thank my Italian community in Heidelberg, especially my flatmate Mike for his daily support. I want to thank Spyros and Hakyung who positively contributed to this time in Heidelberg. A huge thank goes to my long-distance friend Fra, we started this journey together during our master studies and now we are finishing our PhD in different countries but always there for each other. I would like to thank my oldest friend Vale for always being there for me and support with enthusiasm in all my good and bad decisions. I also want to thank Dominik for his support and affection, without which these last months would have been much more complicated. Infine, vorrei ringraziare i miei genitori e tutta la mia famiglia per avermi sostenuto con tanto affetto in questi anni in Germania.

Thank to everyone who somehow has contributed to the realization of this big achievement.

IV. Disclaimer

The work described in this Ph.D. thesis is part of a peer-reviewed published manuscript:

Edoardo Ratto, S. Roy Chowdhury, Nora S. Siefert, Martin Schneider, Marten Wittmann, Dominic Helm and Wilhelm Palm. Direct control of lysosomal catabolic activity by mTORC1 through regulation of V-ATPase assembly. Nature Communications, 2022.

Most of the content, figures, and figure legends in the Introduction, Material, Methods, Results, and Discussion sections described and shown in this thesis, have been taken or adapted from the aforementioned manuscript which have been originally conceived by myself and Wilhelm Palm. For details, see author contributions.

The method sections describing proteomics (**section 3.2.14**) and related analyses (**section 3.2.15, 3.2.16**) contain protocols or parts of them which have been kindly provided by the DKFZ Proteomics Core Facility.

Figure 1 has been adapted from David M. Sabatini, 2017[1].

Figure 3 has been adapted from Michael P. Collins and Michael Forgac, 2018[2].

V. Contributions

Cell lines expressing a doxycycline-inducible Cas9 cassette were generated by Catarina da Silva Pechincha and Franziska Hoffmann.

Lysosensor experiments in **Figure 8a-c** were performed by S. Roy Chowdhury

Generation of knockout cell lines was done by me and Marten Wittmann.

Gibson assembly and site-directed mutagenesis were done by Marten Wittmann.

Endogenously tagged Lamp1-mNeonGreen cell lines and constructs for the encoding of 3xHA-ATP6V1B2, 3xHA-ATP6V1B2-mNeonGreen, 3xFlag-ATP6Voa3, and 3xFlag-ATP6Voa3-mScarlet were generated by Nora S. Siefert.

Generation of cell lines overexpressing V-ATPase subunits or TRiC subunits was done by me, Marten Wittmann and Nora Siefert.

Samples for mass spectrometry analysis were prepared by me, processed by Dominic Helm, and analysed by Martin Schneider at the DKFZ Proteomics Core Facility.

VI. List of abbreviations

4E-BP1	Eukaryotic translation initiation factor 4E-binding protein 1
aa	Amino acid
Atg5	Autophagy related 5
ATP6AP1	ATPase H+ -transporting accessory protein 1
Castor1	Cytosolic arginine sensor for mTORC1 Subunit 1
CCDC115	Coiled-coil domain containing 115
CHX	Cycloheximide
Co-IP	Co-immunoprecipitation
DEPTOR	DEP-domain-containing mTOR-interacting protein
DMSO	Dimethylsulfoxide
DMXL1/2	DMX like protein 1/2
DQ BSA	Dequenched BSA
EDTA	Ethylenediamine tetraacetic acid
eGFP	Enhanced green fluorescence protein
ER	Endoplasmic reticulum
FITC	Fluorescein isothiocyanate conjugate
GATOR1/2	GAP activity towards rags complex 1/2
HEPES	N-2-hydroxyethylpiperazine-N'-2-ethanesulfonic acid
HIF1α	Hypoxia-inducible factor 1α
HIF1α	Hypoxia inducible factor 1 alfa
HRP	Horseradish peroxidase conjugate
kb	Kilo base pair
KO	Knockout
Lamp1	Lysosomal associated membrane protein 1
LDL	Low-density lipoprotein
LSDs	Lysosomal storage disorders
M6P	Mannose-6-phosphate
MEFs	Mouse embryonic fibroblasts
mLST8	mammalian lethal with Sec13 protein 8
mTORC1	Mechanistic target of rapamycin complex 1
Neo	Neomycin
PAK1	p21-activated kinases
PBS	Phosphate-buffered saline
PCR	Polymerase chain reaction

PI	Proteases inhibitor
PI3K	Phosphatidylinositol-3 kinase
PKA	Protein kinase A
Raptor	Regulatory protein associated with mTOR
RAS	Rat sarcoma virus
RAVE	Regulator of ATPase of vacuoles and endosomes
Rheb	Ras homology enriched in brain
RILP	Rab-interacting lysosomal Protein
s.e.m.	Standard error of the mean

VII. List of tables

VIII. List of figures

1 Introduction

1.1 Nutrient sensing and nutrient uptake in mammalian cells.

The ability to detect and respond to changes in environmental nutrient levels is essential for the survival of all living organisms. Mammalian cells are surrounded by different sources of nutrients. The level of intracellular and extracellular lipids, amino acids, and sugar are sensed by several pathways that tightly coordinate cell metabolism with nutrient availability. When nutrients are abundant, nutrients sensing pathways stimulate anabolism and nutrient storage. On the contrary, starvation downregulates anabolism and upregulates mobilization of internal stores and usage of alternative nutrient sources[3].

Proliferating cells require building blocks to produce biomass. In order to increase cellular mass, cells have to acquire nutrients from the extracellular environment for usage in biosynthetic pathways[4]. For example, cells acquire free amino acids from the environment through transmembrane amino acid transporters[5]. Mammalian cells are not able to synthesize *de novo* 10 essential amino acids, which must be acquired from the environment[5]. However, in plasma, the concentration of monomeric amino acids is low compared to the amount of amino acids present in circulating proteins like albumin, which is the most abundant protein in plasma[5]. When monomeric amino acids in the extracellular environment are too low to sustain cellular functions or the demand of proliferation, mammalian cells can use the lysosome to digest extracellular proteins for amino acid generation[6].

1.2 The lysosome

Lysosomes are the endpoint of the endolysosomal system, where extracellular and intracellular macromolecules are degraded. They contain several degradative enzymes, which include proteases, lipase, glycosidases, and nucleases that catabolize macromolecules such as proteins, lipids, glycans, nuclei acids, and also large protein complexes or entire organelles into their monomeric building blocks[7]. Moreover, lysosomes function as a platform for the activation of the nutrient-sensing mTORC1 pathway, as discussed in detail below[8].

1.2.1 Lysosomal enzymes

Lysosomal degradation of protein is carried out by proteases. Proteases in mammals have been categorised into five families based on the type of catalytic site: metallo, serine, threonine, aspartic, and cysteine proteases. Cathepsins are the major lysosomal proteases and exhibit a broad range of proteolytic substrates, such as globular and fibrous proteins as well as proteoglycans. Cathepsins belong to three distinct families of proteases. Cathepsins A and G are serine proteases, cathepsin D and E are aspartic proteases, and cathepsins B, C, F, H, K, L, O, S, V, X, and W are cysteine proteases. Cathepsins exhibit their highest activity in the low pH environment found within lysosomes[9]. However, some cathepsins have also been observed to retain their activity outside of their optimal pH range of 5[10]. For instance, cathepsin S has a pH optimum of 6.5[11], while cathepsin D exhibits optimal activity at pH 4, but can still function at pH 7.4, albeit with reduced kinetics[12]. Additionally, cathepsin K and H have been shown to have stable activity at pH 7[13], indicating a broad range of proteolytic activity. However, there are no clear data on the optimal pH for cathepsin activity in the lysosomal environment, since pH-dependent cathepsin activity has been only measured with purified enzymes so far. In the lysosome, other proteins might influence pH-dependent cathepsin activity differently, since lysosomal luminal composition cannot be reproduced *in vitro*.

Cathepsins are initially produced as preprocathepsins in the endoplasmic reticulum. A signal peptide at the N-terminus, consisting of 20-25 amino acids, targets preprocathepsins to the endoplasmic reticulum. In the endoplasmic reticulum, cathepsins are co-translationally cleaved by a peptidase, resulting in the formation of procathepsins, zymogen forms of the mature cathepsin. During their synthesis in the endoplasmic reticulum, cathepsins undergo N-linked glycosylation. Later, as the procathepsins go through the Golgi, mannose residues on glycan chains are phosphorylated to mannose-6-phosphate (M6P). The M6P-tagged procathepsins are bound by M6P receptors in the trans-Golgi network and trafficked to endosomes for subsequent delivery to lysosomes[9].

Once inside lysosomes, procathepsins are cleaved of their propeptide, resulting in the mature, active cathepsins. The activation process can occur via different modes, including trans-activation or auto-activation, or a combination of both. Auto-activation of cathepsins occurs when the pH inside lysosomes facilitates the cleavage of the propeptide by the catalytic site of the same enzyme[9]. In contrast, trans-activation of the procathepsins requires the assistance of other lysosomal proteases. Examples of cathepsins that are activated by auto-activation include cathepsin B, H, K, L, and S. Cathepsins C and X require the assistance of cathepsins

L and S for their activation. Cathepsin D undergoes partial auto-activation and requires cathepsin B and L for complete maturation.

The acidic pH within the endo/lysosomal compartment promotes the activity of cathepsins and causes conformational changes in their substrates, facilitating their cleavage[9]. The acidic lysosomal pH is generated by the vacuolar H+-ATPase (V-ATPase), an ATP-dependent proton pump that transports protons across the lysosomal membrane, which will be discussed in more detail in section 1.6. The metabolites generated in the lysosomal lumen are exported to the cytoplasm by permeases, which spanned the lysosomal membrane[14]. Interestingly, evidence suggests that lysosomes are used as storage organelles for some metabolites. For instance, during amino acid starvation amino acids produced by lysosomal protein digestion are not immediately exported to the cytoplasm but they remain in the lysosomes for later use[15,16]. Lysosomes are responsible for degrading extracellular and intracellular macromolecules, which are primarily delivered into the lysosomes through endocytosis or autophagy.

1.3 Endocytosis

Endocytosis refers to the process by which cells take up nutrients, macromolecules, and pathogens by engulfing them with the plasma membrane. The cargo is subsequently internalised in a membrane-enclosed vesicle. The engulfed material can be recycled back into the extracellular space or delivered to the lysosome for degradation[17]. Endocytosis has an important role in various cellular processes, such as signal transduction, cell division, cell migration, and nutrient uptake. Several endocytic pathways have evolved to internalize different kinds of cargo with different sizes, such as receptor-mediated endocytosis or macropinocytosis of bulk extracellular fluids[18].

1.3.1 Receptor-Mediated Endocytosis

Receptor-mediated endocytosis mediates uptake of plasma membrane receptors and their bound ligands, including nutrient, adhesion, and signalling receptors[19]. Receptor-mediated endocytosis is mainly mediated by clathrin. Vesicle formation and stabilization are mediated by an adaptor protein complex called AP2, which recognizes specific amino acid sequences in the cytoplasmic portion of the receptors[20]. AP2 recruits clathrin to the membrane, where it polymerizes leading to the formation of membrane invagination[21]. Endocytosis of plasma membrane receptors is critical for cell homeostasis, since the amount of receptor at the plasma

membrane influence intake of nutrients, sensing of extracellular stimuli (growth factors, nutrients) and response to extracellular stresses. For instance, albumin is recognised at the cell surface by several receptors, including Megalin, which drives the uptake of albumin through endocytosis and mediates its degradation in the lysosomes[22]. Moreover, LDL (low-density lipoprotein) is trafficked through receptor-mediated endocytosis. Upon uptake, LDL is transported to the lysosomes where it is broken down to release cholesterol[23,24]. Endocytosis also serves as a mechanism to terminate signal transmission. Once internalised, receptors can either be recycled back to the membrane or be degraded. The removal of receptors from the membrane, whether for recycling or degradation, results in ligand desensitization, while recycling allows for resensitization[25].

1.3.2 Macropinocytosis

Macropinocytosis is the non-selective engulfment of extracellular fluids and their contained solutes. The solutes are contained in large vesicles called macropinosomes[4]. Macropinocytosis is initiated by actin-driven ruffles at the plasma membrane. Cells can use macropinocytosis to ingest any soluble macromolecules from their environment. Moreover, owing to the large size of macropinosomes, cells can internalise cargo through macropinocytosis that is excluded from other endocytic pathways[25]. Upon internalization, macropinosomes can be recycled back to the cell surface or trafficked to the lysosome, where hydrolytic enzymes degrade the macromolecular cargo. Intracellular macropinosome trafficking is similar to trafficking of other endocytic pathways. Thus, macropinosomes do not have specific molecular markers, and they are usually recognised by their large size[4]. In mammalian cells, membrane ruffling and macropinosome formation are initiated by growth factors through the activation of Ras and PI3K signalling. Indeed, one of the first responses to growth factor stimulation is membrane ruffling and macropinosome formation[26]. Ras acts as the proximal signal; it induces PI3K recruitment at the plasma membrane and its activation. In turn, Ras and PI3K activate several downstream effectors such as the small GTPase Rac1 and Rab5 and the kinase PAK1. The activation of these proteins leads to actin polymerization, membrane ruffling, and macropinosome formation[27].

Eukaryotic cells use nutrient transmembrane transporters in order to acquire free nutrients. However, a large fraction of extracellular biomass is contained in macromolecules, which can be accessed by cells through endocytosis[27]. Cancer cells make use of macropinocytosis as a means to supply lysosomes with extracellular proteins. Upon proteolytic degradation, these generate monomeric amino acids, which cancer cells can use to survive and grow in nutrient-

poor tumour environments[28]. Macropinocytosis can provide not only amino acids but also other types of nutrients. For example, albumin, the most abundant protein in serum[29], acts as the main fatty acid binding protein in mammalian plasma, and can be taken up through macropinocyotsis[30]. Moreover, through macropinocytosis cells can take up a complex mix of macromolecules, such as apoptotic bodies[31].

1.4 Autophagy

The lysosome also catabolizes proteins from intracellular sources, which are provided by macroautophagy (hereafter referred to as autophagy). During autophagy, large double-membrane vesicles called autophagosomes are formed, which engulf cytoplasmic materials and subsequently fuse with lysosomes[7]. Through autophagy, cells can degrade large structures such as organelles and protein aggregates. Under basal conditions, autophagy has a housekeeping function, the disposal of damaged components that could be detrimental to normal cellular function. Basal autophagy is particularly important for differentiated cells that cannot reduce damaged components through proliferation[32]. During transient periods of nutrient starvation, autophagy can promote cell survival by recycling intracellular macromolecules. However, during prolonged starvation periods, autophagy progressively leads to cellular atrophy[33].

1.5 Mechanistic target of rapamycin complex 1 (mTORC1)

Mammalian cells regulate anabolic and catabolic activities through growth factors and nutrient-sensing signalling pathways. An important converging point of both signals is the mechanistic target of rapamycin complex 1 (mTORC1), which is activated at the lysosome (**Figure 1a**)[34]. In response to growth factors, like insulin, and nutrient availability mTORC1 promotes cell growth by stimulating anabolic activities such as protein, lipid and nucleotide synthesis. Conceivably, by blocking catabolic processes like lysosomal degradation of materials derived from endocytosis or autophagy[34]. mTORC1 consists of mTOR (a serine/threonine protein kinase that belongs to the family of the PI3K-related kinase), Raptor (regulatory protein associated with mTOR), and mLST8 (mammalian lethal with Sec13 protein 8)[35–37]. mLST8 directly interacts with and stabilised mTOR. Raptor is important for the subcellular localization of the complex and binds to the TOR signalling (TOS) motif on mTORC1 substrates, facilitating the recruitment of downstream mTORC1 effectors[38]. Moreover, Raptor allows the association of the accessory factor proline-rich AKT substrate 40 kDa (PRAS40) and of DEP-domain-

containing mTOR-interacting protein (DEPTOR), which have inhibitory functions on mTORC1 activity[39].

Both growth factors and nutrients have to be available for mTORC1 activation. Nutrients are critical for localisation of mTORC1 at the lysosome through the heterodimeric Rag GTPases. At the lysosome, in the presence of growth factors, the small GTPase Rheb activates mTORC1. Thus, nutrients and growth factors converge through two different pathways on activation of mTORC1.

1.5.1 Rheb-mediated activation of mTORC1.

mTORC1 is downstream of various growth factor-dependent signalling pathways. For instance, the insulin/insulin-like growth factor-1 (IGF-1) pathway activates Akt which leads to mTORC1 activation[40]. Downstream of receptor tyrosine kinases Ras activates mTORC1 through the MAP kinase ERK[41]. These pathways converge on a key negative regulator of mTORC1 signalling, the Tuberous Sclerosis Complex (TSC). TSC is constituted of TSC1, TSC2 and TBC1D7. TSC is the GTPase-activating protein (GAP) for the small GTPase Rheb, which directly interacts with and activates mTORC1[38]. Rheb activity is also regulated by metabolic conditions. For instance, metabolic stress decreasing ATP level in the cell inactivates mTORC1 through the activation of AMP-activated protein kinase and the consequent decrease in TSC activity (**Figure 1b**)[42,43].

1.5.2 Rag-mediated localization of mTORC1

mTORC1 regulation is coupled with amino acid concentrations. The critical components of the amino acids sensing of mTORC1 signalling are the Rag GTPases[44]. The Rags are heterodimers of RagA or RagB with RagC or RagD, anchored to the lysosomal membrane by the pentameric ragulator complex. Ragulator consists of Lamtor1/p18, which wraps around heterodimers of Lamtor2/p14-Lamtor3/MP1 and Lamtor4/p10-Lamtor5/HBXIP. In cells genetically ablated for the Ragulator complex, the Rags and mTORC1 cannot be recruited to the lysosome, thus the pathway is not properly activated[45]. In the presence of amino acids, the Rags are in their active conformation, in which RagA/B is bound to GTP and RagC/D to GDP. This conformation allows them to bind to Raptor and recruit mTORC1 to the lysosomal membrane.

Rags are the converging point of several amino acid-sensing pathways. The presence of leucine and arginine activates the mTORC1 pathway by inhibiting negative regulators of the pathway. Both amino acids signal through the GATOR1 and GATOR2 complex[46]. The GATOR1 complex is constituted of DEPDC5, Nprl2 and Nprl3. GATOR1 functions as a RagA/B GAP, it hydrolyses the GTP bound to RagA/B and inhibits the mTORC1 pathway. The GATOR2 complex is a positive regulator of the mTORC1 pathway and consists of Mios, WDR24, WDR59, Seh1L, and Sec13[38]. Leucine is sensed by Sestrin2. In the absence of leucine, Sestrin2 binds and inhibits GATOR2. The interaction of Sestrin2 with leucine induces the dissociation of Sestrin2 from GATOR2, positively regulating mTORC1 pathway. Similarly, CASTOR1 is the sensor for arginine. It interacts with and inhibits GATOR2 if arginine is not present[38]. Methionine can also activate the mTORC1 pathway. Methionine can be converted into S-adenosylmethionine (SAM), a cellular methyl group donor. However, SAM can be bound by SAMTOR. This interaction induces the dissociation of the SAMTOR-GATOR1 complex, and GATOR1 can no further inhibit the mTORC1 pathway, thus linking mTORC1 with methionine and one-carbon metabolism[47]. The V-ATPase interacts with the Rag-ragulator complex (**Figure 1b**). It has been proposed that the V-ATPase has a function in lysosomal amino acid sensing[48].

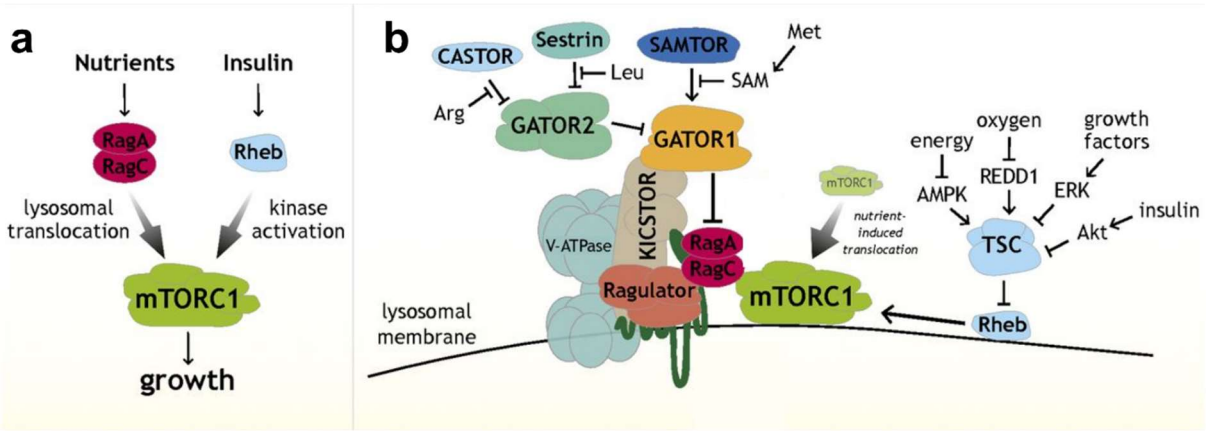

Figure 1. mTORC1 signalling pathway. a. mTORC1 integrates signals from both nutrients and growth factors. Nutrient availability triggers the Rag GTPases to move mTORC1 to the lysosomal surface, while insulin and energy levels activate the Rheb GTPase's kinase activity. **b.** A diagram illustrating the components of the nutrient and growth factors-sensing pathway that are upstream of mTORC1. Adapted from David M. Sabatini, 2017[1].

1.5.3 Downstream effectors of mTORC1

1.5.3.1 Protein Synthesis

Two major mTORC1 effectors are p70S6 Kinase 1/2 (S6K1/2) and eIF4E Binding Proteins 1/2 (4EBP1/2). The phosphorylation and consequent activation of S6K1 by mTORC1 leads to an increase in mRNA biogenesis, translation initiation, and elongation (**Figure 2**). 4E-BP1 is inhibited by mTORC1 through phosphorylation[34]. Phosphorylated 4E-BP1 dissociates from the cap-binding protein eIF4E, allowing the formation of the eIF4F complex required for the initiation of cap-dependent translation. mTORC1 plays an important role in controlling a specific class of transcripts called TOP mRNAs. These have a 5' terminal oligopyrimidine sequence downstream of the N7-methyl guanosine triphosphate cap. mRNAs with TOP motifs are strongly suppressed by mTORC1 inhibition and encode many proteins of the translation machinery, thus slowing down global protein translation and preserving energy and nutrients[49].

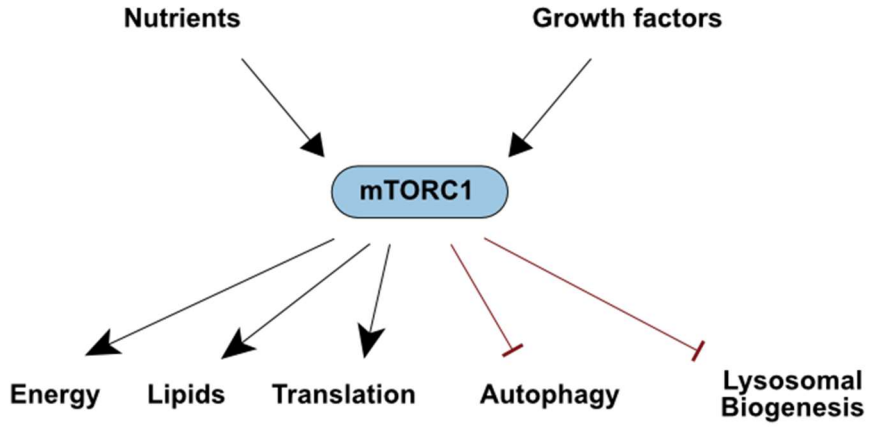

Figure 2. mTORC1 downstream cellular processes. A diagram illustrating the different cellular processes activated or inhibited by mTORC1. mTORC1 is the master regulator of many anabolic and catabolic pathways and balances them depending on nutrient levels and growth factors. In order to grow, cells have to increase the synthesis of proteins, lipids, and energy. In the presence of both growth factors and nutrients, mTORC1 upregulates the synthesis of the aforementioned molecules, while inhibiting lysosomal catabolic pathways. mTORC1 is critical for assessing the abundance of growth factors, energy, and key metabolites and coordinating cellular metabolic pathways consequently.

1.5.3.2 Lipid Synthesis

Besides regulating protein synthesis, mTORC1 controls *de novo* lipid synthesis so that proliferating cells can increase membrane generation. mTORC1 mainly regulates lipid formation by controlling the sterol regulatory element-binding protein 1/2 (SREBP1/2) transcription factors. SREBP1/2 upregulate the expression of several genes involved in fatty acid and cholesterol biosynthesis. SREBP1/2 are normally present as inactive precursors in the endoplasmic reticulum. mTORC1 activation triggers translocation of SREBP1/2 to the Golgi where it is cleaved. The cleavage allows SREBP1/2 to translocate to the nucleus and activate gene expression[50]. mTORC1 also represses Lipin-1 by directly phosphorylating it. Upon mTORC1 inactivation, Lipin-1 get activated. It translocates to the nucleus where it downregulates expression of SREBP1/2 and other genes involved in lipid biosynthesis[51].

1.5.3.3 Energy

For protein and lipid synthesis, mammalian cells need an increasing amount of energy in the form of ATP. Indeed, mTORC1 is able to increase ATP generation. On one hand, mTORC1 increases the expression of hypoxia-inducible factor 1α (HIF1α). HIF1α increases the expression of many glycolytic enzymes, thus rising ATP production through glycolysis[52]. On the other hand, mTORC1 increases mitochondrial biogenesis and oxidative metabolism through increasing mitochondrial gene expression[53].

1.5.3.4 Lysosomal catabolism

Besides regulating anabolic processes, mTORC1 also promotes growth by inhibiting catabolic pathways like lysosomal degradation of extracellular or intracellular materials. mTORC1 blocks lysosomal degradation of intracellular proteins by inhibiting autophagy[7]. In mammals, mTORC1 phosphorylates ULK1 (unc-51-like kinase 1) preventing its activation by AMPK. The complex formed by ULK1 together with ATG13 (mammalian autophagy-related gene 13) and FIP200 (focal adhesion kinase family-interacting protein of 200 kDa) is the first step for autophagosome initiation[54]. mTORC1 also regulates lysosomal catabolism by supressing transcription factor EB (TFEB)-mediated lysosomal biogenesis. TFEB is a basic helix-loop-helix leucine zipper transcription factor that promotes expression of several genes involved in autophagy and lysosomal function, *e.g.*, several lysosomal enzymes and V-ATPase subunits[55]. mTORC1 phosphorylates TFEB, preventing its nuclear translocation. During nutrient

starvation, TFEB is not phosphorylated anymore by mTORC1 and it is translocated into the nucleus where it promotes lysosomal biogenesis[56].

1.6 Lysosomal pH regulation

1.6.1 The vacuolar H^+-ATPase (V-ATPase)

Lysosomal acidification is essential for activating acid-dependent proteases and for coupled transport of small molecules across lysosomal membrane. Lysosomal acidic pH is mainly generated and maintained by the V-ATPase. The V-ATPase is an ATP-dependent proton pump that transports protons from the cytosol into the endo-lysosomal organelles or across the plasma membrane. The V-ATPase is constituted of two multi-subunit domains, the peripheral V_1 and the membrane-integral V_o domain (**Figure 3**). V_1 hydrolyses ATP, whereas V_o transports protons across the membrane[57]. The V_1 domain is composed of eight different subunits (A-H). The V_1 is constituted of 3 copies of the A and B subunits, which are arranged in alternating positions. ATP hydrolysis occurs at 3 catalytic sites each located at the connection point between the A and B subunits. The other V_1 subunits form two stalks that connect the V_1 domain to the V_o domain. The peripheral stalk serves to prevent the rotatory movement of the A-B hexamer complex upon ATP hydrolysis. The central stalk couples ATP hydrolysis with V_o domain movement and proton translocation. The transmembrane V_o domain contains six different subunits. The subunits c, c' and c'' are hydrophobic and arranged in an intramembranous ring. Moreover, c, c' and c'' subunits contain an essential intramembranous glutamate which undergoes protonation during proton transport. The V_o domain contains the peripheral subunit d, which is hydrophobic. It is located above the ring formed by the c subunits, and it connects the V_1 and the V_o domains. The d subunit is critical for reversible assembly of the V-ATPase.

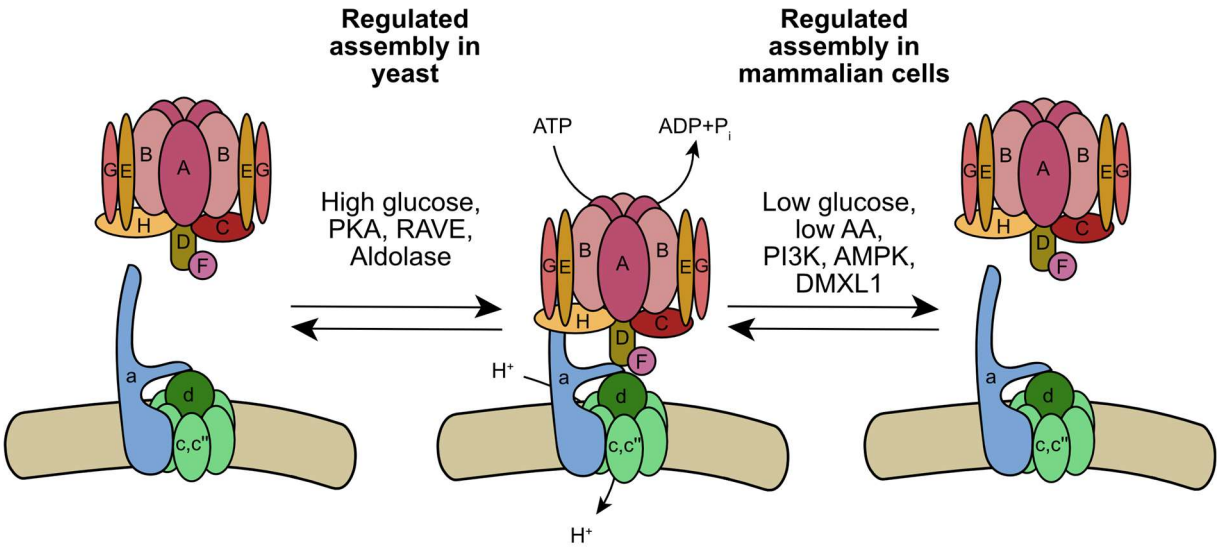

Figure 3. V-ATPase structure and assembly regulation. The assembly of V-ATPases is regulated in response to nutrient availability, with reversible dissociation of the catalytic V_1 and proton-conducting V_0 domains being a major form of regulation. In yeast, V-ATPase assembly increases when glucose is abundant and this process is facilitated by PKA, aldolase, phosphofructokinase, and the assembly factor RAVE. In mammalian cells, glucose starvation instead leads to increased V-ATPase assembly. This process is controlled by the AMPK and PI3K/AKT pathways, but not by PKA. Additionally, increased assembly in mammalian cells is observed in response to amino acid starvation. Adapted from Michael P. Collins and Michael Forgac, 2018[2].

1.6.1.1 V-ATPase role in different organelles.

Acidic pH is important in different organelles. For example, in early endosomes, a decrease in pH allows the dissociation between endocytosed ligands and their receptors, thus allowing signal termination and receptor recycling back to the plasma membrane[25]. As previously discussed, acidification in the endosomes allows the dissociation between lysosomal cathepsins on their way to the lysosome and the mannose 6-phosphate receptors[9]. The Golgi has a mildly acidic pH, which seems to be important for proper trafficking and glycosylation of several proteins[58]. The a subunit of the V_o domain is critical for targeting V-ATPase to different cellular organelles. Mammalian cells have four subunits a isoforms that control the localization of the V-ATPase to the Golgi, lysosomes/endosomes and the plasma membrane[59].

1.6.1.2 Reversible assembly of the V-ATPase.

The V-ATPase is constituted of two distinct domains, the peripheral V_1 and the membrane-associated V_o domain. The V_o domain is a membrane integral domain, whereas the V_1 domain is present in the cytoplasm and can be recruited to membranes where it associates with the V_o domain, forming an active proton pump. The reversible association and dissociation of the two domains is the best-understood mechanism regulating V-ATPase function (**Figure 3**)[60].

1.6.1.3 Reversible association of the V-ATPase in yeast.

In response to several stimuli, the V-ATPase reversibly dissociates, resulting in the termination of ATP-dependent proton transport. In yeast, V_1 and V_o dissociation is induced upon glucose deprivation and it does not require protein synthesis. The disassembled V-ATPase are not functional, and the disassembly during nutrient starvation helps preserve cellular ATP[61]. Only V-ATPases present at the vacuole undergo disassembly in response to glucose starvation, whereas V-ATPases localised to the Golgi are not glucose sensitive. Disassembly is reversible, upon glucose addition, the V_1 domain is recruited to the vacuole. Assembly requires aldolase, phosphofructokinase, and the RAVE complex[60,62]. RAVE is a heterodimeric complex constituted of Rav1, Rav2, and Skp1 subunits. Rav2 interacts with the V_1 subunit C. Rav1 interacts with V_1 subunits E and G but also with the V_o domain[63]. RAVE is recruited to the vacuole and interacts with the V-ATPase in a glucose-dependent manner. Vph1p is the yeast homologue of the Voa subunit, and it is necessary for the interaction of RAVE with the V-ATPase. Glucose-mediated V-ATPase assembly is also mediated by the Ras/cAMP/PKA pathway. Overexpression of Ras or genetic deletion of the regulatory subunit of PKA leads to V-ATPase disruption[64]. Other extracellular stresses control V-ATPase assembly in yeast. For instance, salt and alkaline stress increase V-ATPase assembly, and this assembly modification are regulated by levels of membrane signalling lipid $PI(3,5)P2^2$.

1.6.1.4 Reversible association of the V-ATPase in mammals.

V-ATPase assembly in mammalian cells can be affected by various stimuli, similar to yeast. However, the molecular mechanisms regulating mammalian V-ATPase assembly are not understood. Glucose starvation increases V-ATPase assembly and lysosome activity in mammalian cells. Furthermore, AMPK and PI3K inhibitors block the increased V-ATPase assembly upon glucose deprivation, suggesting that these signalling pathways are critical for

proper V-ATPase regulation[60]. Interestingly, it was observed that amino acids regulate V-ATPase assembly as well. Upon amino acid withdrawal, mammalian cells show a fast and reversible increase in V-ATPase assembly followed by an increase lysosomal acidification. However, it seems that amino acid-mediated V-ATPase assembly is mTORC1 independent. Indeed, the inhibition of mTORC1 with rapamycin did not increase V-ATPase assembly[65]. Moreover, dendritic cells during maturation increase V-ATPase assembly to acidifying lysosome thus facilitating antigen processing[66]. During dendritic cell maturation, treating them with rapamycin for 20 hours prevents the increase in V-ATPase assembly. This observation suggests that mTORC1 regulates the assembly of V-ATPase during maturation process[67].

Several proteins have been implied in V-ATPase assembly in mammals, such as DMXL and RILP. In human, there are two homologues of the yeast Rav1, called DMXL1 and DMXL2[63]. They form two independent heterodimer complexes with WDR7. DMXL1, DMXL2, and WDR7 co-immunoprecipitate with the V-ATPase in the kidney. It has been shown that silencing of DMXL1 or WDR7 blocks the recovery of the lysosome acidification after transient V-ATPase inhibition. However, silencing of DMXL2 has a much weaker effect on organelles reacidification. The function of the DMXL-WDR7 complex in mammals is not well understood. WDR7 is ubiquitously expressed in all tissues. The expression of DMXL1 and DMXL2 seems to be tissue-specific. DMXL1 is more widely expressed, but DMXL2 is enriched in the brain. The different DMXL isoforms might mediate V-ATPase assembly in a tissue-specific manner. It is thought that DMXL1 more broadly mediates V-ATPase assembly in the endolysosomal system, while, DMXL2 facilitates V-ATPase assembly in specialised tissue, like in presynaptic membranes of neurons[63].

Another mammalian protein suggested to regulate V-ATPase assembly is RILP (Rab-Interacting Lysosomal Protein). RILP is recruited to the endolysosomal system by Rab7 and they regulate the delivery of cargo protein to the lysosome. RILP is able to interact with the V_1 domain G1 subunit stabilising the V-ATPase subunit. RILP simultaneously binds to Rab7 with its C-terminal domain and to the G1 subunit with its N-terminal domain. Indeed, RILP inhibition induces proteasomal degradation of the G1 subunit. As a consequence, endolysosomal organelles show an increase in their luminal pH[68]. There are several other proteins, including Aldolase, Phosphofructokinase, ATP6AP2, and CCDC115, which have been proposed to play a role in V-ATPase assembly. However, the molecular mechanisms through which regulate V-ATPase assembly is largely unknown.

1.6.2 Counterion flux.

The V-ATPase proton pumping activity is electrogenic, creating a high, positive charge within the lysosomal lumen, and eventually hindering any further pumping. Thus, the V-ATPase uses ATP to move protons against both a chemical and an electrical gradient. To overcome and dissipate the membrane potential generated by the V-ATPase allowing for efficient proton transport, additional ions must also be transported across the organelle membrane. The movement of secondary ions to dissipate the membrane potential generated by the V-ATPase thus facilitate bulk proton transport is referred to as counterion flux[69]. It has been suggested that either anions entering the lumen or cations leaving the lumen, or both, could be involved in this process[70].

The cytosolic abundant chloride is an important anion participating in the counterion flux at the lysosome. CLC7 is the best studied component of the CLC family of chloride channels and transporters. CLC7 is present in the endolysosomal system and is the primary channel that mediates Cl^- transport at the lysosome[71]. CLC7 is a Cl^-/H^+ exchanger, and transports two Cl^- ions into the lysosome while exporting one proton. Removing protons from the lysosomal lumen increases the luminal pH. However, the transport of two anions reduces the membrane potential and enables the V-ATPase to continue pumping protons[71].

It has been suggested that cation permeability also play a role in facilitating counterion flux[72]. Several cation channels are targeted to the lysosomal membrane. For example, members of the mucolipin family of transient receptor potential (TRP) channels, which includes TRPML1, TRPML2, and TRPML3, have been implicated in lysosomal ion homeostasis. TRPML1 is a Ca2+-permeable cation channel that plays a role in lysosomal acidification and trafficking[73]. TRPML1 is present on the lysosomal membrane, where its inward-rectifying current assists in the movement of ions from the lysosomal lumen to the cytosol[74]. Moreover, TRPML1 is responsive to changes in lysosomal pH, as its activity increases with increasing luminal pH. Another candidate cation channel is the two-pore channels TPCs family, which is sodium-selective and contributes to lysosomal pH regulation and membrane potential maintenance. TPCs are channels composed of two-pore domains that come together as a dimer to form a functional pore. It has been shown that TPC1 and TPC2 are present on the membranes of endosomes and lysosomes[75]. TPC1 is activated by an increase in luminal pH and is voltage-gated, while TPC2 is voltage-independent. In a study conducted on murine myoblasts was observed that TPC2 knockout cells had an elevation in luminal pH along with a decrease in lysosomal protease levels[76]. Additionally, overexpression of TPC2 in HeLa cells led to an increase in lysosomal pH[71]. These studies suggest that TCP2 is involved in the regulation of

lysosomal pH by maintaining lysosomal membrane potential. Finally, the TMEM175 potassium channel is present in the lysosomes and late endosomes, and plays a crucial role in regulating lysosomal membrane potential and pH stability. TMEM175 knockout model has shown impaired lysosomal degradation and lysosome-mediated autophagosome clearance[77].

1.7 Lysosome dysfunction in hereditary diseases and human ageing

Dysfunction of lysosomal enzyme activity or a block in the trafficking of these enzymes to the lysosome leads to a class of disorders called lysosomal storage disorders (LSDs). Lysosomal storage disorders are a family of diseases characterised by a malfunction of the lysosomes. Lysosomal storage disorders can be caused by mutations in 50 different genes encoding hydrolases, permeases or proteins involved in the M6P pathway. Abnormal activity of these proteins leads to an accumulation of materials in the lysosomal lumen, such as lipids, sugars, nucleotides and amino acids due to defective lysosomal catabolism[78]. Storage of abnormal levels of substrates in the lysosomal lumen impairs the organelle's basic functions, such as degradative capacity, trafficking and, fusion with autophagosome. Thus, cells lose the ability to recycle damaged organelles and proteins aggregates through autophagy leading to a loss of cellular quality control. Patients affected by lysosomal storage disorders generally show neurodegenerative symptoms, metabolic imbalance and severe impairment during growth[54].

Cellular and organismal ageing is characterised by a gradual decline in physiological functions that occurs throughout multiple pathways. Alterations in the endolysosomal system are evident during ageing[79]. Lysosomal capacity for degradation diminishes, and cells accumulate misfolded and damaged components over time. Increasing evidence suggests that reduced lysosomal function is the most important change in the autophagy pathway that contributes to cellular ageing. Indeed, one of the most well-established indicators of neuronal ageing is the presence of lysosomes containing undigested materials[79]. Studies in yeast have revealed that lysosomes, and particularly the lysosomal proton pump V-ATPase, play a crucial role in determining longevity[80]. In yeast, a loss of lysosomal acidity results in a shortened lifespan, in part due to mitochondrial dysfunction. Cells that lack V-ATPase subunits or are treated with V-ATPase inhibitors have a significantly shorter lifespan and show various mitochondrial impairments. When the ATP6AP2 gene, which expresses a crucial protein for regulating the V-ATPase, is conditionally deleted, V-ATPase activity is reduced. The loss of function of ATP6AP2 leads to the accumulation of autophagic vacuoles, as well as cognitive impairment and neurodegeneration in both mice and flies[81]. These findings suggest that a partial loss of acidification may not immediately hinder the autophagic-lysosomal system, but make it more

susceptible to failure over time. It appears evident that alterations in pH due to ageing can significantly alter the proteolytic activity balance within lysosomes and have a disruptive impact on the breakdown of specific cellular components[80]. Lysosomal impairment is also involved in the progression of neurodegenerative diseases, such as Alzheimer's disease, Huntington's disease, and Parkinson's disease, in which the degradative function of the lysosome is progressively compromised, which eventually leads to reduced neuron viability[82]. Neurons rely on the lysosomal catabolic capacity since they are unable to proliferate and dilute damaged organelles and proteins aggregates during mitosis[7].

1.8 Exploitation of lysosomal activity in virus infection and cancer

Lysosomes are exploited in several pathological conditions. For example, acidic organelles are essential for proper infection of several viruses. For viruses to infect host cells, they must efficiently release their genome after entering the cell, allowing for translation and replication. Although viruses use a variety of receptors to initiate entry, studies on both enveloped and non-enveloped viruses suggest that intracellular acidic compartments play a crucial role in the entry of many viruses[83]. Endolysosomal compartments with an acidic pH can activate molecular mechanisms that result in the disassembly of viral particles. Acidic pH-dependent endosomal proteases cleave the glycoprotein segments of certain viruses, which facilitates efficient delivery of the viral genome into the cytosol. Without endolysosomal acidification and cleavage of the viral particle, viral replication and infection are interrupted[84].

Lysosomal activity can affect cancer development. Cancer cells that reside in solid tumour are exposed to limited nutrients due to poor vasculature, and their aberrant proliferation creates energetic and nutrient demands. Lysosomes play important roles in the progression of several human cancers. Indeed, cancer cells also upregulate the uptake of extracellular macromolecules. Oncogenic Ras upregulates the uptake of extracellular materials through macropinocytosis, decreases the dependence on free glutamine for growth[85]. Moreover, cells with oncogenic Ras mutations can proliferate in the absence of essential amino acids, such as leucine, when supplemented with extracellular proteins. Overall, evidence suggests that lysosomal digestion of extracellular macromolecules is an important nutritional source for cancer cells that grow in poorly vascularised tumours[28].

2 Aims of the project

mTORC1 promotes cellular growth in the presence of amino acids by upregulating anabolic processes and by blocking lysosomal catabolism of macromolecules. Upon nutrient starvation, mTORC1 inhibition leads to an upregulation in nutrient generation through lysosomal catabolism of proteins from extracellular and intracellular sources. However, it was not known how mTORC1 regulates lysosomal catabolism of extracellular proteins. In my Ph.D., my objective was to elucidate the cellular process through which the inhibition of mTORC1 increases the generation of nutrients from extracellular proteins within lysosomes. Upon discovering that mTORC1 regulates lysosomal pH, I went on to study in detail the molecular mechanism by which mTORC1 regulates lysosomal pH. I found out that mTORC1 regulates lysosomal pH by controlling V-ATPase assembly at the lysosomal membrane. Finally, I investigated how mTORC1-dependent regulation of lysosomal pH impacts lysosomal function and global lysosomal catabolism. My research provided new insights into the complex interplay between mTORC1, lysosomal catabolic activity, and cellular metabolism.

3 Materials and Methods

3.1 Materials

3.1.1 Primary antibodies

Table 1. Primary antibodies used in this study

Antibody	Provider	Catalogue number
SQSTM1(D1Q5S)	Cell Signaling	39749
HA-tag	Cell Signaling	3724
S6K (49D7)	Cell Signaling	2708
S6K pT389 (108D2)	Cell Signaling	9234
ATG5 (D5F5U)	Cell Signaling	12994
myc-tag (9B11)	Cell Signaling	2276
Cathepsin B	R&D Systems	AF965
Cathepsin L	R&D Systems	AF1515
Cathepsin D	R&D Systems	AF1029
Cathepsin X/Z/P	R&D Systems	AF1033
CCT1(91A)	Invitrogen	MA3-026
β-actin	Sigma Aldrich	A5441
ATP6V1E1	Proteintech	15280
GAPDH(OTI2D9)	Origene	TA802519
ATP6V0d1	Abcam	ab202899
ATP6V1A	Abcam	ab199326
CCT2	Abcam	ab92746
LC3	gift from Tullia Lindsten	Cheong et al. Autophagy, 2013[86].

3.1.2 Secondary antibodies

Table 2. Secondary antibodies used in this study

Antibody	Provider	Catalogue number
HRP anti-goat	Life Technologies	31402
HRP anti-mouse	Cytiva	NA931
HRP anti-rabbit	Cytiva	NA934
HRP anti-rat	Jackson ImmunoResearch	A10549

3.1.3 Fluorescent probes

Table 3. Fluorescent probes used in this study

Probe	Provider	Catalogue number
Oregon Green 488 70 kDa dextran	Life Technologies	D7172
Alexa Fluor 568 10 kDa dextran	Life Technologies	D22912
FITC dextran 10 kDa	Life Technologies	D1821
DQ Green BSA	Life Technologies	D12050
Hoechst 33342	Life Technologies	H1399
Lysotracker	Life Technologies	L7528
Lysosensor Yellow/Blue DND160 dextran	Life Technologies	L22460
Cresyl Violet	MP biomedicals	150727
Magic Red Cathepsin B	Immunochemistry Technologies	KF17308
Magic Red Cathepsin L	Immunochemistry Technologies	KF17312

3.1.4 Chemicals and inhibitors

Table 4. Chemicals and inhibitors used in this study

Inhibitor name	Provider	Catalogue number
Torin 1	Tocris	4247
Bafilomycin A1	Cayman Chemical	AZD8055
Rapamycin	EMD Chemicals	AY-22989
Cycloheximide	Santa Cruz Biotechnology	CAS 66-81-9
LY2584702	Selleckchem	S7698
E64	Serva	21100
AEBSF	Serva	12745
Leupeptin	Serva	51867
Pepstatin	Serva	52682
Halt Protease Inhibitor Mix	Thermo Fisher Scientific	78429
Halt protease and phosphatase Inhibitor Mix	Thermo Fisher Scientific	78444
Sodium orthovanadate	MP Biomedicals	159664
Sodium fluoride	Alfa Aesar	A13019
Sodium pyrophosphate	Alfa Aesar	A17546
Sodium glycerophosphate	Alfa Aesar	A16269
Puromycin	Santa Cruz Biotechnology	sc-108071A
Blasticidin	Santa Cruz Biotechnology	sc-495389
Geneticin (G418)	GIBCO/Invitrogen	10131035
Hygromycin	GIBCO/Invitrogen	10687010

Doxycycline	Sigma Aldrich	J67043
Polyethylenimine (PEI, MW 25000)	Polysciences	24314
Polybrene	Tocris	7711
Skim milk powder	Gerbu Biotechnik	1602
Mass Spec Grade water	Thermo Fisher Scientific	51140
Triton X-100	Sigma Aldrich	93443
Agarose	Sigma Aldrich	A9539
Acrylamide	Carl Roth	A121.1
β-mercaptoethanol	Sigma Aldrich	M3148
fatty acid-free BSA	EMD Millipore	126579
BSA for blocking solutions	Serva	11930
Clarity Western ECL	BioRad	170-5061
Lipofectamine 3000	ThermoFisher Scientific	L3000001
TEMED	Carl Roth	2367
APS	ThermoFisher Scientific	17874
SDS	Serva	20765
Tris Base	Sigma Aldrich	648310
Monensin	Selleckchem	S2324
Nigericin	Tocris	4312

3.1.5 Cell lines

Table 5. Cell lines used in this study

Cell line	Reference
MEFs	Palm et al. Cell, 2015[28].
MIA PaCa-2	ATCC CRL-1420
A549	ATCC CRM-CCL-185
MRC-5	ATCC CCL-171
HEK 293T	ATCC CRL-3216

3.1.6 Commercial plasmids

Table 6. Backbone vectors used in this study

Vectors	Reference
pCMVR8.74	Addgene 22036
pCMV-VSV-G	Addgene 8454
Gag-Pol	Addgene 14887
pRRL-SFFV-rtTA3-IRES-EcoR-PGK-HygroR	de Almeida M. et al. Nature, 2021[87].
pLentiv2-TRE3G-Cas9-P2A-BFP	de Almeida M. et al. Nature, 2021[87].
Dual-hU6-sgRNA-mU6-sgRNA-Ef1a-Thy1.1-P2A-NeoR	de Almeida M. et al. Nature, 2021[87].
Dual-hU6-sgRNA-mU6-sgRNA-EF1αs-BFP	de Almeida M. et al. Nature, 2021[87].
pLenti-CRISPR v2-PuroR	Addgene 52961
pMaCTag-Z07	Addgene 124790

pMaCTag-Z11	Addgene 120054
pLV-EF1a-IRES-BlastR	Addgene 85133
pLV-EF1a-IRES-HygroR	Addgene 85134
pcDNA3.1-hAsCpf1	Addgene 89353

3.1.7 Generated plasmids

Table 7. Generated plasmids in this study

Generated plasmids	**Backbone vector**
pLenti-hU6-sgRNA-iT-EF1α-mCherry-P2A-NeoR + **sgRNAs**	pLenti-hU6-sgRNA-iT-EF1α-mCherry-P2A-NeoR
pLenti-hU6-sgRNA-iT-EF1α-EF1αs-BFP+**sgRNAs**	pLenti-hU6-sgRNA-iT-EF1α-EF1αs-BFP
LentiCRISPR v2 + **sgRNAs**	LentiCRISPR v2
pLV-EF1a-IRES-BlastR- HA-V1B2	pLV-EF1a-IRES-BlastR
pLV-EF1a-IRES-BlastR- HA-V1B2-NeonGreen	pLV-EF1a-IRES-BlastR
pLV-EF1a-IRES-HygroR- Flag-Voa3	pLV-EF1a-IRES-HygroR
pLV-EF1a-IRES-HygroR- Flag-Voa3-mScarlet-I	pLV-EF1a-IRES-HygroR
pLV-EF1a-IRES-BlastR- eGFP-V1A	pLV-EF1a-IRES-BlastR
pLV-EF1a-IRES-HygroR-Myc-Tag-CCT1	pLV-EF1a-IRES-HygroR
pLV-EF1a-IRES-HygroR-Myc-Tag-CCT2	pLV-EF1a-IRES-HygroR

3.1.8 sgRNAs

Table 8. sgRNA used in this study

Gene	Species	Name	sgRNA sequence 1	sgRNA sequence 2
Chr1.1	mouse	Control_sgRNA1	GACAATGAACATAAGCACAT	
Rosa1	mouse	Control_sgRNA2	GAAGATGGGCGGGAGTCTTC	
Cct1	mouse	CCT1_sgRNA1	GGTGGCACCATCGTTAGTAA	
Cct2	mouse	CCT2_sgRNA1	GGTTGGAGAGAAGCCACAA	
Atg5	mouse	ATG5_dsgRNA	ATCAAATAGTAAACCAAT	GAACATCACAGTACATTTCA
Rilp1	mouse	RILP1_dsgRNA1	TCTTGGAAAAGGCCGCCGTG	GCTCGTGTACCATCTAGCGG
Rilp1	mouse	RILP1_dsgRNA2	GGAGGTGACAGACAGACAGC	TCTTGGAAAAGGCCGCCGTG
Dmxl1	mouse	DMXL1_dsgRNA1	AGTTGGGGAAAGTACATGAG	TGATGGTGAGAGATCTAAGG
Dmxl1	mouse	DMXL1_dsgRNA2	AGTAGGGAGCCATGCCACAT	GCATTAAGGACACCAAATGT
Dmxl2	mouse	DMXL2_dsgRNA1	GTGGGACACAGTCAGAACAG	TATATGACAAAGGTCCAATG
Dmxl2	mouse	DMXL2_dsgRNA2	GGTAAGAGATGGAATATTGG	TTGAATGCGAATCTACAGGA
CtsB	mouse	CTSB_dsgRNA1	GGAGTCTACAATTCTCATGT	CTGGAGAAGGAGATACTCCC
CtsB	mouse	CTSB_dsgRNA2	TCGGCCATTGGTGTGAATGC	ATTGGACAGATTAGAGACCA
CtsD	mouse	CTSD_dsgRNA1	GTATCTTGCAATGAATGGAG	CCTGAGCCAGGACACTGTAT
CtsD	mouse	CTSD_dsgRNA2	GGGGCAGTGCCTCTTATCCA	CACTCGAAAGGCCTACTGGC
CtsL	mouse	CTSL_dsgRNA1	GCAAGAGAAAGCCCTCATGA	GGACAGATGTTCCTTAAGAC
CtsL	mouse	CTSL_dsgRNA2	AAGAGTGGAGGAGAGCGATA	CCAAGCAGAGGACAGCCAAA
Cct1	mouse	CCT1_dsgRNA1	AGTTGGCTTGGATAAAATGT	GTTCGGGGACCGCAGCACTG
Cct1	mouse	CCT1_dsgRNA2	GTTCGGGGACCGCAGCACTG	CAGATCATCAATCCGAAGGA

Cct2	mouse	CCT2_dsgRNA1	AGTGGCACCACGAAGCACAA	GATCCTAGAACAGTTTACGG

3.1.9 Standard kits

Table 9. Standard kit used in this study

Kit	Provider	Catalogue number
Pierce BCA Protein Assay Kit	Thermo Fisher Scientific	23227
Bio-Rad Protein Assay Dye Reagent	Bio-Rad	5000006
DNA 1Kb ladder	NEB	N3200L
Precision Plus Protein Dual Color Standards	BioRad	1610374EDU
QIAprep Spin Miniprep Kit	QIAGEN	27106
QIAquick PCR Purification Kit	QIAGEN	28106
QIAquick Gel Extraction Kit	QIAGEN	28706X4
HiFi DNA Assembly Master Mix	NEB	E2621L
MycoAlertTM Mycoplasma Detection	Lonza	LT07-318
Q5 Site-Directed Mutagenesis Kit	NEB	E0554S

3.1.10 Enzymes

Table 10. Enzymes used in this study

Enzymes	Provider	Catalogue number
SuperScript III Reverse Transcriptase	Invitrogen	18080093
T7 DNA Ligase	NEB	M0318
T4 Polynucleotide Kinase	NEB	M0201
FastDigest BpiI	Thermo Fisher Scientific	FD1014
EcoRI-HF	NEB	R3101
BamHI	NEB	R3136
Endo H	NEB	P0702
PNGase F	NEB	P0710
DnpI	NEB	R0176S
Velocity HiFi-polymerase	Bioline	BIO-21098

3.1.11 Buffers

Table 11. Buffers used in this study

Buffer	Composition
Genomic DNA extraction lysis buffer	10 mM Tris-HCl 150 mM NaCl 10 mM EDTA 0.1 % SDS
Standard protein lysis buffer	50 mM HEPES pH 7.4 40 mM NaCl 2 mM EDTA 1 mM Na orthovanadate 50 mM NaF 10 mM Na pyrophosphate 10 mM Na glycerophosphate 1 % Triton X-100 1x Halt protease and phosphatase inhibitor cocktails
Homogenisation buffer	20 mM HEPES (pH 7.5) 50 mM sucrose 125 mM KCl 1 mM EDTA 1x Halt protease and phosphatase inhibitor cocktails
Laemmli Sample Buffer (4x)	250 mM Tris pH 6,8 50 % Glycerol 5 % SDS (20 %) 0.05 % Bromophenol Blue

	10 % beta-Mercaptoethanol
Tris-buffered saline (TBST)	20 mM Tris base
	150 mM NaCl
	0.1 % Tween-20
	pH to 7.5
1 L Phosphate-buffered saline (PBS) (10x)	80 g NaCl
	14.4 g Na_2HPO_4
	2.4 g KH_2PO_4
	2 g KCl
1L SDS-PAGE Running & Transfer Buffer (10x)	30.3 g Tris base
	144 g Glycine
SDS-PAGE Running Buffer	1x SDS-PAGE Running & Transfer Buffer
	0.1 % SDS
Transfer Buffer	1x SDS-PAGE Running & Transfer Buffer
	0.01 % SDS
	20 % methanol
Western Blot Stripping Buffer	200 mM Glycine
	0.1 % SDS
	pH 2.2
Ponceau S Staining Solution	0.2 % Ponceau S
	5 % Glacial Acetic Acid
Tris-borate-EDTA Buffer (TBE)	89 mM Tris base
	89 mM Boric acid
	2 mM Na_2EDTA pH 8
BSA solution for Antibodies	5 % BSA
	0.2125 % NaCl

	0.025 % NaAzide
1L 1,5 M Tris pH 8,8	181.71 g Tris base
	Adjust pH to 8.8 with concentrated HCl
1L 1,5 M Tris pH 6,8	121.14 g Tris base
	Adjust pH to 6.8 with concentrated HCl
Co-IP lysis buffer	40 mM HEPES-KOH pH 7.4
	150 NaCl
	2 mM EDTA
	2,5 mM $MgCl_2$
	5 % glycerol
	1 % Triton X-100
	protease and phosphatase inhibitors Cocktail
PCR buffer	200 mM Tris-HCl pH 8.8
	100 mM $(NH_4)_2SO_4$
	500 mM KCl
	1% Triton X-100
	1 mg/ml BSA
	20 mM $MgCl_2$
	500 mM betaine
Peptides resuspension buffer	2.5 % Hexafluoro-2-propanol
	0.1 % TFA
Proteomic solvent A	0.1 % formic acid in water
Proteomic solvent B	0.1 % formic acid in acetonitrile

3.1.12 Acrylamide gels

Table 12. Acrylamide gels used in this study

Resolving Gel %	Solutions	5 mL
7.5 %	H2O	2.45 mL
	1,5 M Tris pH 8,8	1.25 mL
	30 % Rotiphorese	1.25 mL
	10 % SDS	50 µL
	10 % APS	50 µL
	TEMED	5 µL
10 %	H2O	1.979 mL
	1,5 M Tris pH 8,8	1.237 mL
	30 % Rotiphorese	1.633 mL
	10 % SDS	50 µL
	10 % APS	50 µL
	TEMED	5 µL
12 %	H2O	1.732 mL
	1,5 M Tris pH 8,8	1.237 mL
	30 % Rotiphorese	1.93 mL
	10 % SDS	50 µL
	10 % APS	50 µL
	TEMED	5 µL
15 %	H2O	1.237 mL

	1,5 M Tris pH 8,8	1.237 mL
	30 % Rotiphorese	2.425 mL
	10 % SDS	50 µL
	10 % APS	50 µL
	TEMED	5 µL

Stacking Gel %	**Solutions**	**5 mL**
5 %	H2O	3.424 mL
	1,5 M Tris pH 6,8	634 µL
	30% Rotiphorese	836 µL
	10% SDS	50.352 µL
	10% APS	50 µL
	TEMED	5 µL

3.1.13 Instruments

Table 13. Instruments used in this study

Instrument	**Provider**
ChemiDoc Touch imaging system	Bio-Rad
Leica TCS SP5 confocal microscope	Leica
CASY Cell Counter and Analyzer	OMNI Life Sciences

Infinite 200 Pro plate reader	Tecan
Synergy H1 plate reader	BioTek
FACSAria III cell sorter	Becton Dickinson (BD)
DigestPro MSi robotic system	INTAVIS Bioanalytical Instruments AG
Ultimate 3000 UPLC system	Thermo Fisher Scientific
Orbitrap Exploris 480 mass spectrometer	Thermo Fisher Scientific
Multi-Mode Plate Reader Synergy H1	BioTek

3.1.14 Software

Table 14. Software used in this study

Software	
NEBbuilder Assembly Tool	nebuilder.neb.com
online oligo design tool	www.pcr-tagging.com
Image Lab (v3.0.1.14)	BioRad
Fiji	Schindelin J, et al. Nature Methods, 2012[88].
MaxQuant	Tyanova S, et al. Nature Protocols 2016[89].
GraphPad Prism version 9.0.0 (471)	Prism
Leica LAS AF software (v2.6.3.8173)	Leica
FACSDiva software (v8.0, FACSAria I)	Becton Dickinson (BD)
R-package limma	Ritchie ME, et al Nucleic acids research 2015[90].

3.1.15 Miscellaneous

Table 15. Miscellaneous

Other	Provider
PVDF	Biorad 1620184
Nitrocellulose	Biorad 1620112
KIMBLE Dounce tissue grinder	Sigma Aldrich
8-well chambered coverslips	IBIDI
Acclaim PepMap300 C18, 5 µm, 300 Å wide pore	Thermo Fisher Scientific
nanoEase MZ Peptide analytical column	Thermo Fisher Scientific

3.2 Methods

3.2.1 Cell culture

MIA PaCa-2, A549 and MRC-5 cells, and SV40 large T antigen-immortalised mouse embryonic fibroblasts (MEFs) were maintained in DMEM/F-12 supplemented with 10 % FBS. HEK 293T were cultured in DMEM supplemented with 10 % FBS. All cell lines were maintained at 37 °C and 5 % CO_2 and a mycoplasma contamination test was regularly performed (MycoAlertTM Mycoplasma Detection, Lonza). All human cell lines were authenticated using Single Nucleotide Polymorphism (SNP) typing by Multiplexion or by sequencing analysis. Amino acid-deficient cell culture media were performed with amino acid-free, glucose-free DMEM/F-12 (USBiological D9807-11) and dialyzed FBS (Gibco). Glucose and bicarbonate (Sigma Aldrich) were added back to the same concentration of DMEM/F-12 and the pH was adjust to 7.3 by using HCl. All amino acids were re-added at the same concentration as in DMEM/F-12 in media used for full media or restimulation (+aa) condition (**Table 16**). For SILAC experiment also medium and heavy isotopes of Arginine and Lysine were used, maintaining the same concentration of DMEM/F-12.

Table 16. Amino acid concentration in the cell culture media used in this study

Media composition	Final concentration	Provider	Catalogue number
Alanine	50 µM	Sigma Aldrich	A0325000
Arginine:HCl	699 µM/480 µM (SILAC)	Sigma Aldrich	A1271000
Asparagine:H2O	50 µM	Sigma Aldrich	Y0000305
Aspartate	50 µM	Sigma Aldrich	A9256
Cysteine:HCl:H2O	100 µM	Sigma Aldrich	C3290000
Cystine:2HCl	100 µM	Sigma Aldrich	C3300000
Glutamate	50 µM	Sigma Aldrich	G8415
Glutamine	2500 µM	Gibco	25030

Glycine	250 µM	Sigma Aldrich	G5417
Histidine:HCl:H2O	150 µM	Sigma Aldrich	H0755000
Isoleucine	416 µM	Sigma Aldrich	I0460000
Leucine	450 µM	Sigma Aldrich	L0375000
Lysine:HCl	499 µM	Sigma Aldrich	L0900000
Methionine	116 µM	Sigma Aldrich	M0960000
Phenylalanine	215 µM	Sigma Aldrich	P1150000
Proline	150 µM	Sigma Aldrich	P3350000
Serine	250 µM	Sigma Aldrich	S0450000
Threonine	449 µM	Sigma Aldrich	T8441
Tryptophan	44 µM	Sigma Aldrich	T2610000
Tyrosine:2Na:H2O	248 µM	Sigma Aldrich	T1145
Valine	452 µM	Sigma Aldrich	V0030000
Glucose	17,5 mM	Sigma Aldrich	G7021
Bicarbonate	2.4 g/L	Sigma Aldrich	S5761
L-Arginine:HCL (13C6)	480 µM	Cambridge Isotopes Laboratories	201204102
L-Arginine:HCL (13C6, 15N4)	480 µM	Cambridge Isotopes Laboratories	201604102
L-Lysine:2HCL (4,4,5,5-D4)	499 µM	Cambridge Isotopes Laboratories	DLM-2640-1
L-Lysine:2HCL (D9)	499 µM	Cambridge Isotopes Laboratories	DLM-570-PK

3.2.2 Lentivirus production and transduction

For lentiviral production, HEK 293T cells were co-transfected with the expression lentiviral plasmid, pCMVR8.74 and pCMV-VSV-G. DNA was transfected into HEK293T using polyethyleneimine (PEI, MW 25000) and cell culture medium changed after 6 h and 24 h. Two days after transfection, supernatants containing the viral particles were filtered through a 0.45 µm PES filter. Target cells were infected at 50 % transduction efficiency by the addition of viral supernatant and 10 µg/ml polybrene.

3.2.3 Generation of iCas9 cells

Cell lines expressing a doxycycline-inducible Cas9 cassette were generated essentially as described previously (11). MEFs were sequentially transduced with pRRL-SFFV-rtTA3-IRES-EcoR-PGK-HygroR and pLentiv2-TRE3G-Cas9-P2A-BFP subsequently, cells were selected with 100 µg/ml hygromycin B by Catarina Pechincha. After antibiotic selection cells were sorted as single cells into 96-well plates using a FACSAria III cell sorter (BD Bioscience) by Catarina Pechincha or Franziska Hoffmann. Cas9-BFP expression was induced with 1 µg/ml doxycycline. Finally, the detected single clones were tested for Cas9 induction, gene editing, and TRE3G promoter tightness by flow cytometry and immunoblotting.

3.2.4 Generation of knockout cells

Inducible Cas9 MEFs knockout (iKO) were generated by lentiviral transduction of Dual-hU6-sgRNA-mU6-sgRNA-Ef1a-Thy1.1-P2A-NeoR or Dual-hU6-sgRNA-mU6-sgRNA-EF1-s-BFP containing the dual single guide RNA against the gene of choice (**Table 8**). Subsequently, MEFs were selected with 0,4 mg/mL geneticin or FACS sort for BFP to obtain a sgRNA-positive population. Knockout specificity was confirmed by immunoblotting. Knockout generation was achieved by treating the cell with 400 ng/mL of doxycycline for 3 days. For inducible CRISPR-Cas9 editing experiments, cells used as control were not treated with doxycycline. For **Figure 6** sgRNAs targeting non-coding chromosome regions were used as controls. For **Figure 15c** constitutive knockouts were used. In this case, MEFs were transduced with LentiCRISPR v2 (Addgene 52961), carrying sgRNAs against target genes or targeting non-coding chromosome regions (used as control sgRNA).

3.2.5 Generation of V-ATPase and TRiC expression constructs

For the generation of the expression construct I designed the primers and the cloning strategy which was carried out by Marten Wittmann. Gibson Assembly workflow was used in order to generate V-ATPases and TRiC expression construct. Human ATP6V1B2 and ATP6Voa3 (TCIRG1) ORFs were obtained from the Genomics and Proteomics Core Facility at the DKFZ. 3xHA-Tag or 3xFlag-Tag were added to the primer used to amply the ORFs in order to introduce the tag at the 5' of the fragment. Whereas, mNeonGreen and mScarlet-I were amplified from pMaCTag-Z07 (Addgene 124790) and pMaCTag-Z11 (Addgene 120054), respectively to tag the C-terminal of the gene of interest. Finally, HA-V1B2 and HA-V1B2-mNeonGreen were cloned into pLV-EF1a-IRES-BlastR (Addgene 85133), Flag-Voa3 and Flag-Voa3-mScarlet-I were cloned into pLV-EF1a-IRES-HygroR (Addgene 85134). For murine Cct1 and Cct2 expression construct, fragments containing the gene were synthesised by Genewiz. To generate constructs resistant to Cas9 editing 5 synonymous nucleotide mutations were added in the sgRNA binding site. Myc-Tag was added to the primer used to amply the DNA fragments of Cct1 and Cct2 in order to introduce the tag at the 5' of the gene. The fragments were then cloned into pLV-EF1a-IRES-HygroR. Cct2 was additionally mutated to Cct2 S260A and Cct2 S260D by site-directed mutagenesis (Q5 Site-Directed Mutagenesis Kit, NEB).

Primers for cDNA amplification and cloning were designed using the NEBuilder Assembly Tool (**Table 17**). Cloning was performed using the HiFi DNA Assembly Master Mix.

Table 17. Oligonucleotide used for V-ATPase cloning

Primer ID	Sequence (5' to 3')
pLV-3xHA-hATP6V1B2 FWD	tccatttcaggtgtcgtgagatgtacccatacgatgttcctgactatgcgggctatcccta tgacgtcccggactatgcaggatcctatccatatgacgttccagattacgctGCGCT GCGGGCGATGCGG
pLV-hATP6V1B2 REV	agagcggccgccctcgaggCTATGCCACACTGTCGTCGTTATTG
pLV-3xFLAG-hATP6V0a3 FWD	tccatttcaggtgtcgtgagatggactacaaagaccatgacggtgattataaagatcat gatatcgattacaaggatgacgatgacaagGGCTCCATGTTCCGGAGC
pLV-hATP6V0a3 REV	tgcaaagcatggcggaggcggatccgtgagcaagggcgaggag
mNeonGreen-hATP6V1B2 REV	cccgcagcgcggagcctccacctcccttgtacagctcgtccatgc
hATP6V1B2-mNeonGreen FWD	tgcaaagcatggcggaggcggatccgtgagcaagggcgaggag
pLV-NeonGreen REV	tagagcggccgccctcgaggCTAATGCTTTGCAGAGTCTCGAGGG
mScarlet-hATP6V0a3 REV	acatggagccggatccgcctccgcccttgtacagctcgtccatgc
hATP6V0a3-mScarlet FWD	gctgtacaagggcggaggcggatccggctccatgttccggagc

pLV-mScarlet REV	tagagcggccgccctcgaggCTAGTCATCTGTGGCAGCG
pLV-Myc-Cct1 FWD	tccatttcaggtgtcgtgagatggaacaaaaacttattagcgaagaagatcttGAGG GTCCTTTGTCCGTG
pLV-Myc-Cct2 FWD	tccatttcaggtgtcgtgagatggaacaaaaacttattagcgaagaagatcttGCTT CCCTTTCCCTCGCAC
pLV-Cct1 REV	tagagcggccgccctcgaggTCAGTCATCAAGGGCTCC
pLV-Cct2 REV	tagagcggccgccctcgaggTTAACAGGGGTGGTGATCG

3.2.6 Generation of endogenously tagged Lamp1-mNeonGreen cell lines

Lamp1-mNeonGreen cell lines were generated by Nora Siefert in our laboratory as previously described[91]. pMaCTag-Z07 (Addgene 124790) was used to amplify mNeonGreen by using primers modified with phosphothioate groups (*) at the five terminal 5' end bases (**Table 18. Oligonucleotide used for LAMP1 endogenous tagging**). The PCR was performed using Velocity HiFi-polymerase (Bioline BIO-21098) and PCR buffer (200 mM Tris-HCl pH 8.8, 100 mM (NH4)2SO4, 500 mM KCl, 1% Triton X-100, 1 mg/ml BSA, 20 mM MgCl2, 500 mM betaine). For the transfection, 100.000 MEFs were plated on 6-well plates. The following day 500 ng of the PCR product and 500 ng pcDNA3.1-hAsCpf1 (Addgene 89353) were co-transduced using Lipofectamine 3000 (ThermoFisher Scientific). After 1 week from transfection, mNeonGreen-positive MEFs were sorted as single cells in 96 well plates using a FACSAria III cell sorter. Finally, single clones were tested by immunoblotting and confocal microscopy to detect successful incorporation of mNeonGreen.

Table 18. Oligonucleotide used for LAMP1 endogenous tagging

Primer ID	Sequence (5' to 3')
M1_mLAMP1	G*T*G*G*G*CGGTGCCCTGGCAGGGCTGGTCCTCATCGTCCTCATTGCCTACCTCATTGG CAGGAAGAGGAGTCACGCCGGCTATCAGACCATCTCAGGTGGAGGAGGTAGTG
M2_mLAMP1	G*C*T*T*G*GGGATGTGAGAACAGGCCCCTGTGCATCTCTGGTGCACCTGCCCACCAGGA AAAAACCCACCAGGCTAGATGGTCTATCTACAAGAGTAGAAATTAGCTAGCTGCATCGGT ACC

3.2.7 Proliferation assay

Proliferation assay was performed using MEFs. They were first transduced with sgRNA against Cct2 and subsequently, transduced with empty control vector, Cct2 wild type, phosphomimetic Cct2 S260A, or Cct2 S260D. Upon antibiotic selection for cells expressing the sgRNA and the corresponding expression construct, Cas9 expression was induced by using 400 ng/ml of doxycycline for three days before the start of the experiment. On the day of the experiment (day 0), MEFs were plated in 12 well plates and after 5 hours medium changed to 1.5 mL of experimental media. Cells were counted from day 0 to day 3 in triplicate using a CASY Cell Counter and Analyzer (OMNI Life Sciences), and plotted as fold change compared to day 0 measurements.

3.2.8 Lysosomal pH measurement with lysosensor

To conduct the lysosensor assay, 15.000 MEFs were seeded onto a clear bottom 96-well black border plate and allowed to attach overnight. Next, cells were treated with media containing 0.2 mg/ml Lysosensor Yellow/Blue DND160 dextran for 4 hours. Then washed three times and incubated in fresh media for an additional 4 hours, during which any specified treatments were administered. For each experiment, a pH calibration curve was constructed by incubating cells in sodium acetate-acetic acid calibration buffers with varying pH levels (ranging from pH 4.2 to pH 5.2) for 10 minutes at 37°C. The lysosomal pH was then clamped to the buffer pH through the addition of 10 µM nigericin and 10 µM monensin. A Multi-Mode Plate Reader Synergy H1 (BioTek) was used to perform dual-emission ratiometric measurements. For lysosensor measurements excitation 329 nm/emission 440 nm and excitation 380 nm/emission 540 nm were used. Lysosomal pH values were calculated based on the emission intensity ratio of 440 nm/540 nm and the calibration curve.

3.2.9 Protein extraction

3.2.9.1 Cytosolic protein lysis

For full protein extraction, 300,000 MEFs were plated in a 6-well plate and left to attach overnight. Then, cells were washed once with ice-cold PBS, lysed in ice-cold lysis buffer (50 mM HEPES pH 7.4, 40 mM NaCl, 2 mM EDTA, 1 mM sodium orthovanadate, 50 mM sodium fluoride, 10 mM sodium pyrophosphate, 10 mM sodium glycerophosphate, 1 %

Triton X-100, 1x Halt protease and phosphatase inhibitor cocktails). After 15 min incubation on ice with occasional vortexing, samples were centrifuged at 14,000 g for 5 min at 4 C, and supernatant with solubilised proteins was collected.

3.2.9.2 Lysosome-containing membrane fractions

For membrane fractionation, 300,000 MEFs were plated and incubated overnight with 2 mg/ml 10 kDa Dextran (Sigma Aldrich). The following day, cells were washed twice with fresh media and maintained for 4 h in fresh media without dextran. Then, MEFs were washed once with ice-cold PBS and resuspended in ice-cold homogenization buffer (20 mM HEPES (pH 7.5), 125 KCl, 50 mM sucrose, 1 mM EDTA, protease, and phosphatase inhibitors). Lysis was carried out by 12 strokes with a KIMBLE Dounce tissue grinder with a large clearance pestle (Sigma Aldrich). Next, the samples were centrifuged at 800 g for 5 minutes to pellet the nuclei. The supernatant was centrifuged at 18,000 g for 20 minutes. The lysosome-containing membrane pellet so obtained was resuspended and lysate in lysis buffer (50 mM HEPES pH 7.4, 40 mM NaCl, 2 mM EDTA, 1 mM sodium orthovanadate, 50 mM sodium fluoride, 10 mM sodium pyrophosphate, 10 mM sodium glycerophosphate, 1 % Triton X-100, 1x Halt protease and phosphatase inhibitor cocktails).

3.2.10 Immunoblotting

The protein concentration was determined using the Pierce™ BCA Protein Assay Kit (ThermoFisher Scientific). Equal protein amount was used for the following analysis. Specifically, proteins from cell lysate preparations were mixed with Laemmli sample buffer 4x (250 mM Tris pH 6.8, 50 % Glycerol, 5 % SDS (20 %), 0.05 % Bromophenol Blue, 10 % beta Mercaptoethanol) in a final maximum volume of 50 µL. Then, samples were separated on SDS gel (different percentage of acrylamide were used, depending on the protein of interest) at room temperature at 150 V until the running front ran out. For LC3 detection proteins were blotted on PVDF membranes otherwise on nitrocellulose membranes at 4 C at 100 V for 70 minutes. Membranes were rinsed in dH_2O and incubated for 2 minutes in Ponceau S solution to asses blotting efficiency. Membranes were destained with TBST and then blocked in 5% (w/v) non-fat dry milk in TBST for 30 minutes. Membranes were then incubated overnight with primary antibody at 4 degrees. The following day membranes were washed 3 times for 5 minutes each in TBST, then incubated with the HRP-coupled secondary antibody at room

temperature for 2 hours. Membranes were washed 3 times for 10 minutes each and finally incubate with Clarity Western ECL (BioRad) substrates and imagined in the ChemiDoc Touch imaging system (BioRad). When samples were analysed using multiple antibodies on different membranes, sample preparation, electrophoresis, and immunoblotting were performed in parallel under identical conditions. Immunoblotting quantification and further analysis were done with Image Lab software (BioRad).

3.2.11 Confocal microscopy

For confocal microscopy, 12,000-15,000 cells were plated the day before on 8-well chambered coverslips (IBIDI). Live cell imaging was performed in a humidified chamber at 37° C and 5 % CO_2. Torin 1 treatment and amino acid restimulation were performed at the microscope immediately prior to imaging, if not otherwise indicated. For live imaging 0.5 µg/ml Hoechst and 1 µM cresyl violet or 10 nM of lysotracker red was added 30 min prior to imaging, where indicated. All microscopy experiments were imaged with a Leica TCS SP5 confocal microscope using a 40x or 63x, 1.40 oil objective.

3.2.11.1 Dextran uptake

70 kDa Oregon Green 488 dextran or 10 kDa Alexa Fluor 568 dextran were incubated with MEFs for 45 minutes at a concentration of 0.1 mg/ml. Next, cells were washed three times with PBS, and fixed in 4% PFA for 15 minutes at room temperature. Finally, cells were stained with 10 µg/ml Hoechst in PBS for 5 min and washed with PBS. The cells were maintained in PBS for the imagining.

3.2.11.2 Cathepsin activity

Cathepsin activity was measured by using Magic Red substrates for cathepsin B and cathepsin L. The probe was first resuspended in DMSO, then diluted 1:250 in DMEM/F12, and incubated for 10-12 minutes before starting imaging.

3.2.11.3 Extracellular protein degradation assay

Cells were incubated with DQ-BSA and imaged after 5 h of incubation. Cells were treated with torin 1 as indicated. In **Figure 4f** and **Figure 19c**, MEFs were first incubated for 4 h with DQ-BSA, then washed once with PBS and incubated for 3 h in fresh media in the absence of any probe. In Figure 9a, c, to have a comparable treatment as with lysosensor, MEFs were first incubated for 4 h with DQ-BSA, then washed once with PBS and incubated for 4 h in fresh media in the absence of any probe. During this chase time, MEFs were treated with torin 1 where indicated.

3.2.11.4 Lysosomal acidity assay

MEFs were incubated overnight with 1 mg/mL 10 kDa FITC dextran, washed once with PBS, and then incubated in fresh media for 4 h. To quantify V-ATPases activity, during the 4 h chase MEFs were treated for 1 h with torin 1 to maximize V-ATPases assembly and treated with 20 nM bafilomycin A1 for the last 30 minutes. Immediately before imaging bafilomycin A1 was removed by one wash with 5 mg/mL fatty acid-free BSA in DMEM/F12, and the quenching of FITC fluorescence was measured over time.

3.2.11.5 V-ATPases assembly

To analyse V-ATPases assembly, MEFs expressing HA-ATP6V1B2-mNeonGreen and Flag-ATP6Voa3-mScarlet-I were followed over time. Any treatment indicated in the figures was done immediately prior start of imaging.

3.2.12 Image analysis

Confocal imaging was quantified using Fiji[88]. Briefly, integrated density was quantified in randomly chosen fields of view across the sample. Then, it was normalised on the cell number and plotted as mean cell fluorescence. Mander's Correlation Coefficients were calculated using the Fiji plugin Coloc 2. To examine the changes in fluorescent probes at the subcellular level, Lamp1-mNeonGreen or Voa3-mScarlet were expressed to label lysosomes. Both proteins showed high levels of colocalization regardless of mTORC1 activity. To determine the region of interest (ROI) corresponding to Lamp1-mNeonGreen or Voa3-mScarlet-positive lysosomes,

images were processed using Fiji. The background signal was removed, and a Gaussian Blur function was applied to accurately demarcate the lysosomal area, including the organelle lumen. The threshold and particle analyser functions of Fiji were utilised to identify ROIs. For DQ BSA, Cathepsin Magic Red, and V1B2-mNeonGreen, the background signal was removed, and the integrated signal density was quantified in lysosomal ROIs defined by Lamp1-mNeonGreen or Voa3-mScarlet. To specifically quantify the organellar population of V1B2-mNeonGreen, background subtraction was used to reduce the diffuse cytosolic signal. To quantify lysosomal DQ BSA fluorescence dequenching, the DQ BSA integrated density was normalised to the total area of Lamp1-mNeonGreen. In order to measure the movement of V1B2-mNeonGreen towards Voa3-mScarlet-positive lysosomes, the integrated density of V1B2-mNeonGreen was normalised to the area of Voa3-mScarlet for each individual particle. To determine the proportion of lysosomes with high proteolytic activity, as measured by fluorescence dequenching of DQ BSA or Cathepsin Magic Red in **Figure 19** the Fiji auto threshold function was employed in cells treated with torin 1, which exhibited elevated lysosomal catabolic activity. Subsequently, the average auto-threshold value was utilised for all conditions within the same experiment, and the DQ BSA or Cathepsin Magic Red signal area was expressed as a percentage of the total lysosomal area, defined by Lamp1-mNeonGreen, and plotted.

3.2.13 Sample preparation for proteomics

MEFs expressing empty vector and HA-V1B2 or Flag-Voa3 were used for the SILAC-based Co-IP proteomics. These cell lines were cultured for three passages in media containing light, medium and heavy isotopes (**Table 16**). Biological replicates were generated on 4 different days and isotope labelling was swapped among conditions to avoid technical bias. 1.2 million MEFs were plated 2 days before the experiment in 15 cm plates, so that they reached 80% confluency on the day of the experiment. On the day of the experiment, cells were incubated with fresh full media or starved (-aa) for 1 hour followed by amino acids restimulation (+aa) for 30 minutes, where indicated. After the treatments, MEFs were washed once with ice-cold PBS and lysed in ice-cold Co-IP buffer (40 mM HEPES pH 7.4, 150 mM NaCl2, 2 mM EDTA, 2,5 mgCl2, 1 % Triton X-100, 5 % glycerol, protease, and phosphatase inhibitors) for 15 minutes. Lysates were centrifuged at 18,000 g for 5 min at 4 °C, and protein concentration was determined by Pierce BCA Protein Assay (Thermo Fisher Scientific). Finally, 5 mg of protein per condition, with different isotopes labelling, were mixed and incubated with 15 µg primary antibody and 15 µg dynabeads protein G (Life Technologies) for 2 hours at 4° C. Then, the bead-antibody-protein complex was washed once with ice-cold Co-IP lysis buffer. Proteins

were eluted in 2x Laemmli buffer by incubation for 15 min at 65 °C while shaking. Finally, the samples were handed over to the Proteomic Core Facility where proteins were precipitated with chloroform-methanol and further processed for Mass Spec analysis.

3.2.14 LC-MS/MS analysis

Proteins were run for 0.5 cm into an SDS-PAGE. After Coomassie staining, the total sample was cut out and used for subsequent digestion using trypsin as described previously50, adapted to a DigestPro MSi robotic system (INTAVIS Bioanalytical Instruments AG). Peptides were re-suspended in loading buffer containing 2.5 % Hexafluoro-2-propanol, 0.1 % TFA in water. Analysis was carried out on an Ultimate 3000 UPLC system (Thermo Fisher Scientific) directly connected to an Orbitrap Exploris 480 mass spectrometer. Analysis time and method were chosen to accompany expected sample complexity and set to 120 min. Prior to the analytical separation, peptides were online desalted on a trapping cartridge (Acclaim PepMap300 C18, 5 µm, 300 Å wide pore; Thermo Fisher Scientific) for 3 min using 30 µl/min flow of 0.05 % TFA in water. The analytical multistep gradient was carried out on a nanoEase MZ Peptide analytical column (300 Å, 1.7 µm, 75 µm x 200 mm, Waters) using solvent A (0.1 % formic acid in water) and solvent B (0.1 % formic acid in acetonitrile). The concentration of B was linearly ramped from 2 % to 38 % for a varying time with respect to the total analysis procedure (72 min or 102 min), followed by a quick ramp to 95 % B, after two minutes the concentration of B was lowered back to 2 % and a 10 min equilibration step appended. Eluting peptides were analyzed in the mass spectrometer using data-dependent acquisition (DDA) mode. A full scan (OE480: 60 000 resolution, 380-1400 m/z, 300 % AGC target, 45 ms maxIT; HF-X: 120 000 resolution, 375-1500 mz/, 3e6 AGC target, 54 ms maxIT) was followed by 2 s (OE480) or up to 18 (HF-X) MS/MS scans. Peptide features were isolated with a window of 1.4 m/z (OE480) or 1.6 m/z (HF-X) and fragmented using 26 % NCE (OE480) or 27 % (HF-X). Fragment spectra were recorded at 15k resolution (OE480: 100 % AGC target, 54 ms maxIT; HF-X: 1e5 AGC target and 22 ms maxIT). Unassigned and singly charged eluting features were excluded from fragmentation.

3.2.15 Proteomics data analysis

Data analysis was carried out by MaxQuant[89] using an organism-specific database extracted from Uniprot.org (UP000000589_10090.fasta download 2020-02-26; number of entries 55435) under default settings. Identification FDR cut-offs were 0.01 on peptide level and 0.01 on protein level. The match between runs option was enabled to transfer peptide identifications across RAW files based on accurate retention time and m/z. LFQ quantification was done using a label-free quantification approach based on the MaxLFQ algorithm[92]. A minimum of 2 quantified peptides per protein was required for protein quantification. SILAC quantification was done using triplex approach with medium channel Arg6, Lys4 and heavy channel Arg10, Lys9, and unlabelled amino acid as light channel. Re-quantify option was enabled to stabilize very large or small ratios[93].

3.2.16 Proteomics statistical analysis

The statistical analysis was performed with the R-package limma[90]. SILAC ratios were normalised via quantile normalization[94]. Adapted from the Perseus recommendations[95], protein groups with a valid SILAC ratio in 70% of the samples of at least one of the conditions were used for statistics. For missing SILAC ratios, random values drawn from a narrowed (0.3 standard deviation) intensity distribution around 0 of the individual sample were imputed. The p-values were adjusted with the Benjamini–Hochberg method for multiple testing[96].

3.2.17 Statistical analysis

For proteomics data, p-values were calculated using limma moderated t-statistic and, where indicated, adjusted with the Benjamini–Hochberg method for multiple testing. For other experiments, p-values were calculated using a one sample t-test with a hypothetical mean of 1 or a two-tailed unpaired t-test with Welch correction as indicated in the figure legends.

4 Results

4.1 mTORC1 does not regulate the uptake of extracellular macromolecules through fluid-phase endocytosis

Previous data from our laboratory showed that mTORC1 suppresses the catabolism of extracellular proteins in the lysosome[28]. How does mTORC1 inhibition promote lysosomal degradation of extracellular proteins?

To determine how mTORC1 regulates the catabolism of extracellular proteins, I used SV40 large T antigen-immortalised mouse embryonic fibroblasts (MEFs). MEFs are non-transformed cells that are widely used to study mTORC1 signalling pathways. Our laboratory showed that mTORC1 inhibition increases the lysosomal degradation of DQ BSA, a self-quenched albumin probe that fluoresces upon degradation[97]. However, this assay could not discriminate at which step of the endolysosomal system mTORC1 regulated protein catabolism. Conceivably, mTORC1 blocks lysosomal degradation of extracellular proteins by interfering at any step from protein uptake to lysosomal catabolism. Uptake of macromolecules through endocytosis can be studied by using fluorescent probes. Specifically, I used fluorescent Alexa Fluor 568 10 kDa dextran as a marker of general fluid-phase endocytosis, and Alexa Fluor 488 70 kDa dextran as a marker of macropinocytosis. In order to study the possible role of mTORC1 in the uptake of extracellular macromolecules, I inhibited the kinase by using the mTOR kinase inhibitor torin 1. Cells were pre-treated with DMSO or torin 1 for 1 hour. Next, I incubated MEFs with 10 kDa dextran or 70 kDa dextran for 45 minutes. After the incubation period, MEFs were fixed and uptake of extracellular dextran was measured by confocal microscopy. The amount of uptaken probes was then quantified by using the software Fiji[88]. The integrated density of the dextran signal was quantified in randomly chosen fields of view across the sample. Then, it was normalised on the cell number and plotted as mean cell fluorescence. I could not detect any changes in the uptake of either the 10 kDa dextran or the 70 kDa dextran probes (**Figure 4a-d**). This suggests that mTORC1 does not regulate the uptake of extracellular macromolecules through fluid-phase endocytosis or macropinocytosis.

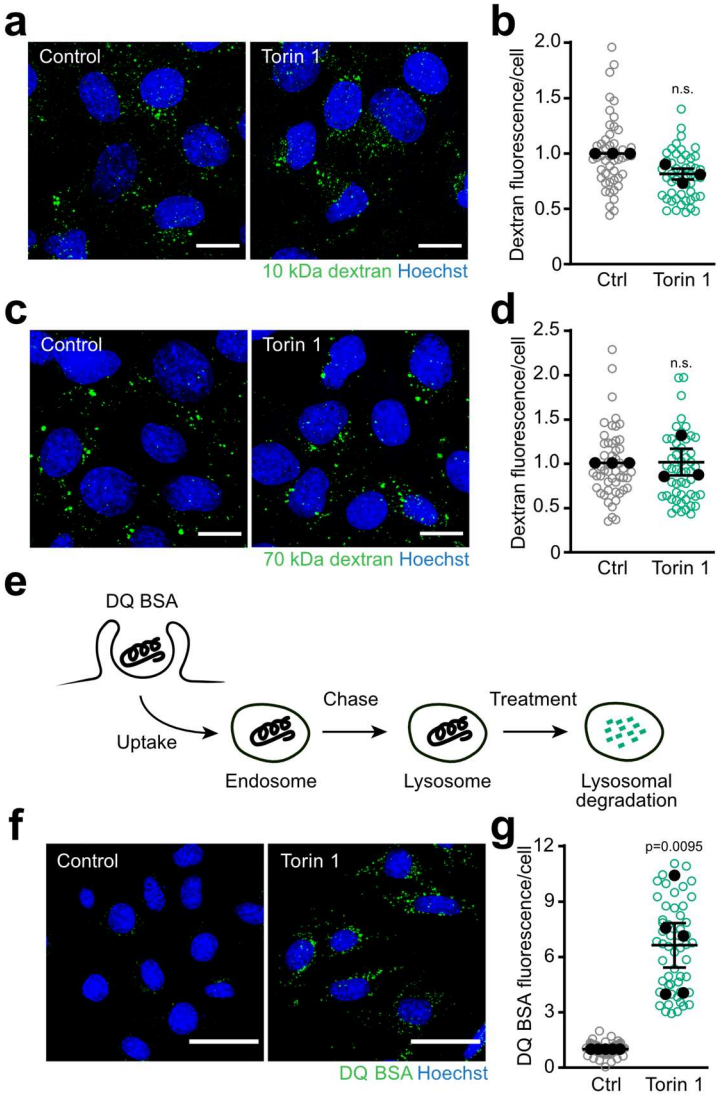

Figure 4. mTORC1 affects digestion of extracellular protein directly at the lysosome. a. Confocal microscopy images of MEFs incubated with Alexa Fluor 568 10 kDa dextran for 45 minutes and treated with DMSO (control) or torin 1 (400 nM) for 1 hour. Scale bars = 20 μm. **b.** Quantification of Alexa Fluor 568 10 kDa dextran fluorescent per cell in MEFs treated as in a. **c.** Confocal microscopy images of MEFs incubated with Alexa Fluor 488 70 kDa dextran for 45 minutes and treated with DMSO (control) or torin 1 (400 nM) for 1 hour. Scale bars = 20 μm. **d.** Quantification of Alexa Fluor 488 70 kDa dextran fluorescent per cell in MEFs treated as in c. **e.** Schematic for lysosomal loading with DQ BSA. Cells were preloaded with DQ BSA. During chase with fresh media the internalised DQ BSA chased out of endosomes. After 3 hours of chase the majority of the DQ BSA is in the lysosomes and treatments to measure specific lysosomal catabolism were started. **f.** Confocal microscopy images of MEFs pre-loaded with DQ BSA for 4 hours, chased for 3 hours and treated with DMSO (control) or torin 1 (400 nM) for 1 hour. Scale bars = 50 μm. **g**. Quantification of DQ BSA fluorescent per cell in MEFs treated as in f.

Data are plotted as normalised replicate mean ± s.e.m. (closed circles) for 3 biologically independent experiments for b) and d) or 5 biologically independent experiments for g) and fields of view (open circles, ≥ 10 per replicate). A two-tailed unpaired t-test with Welch correction was used to calculate p-values. n.s. not significant.

4.2 mTORC1 inhibition increases lysosomal protein degradation by increasing lysosomal protease activity

I then tested the role of mTORC1 directly on lysosomal catabolism of extracellular macromolecules by using an alternative assay with DQ BSA. Specifically, MEFs were incubated for 4 hours with DQ BSA, then washed and chased for 3 hours with fresh medium to remove the probe from the endosomal system and allow the probe to accumulate in lysosomes. Only after the chase period, torin 1 was added to the cells for 1 hour (**Figure 4e**). With this assay, it is possible to analyse the effect of mTORC1 inhibition specifically on lysosomes, excluding confounding contributions of upstream steps, like DQ BSA uptake or vesicular trafficking. After one hour of torin 1 treatment, MEFs were imaged live by confocal microscopy, and the DQ BSA signal per cell was quantified as previously described. A strong increase in DQ BSA degradation in the lysosomes was observed (**Figure 4f, g**). These data show that mTORC1 inhibition directly impacts lysosomal catabolism, independently of upstream events.

Protein degradation in the lysosomes is mediated by proteases. Thus, a change in protease activity or abundance may explain the increase in DQ BSA signal upon mTORC1 inhibition. To measure cathepsin activity upon mTORC1 inhibition, Magic Red cathepsin substrates (MR) were used. Magic Red (MR) is a cell-permeable probe that crosses the cell membrane and the membranes of cellular organelles. It is constituted of a cathepsin substrate that is specific for the different lysosomal cathepsins linked to cresyl violet. The probe becomes dequenched upon cleavage by cathepsins[98]. I used Magic Red substrates for the ubiquitous lysosomal proteases cathepsin B and cathepsin L. MEFs were pretreated with DMSO or torin 1 for 1 hour, then incubated with the MR substrates for either cathepsin for 10-12 minutes. Torin 1 treatment caused a significant increase in MR signal for both cathepsin B and cathepsin L (**Figure 5a-d**). To test if mTORC1 inhibition increases the trafficking of cathepsins to the lysosomes, which could explain the increase in Magic Red dequenching, I assessed the abundance of several major cathepsins by western blotting. After 1 hour of torin 1 treatment, the levels of the mature forms of cathepsin B, cathepsin D, cathepsin L and cathepsins X/L did not change (**Figure 5e**). These data suggest that short-term mTORC1 inhibition increases lysosomal cathepsin activity directly, but does not change their abundance in the lysosomes.

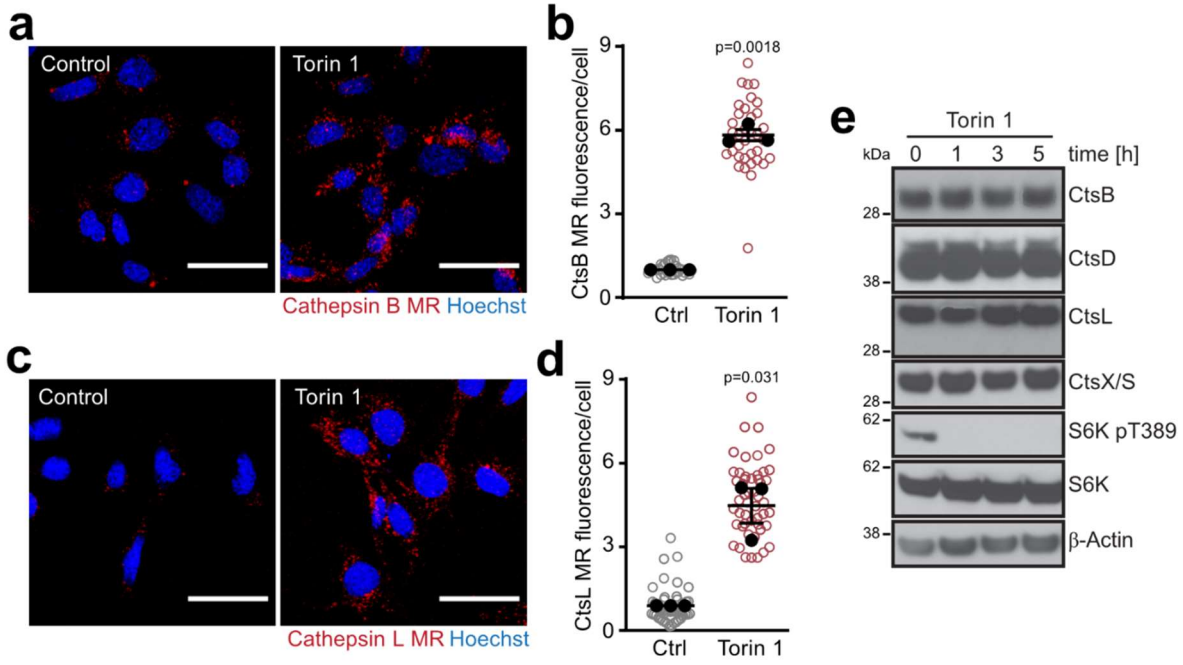

Figure 5. Cathepsin activity increases upon mTORC1 inhibition. a. Confocal microscopy images of MEFs incubated with cathepsin B MR for 10-12 minutes and treated with DMSO (control) or torin 1 (400 nM) for 1 hour. Scale bars = 50 µm. **b.** Quantification of cathepsin B MR fluorescent per cell in MEFs treated as in a. **c.** Confocal microscopy images of MEFs incubated with cathepsin L MR for 10-12 minutes and treated with DMSO (control) or torin 1 (400 nM) for 1 hour. Scale bars = 50 µm. **d.** Quantification of cathepsin L MR fluorescent per cell in MEFs treated as in c. **e.** Western blot of whole cell lysates of MEFs treated with DMSO (control) or torin 1 (250 nM) for the indicated amount of time.

Data are plotted as normalized replicate mean ± s.e.m. (closed circles) for 3 biologically independent experiments, and fields of view (open circles, ≥ 10 per replicate). A two-tailed unpaired t-test with Welch correction was used to calculate p-values.

To understand if specific cathepsins were essential for lysosomal protein degradation in response to torin 1 treatment, cathepsin B, D, or L were genetically ablated by using a doxycycline-inducible CRISPR/Cas9 system. Two different control sgRNAs and two different sgRNAs per gene were used to generate knockout cells. sgRNAs were ectopically transduced in MEFs expressing a doxycycline-inducible Cas9 cassette. Knockout generation was achieved by treating the cells with 400 ng/mL of doxycycline for 3 days. Western blotting showed a strong reduction of the target cathepsins, demonstrating efficient gene editing (**Figure 6a**). Upon knockout generation, cells were incubated with DQ BSA and treated with torin 1. DQ BSA degradation was monitored by confocal microscopy. No difference was detected in the DQ BSA signal per cell in cathepsin knockout compared to control cells. Conversely, a broad specificity mix of protease inhibitors almost completely abrogated DQ BSA dequenching (**Figure 6 b, c**).

Overall, these data suggest that short-term mTORC1 inhibition increases the global activity of lysosomal proteases but not their abundance, resulting in an up-regulation of extracellular protein catabolism in the lysosome within one hour.

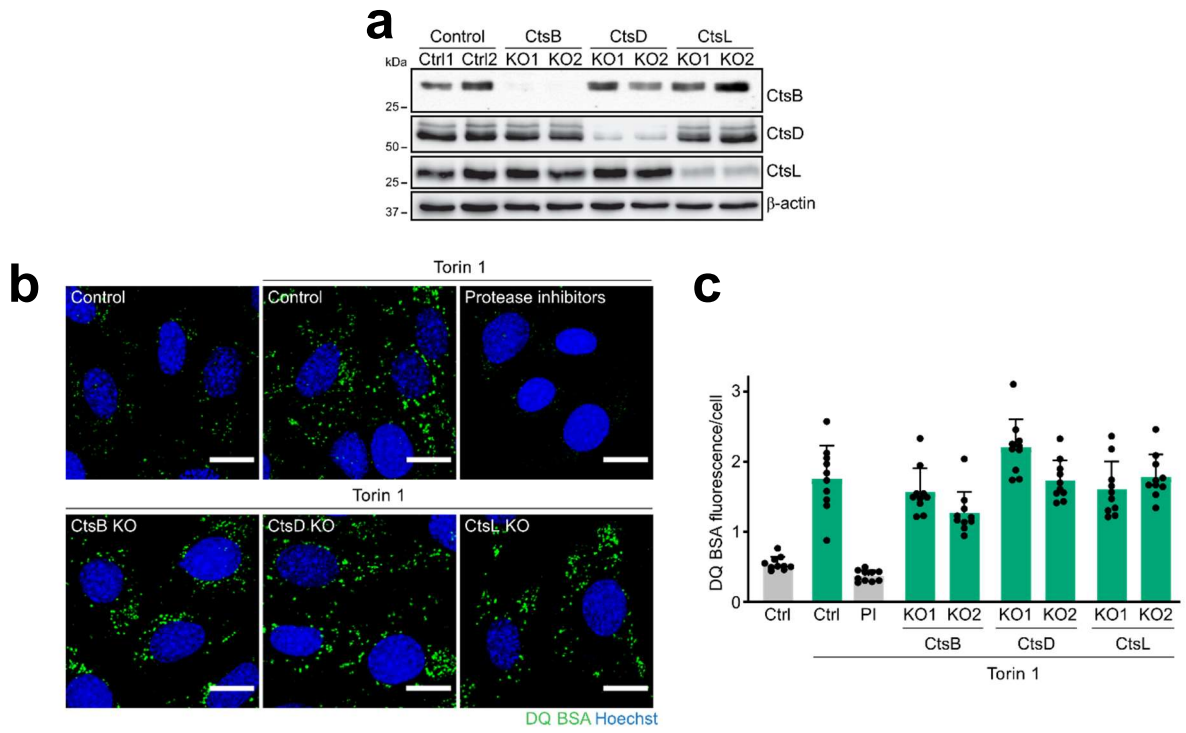

Figure 6. Overall protease activity is required for mTORC1-dependent increase in extracellular protein digestion. a. Western blot of MEFs expressing doxycycline-inducible Cas9 transduce with sgRNA targeting non-coding chromosome regions (Ctrl) or cathepsin B, cathepsin D, or cathepsin L doxycycline-inducible treated with doxycycline (400 ng/mL) for 3 days before the start of the experiment. **b.** Confocal microscopy images of control, cathepsin B, cathepsin D, or cathepsin L KO MEFs incubated with DQ BSA and treated with DMSO (control), torin 1 (400 nM) or Proteases inhibitor mix (PI: 20 µM pepstatin, leupeptin, E64, AEBSF) as indicated for 5 hours. Scale bars = 20 µm. **c.** Quantification of DQ BSA fluorescent per cell in MEFs treated as in b.

Mean ±SD of one biologically independent replicate out of 3 is plotted (≥ 10 fields of view).

4.3 mTORC1-mediated regulation of protein translation does not mediate the acute increase in lysosomal catabolism of extracellular protein

mTORC1 suppresses lysosomal biogenesis and catabolism by antagonising TFEB activation[55]. To rule out that the fast increase in DQ BSA dequenching is not mediated by TFEB activation, MEFs were co-treated with torin 1 and the translation inhibitor cycloheximide (CHX). Increasing concentrations of CHX did not prevent the increase in DQ BSA signal upon torin 1 treatment (**Figure 7a, b**). Thus, translation of new proteins is not involved in the short-term increase in DQ BSA degradation upon mTORC1 inactivation.

mTORC1 suppresses autophagy and thus delivery of intracellular substrates to the lysosomes. Therefore, I tested if autophagy affects the mTORC1-mediated increase in lysosomal catabolism. MEFs expressing a doxycycline-inducible Cas9 were transduced with a sgRNA against ATG5, an essential component of the autophagic pathway. Knockout cells were generated by treating MEFs for 3 days with doxycycline. Untreated cells were used as control. ATG5 levels were undetectable by western blotting (**Figure 7c**). ATG5 lipidates LC3 allowing LC3 recruitment to the autophagosome, an essential step for autophagy progression. As a consequence, lipidation of LC3 is abrogated in ATG5 knockout MEFs. P62 mediates the recruitment of autophagic cargo to the autophagosome and gets degraded in the process. Thus, P62 accumulation in ATG5 knockout MEFs also correlates with autophagy suppression. ATG5 knockout MEFs were incubated with DQ BSA. Cells did not display defects in DQ BSA catabolism in the DMSO-treated condition. Moreover, ATG5 ablation did not prevent the increase in DQ BSA dequenching mediated by torin 1 **(Figure 7d, e)**. Collectively, these data demonstrate that mTORC1 inhibition increases extracellular protein degradation independently of changes in translation or autophagy.

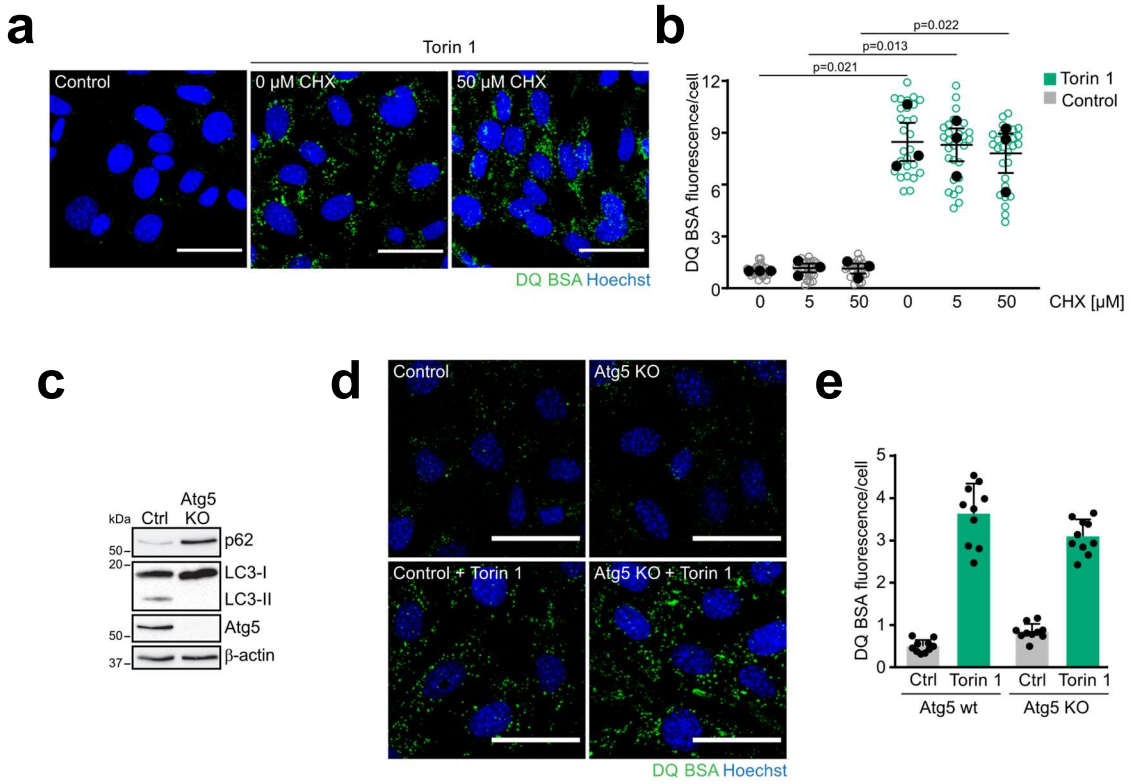

Figure 7. Translation of new proteins and autophagy are dispensable for mTORC1-dependent increase in extracellular protein digestion. a. Confocal microscopy images of MEFs incubated with DQ BSA treated with DMSO (control) or torin 1 (250 nM) and cycloheximide (CHX) at indicated concentration for 5 hours. Scale bars = 50 μm. **b.** Quantification of DQ BSA fluorescent per cell in MEFs treated as in a. **c.** Western blot of MEFs expressing doxycycline-inducible Cas9 transduce with sgRNA targeting Atg5 untreated (ctrl) or treated (KO) with doxycycline (400 ng/mL) for 3 days before the start of the experiment. **d.** Confocal microscopy images of control or Atg5 KO MEFs incubated with DQ BSA and treated with DMSO (control) or torin 1 (400 nM) for 5 hours. Scale bars = 20 μm. **e.** Quantification of DQ BSA fluorescence per cell in MEFs treated as in d.

In b data are plotted as normalised replicate mean ± s.e.m. (closed circles) for 3 biologically independent experiments, and fields of view (open circles, ≥ 10 per replicate). A two-tailed unpaired t-test with Welch correction was used to calculate p-values. In e mean ± SD of one biologically independent replicate out of 3 is plotted (≥10 fields of view).

4.4 mTORC1 inactivation increases lysosomal protease activity by increasing lysosomal acidity.

Lysosomal protease activity is pH dependent[99,100]. To verify if the mTORC1-mediated increase in lysosomal cathepsin activity was mediated by increased acidification, lysosomal pH was measured. First, to analyse lysosomal pH, the fluorophores cresyl violet and lysotracker red were used in a confocal live imaging assay[101]. These probes are acidotropic, thus they

accumulate in acidic compartments. After one hour of torin 1 treatment, cresyl violet and lysotracker red showed a strong lysosomal accumulation (**Figure 8a-d**). This suggests that mTORC1 inhibition decreases lysosomal pH. When MEFs were treated with rapamycin, a partial mTORC1 inhibitor, cresyl violet and DQ BSA did not increase (**Figure 8e-h**).

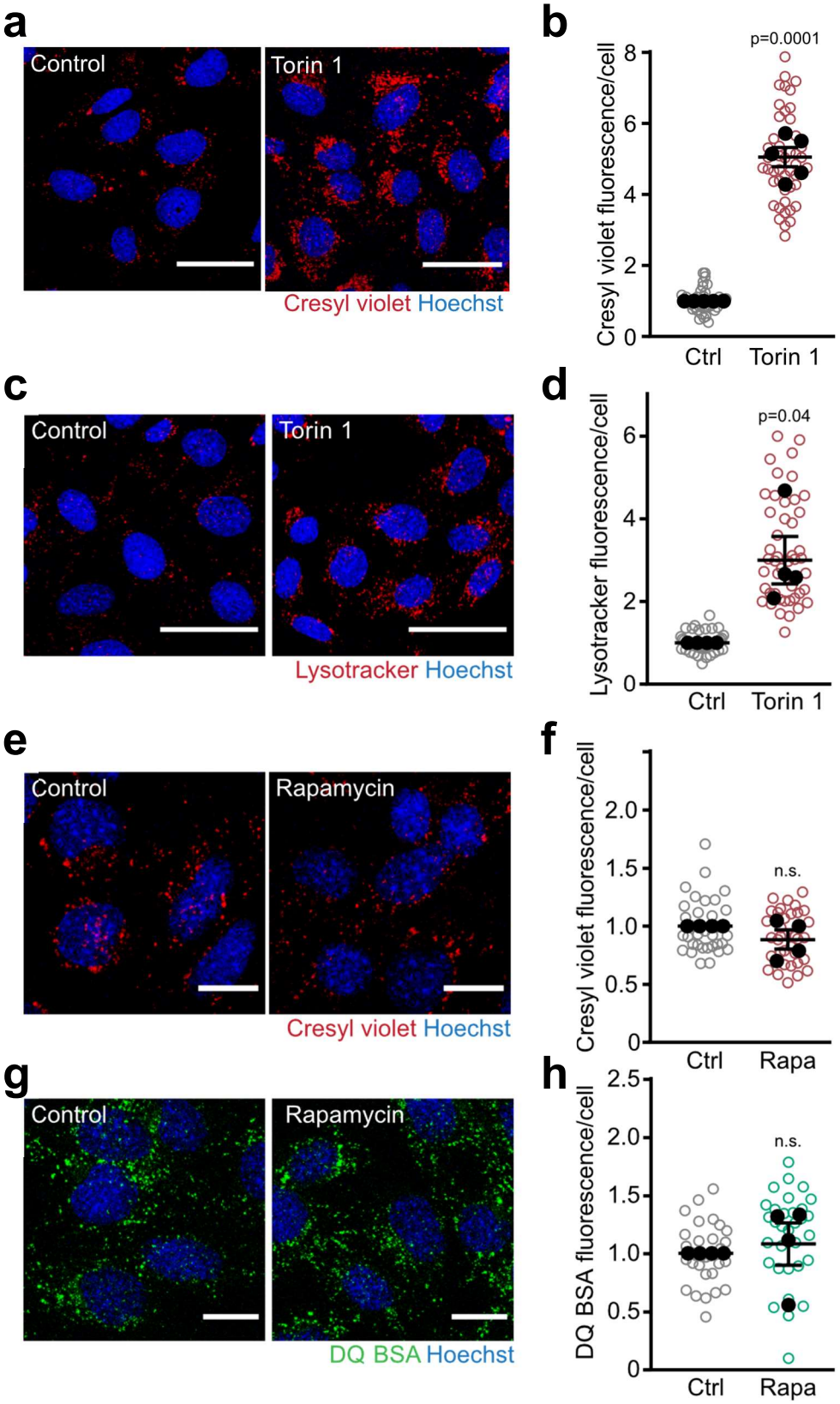

Figure 8. mTORC1 inactivation increases lysosomal acidification. a. Confocal microscopy images of MEFs incubated with cresyl violet (1 μM) and treated with DMSO (control) or torin 1 (400 nM) for 1 hour. Scale bars = 50 μm. **b.** Quantification of cresyl violet fluorescent per cell in MEFs treated as in a. **c.** Confocal microscopy images of MEFs incubated with lysotracker red (10 nM) and treated with DMSO (control) or torin 1 (400 nM) for 1 hour. Scale bars = 50 μm. **d.** Quantification of lysotracker red fluorescent per cell in MEFs treated as in c. **e**. Confocal microscopy images of MEFs incubated with cresyl violet and treated with DMSO (control) or rapamycin (200 nM) for 1 hour. Scale bars = 20 μm. **f.** Quantification of cresyl violet fluorescent per cell in MEFs treated as in e. **g.** Confocal microscopy images of MEFs incubated with DQ BSA and treated with DMSO (control) or rapamycin (200 nM) for 5 hours. Scale bars = 20 μm. **h.** Quantification of DQ BSA fluorescent per cell in MEFs treated as in g.

Data are plotted as normalised replicate mean ± s.e.m. (closed circles) for 5 biologically independent experiments for b or 4 biologically independent experiments for d, f and h, and fields of view (open circles, ≥10 per replicate). A two-tailed unpaired t-test with Welch correction was used to calculate p-values. n.s. not significant.

To quantify lysosomal pH directly during mTORC1 inhibition, Roy Chowdhury in our laboratory used dextran-conjugated lysosensor yellow/blue DND-160 (lysosensor). Lysosensor is a ratiometric dye that has dual emission spectra which are pH dependent used for absolute quantification of lysosomal pH. MEFs incubated with DQ BSA or lysosensor were used and treated with several concentrations of torin 1, ranging from 50 to 500 nM. Increasing torin 1 concentration promoted DQ BSA degradation, and simultaneous decrease in lysosomal pH (**Figure 9a**). To directly test whether lysosomal lumen acidification is required for increased DQ BSA degradation, Roy Chowdhury maintained lysosomal pH stable upon mTORC1 inhibition using the V-ATPase inhibitor bafilomycin A1. 5 nM of bafilomycin A1 was able to abrogate the torin 1-mediated drop in lysosomal pH (**Figure 9b**). Consistently, MEFs treated with torin 1 and 5 nM of bafilomycin A1 completely suppress the torin 1-mediated increase in DQ BSA degradation (**Figure 9c**). Finally, to understand if mTORC1 regulation of lysosomal pH is conserved in humans and different cell types, I treated human pancreatic and lung carcinoma cell lines (MIA PaCa-2, A549) and immortalised human fibroblasts (MRC-5) with torin 1. All three cell lines responded to torin 1, showing an increase of DQ BSA and an associated accumulation of cresyl violet in the lysosomes (**Figure 9d-f**). These results show that mTORC1 can regulate lysosomal pH in various human and mouse cell types. Moreover, the acidification of the lysosomal lumen is also required for the increased DQ BSA degradation upon mTORC1 inhibition.

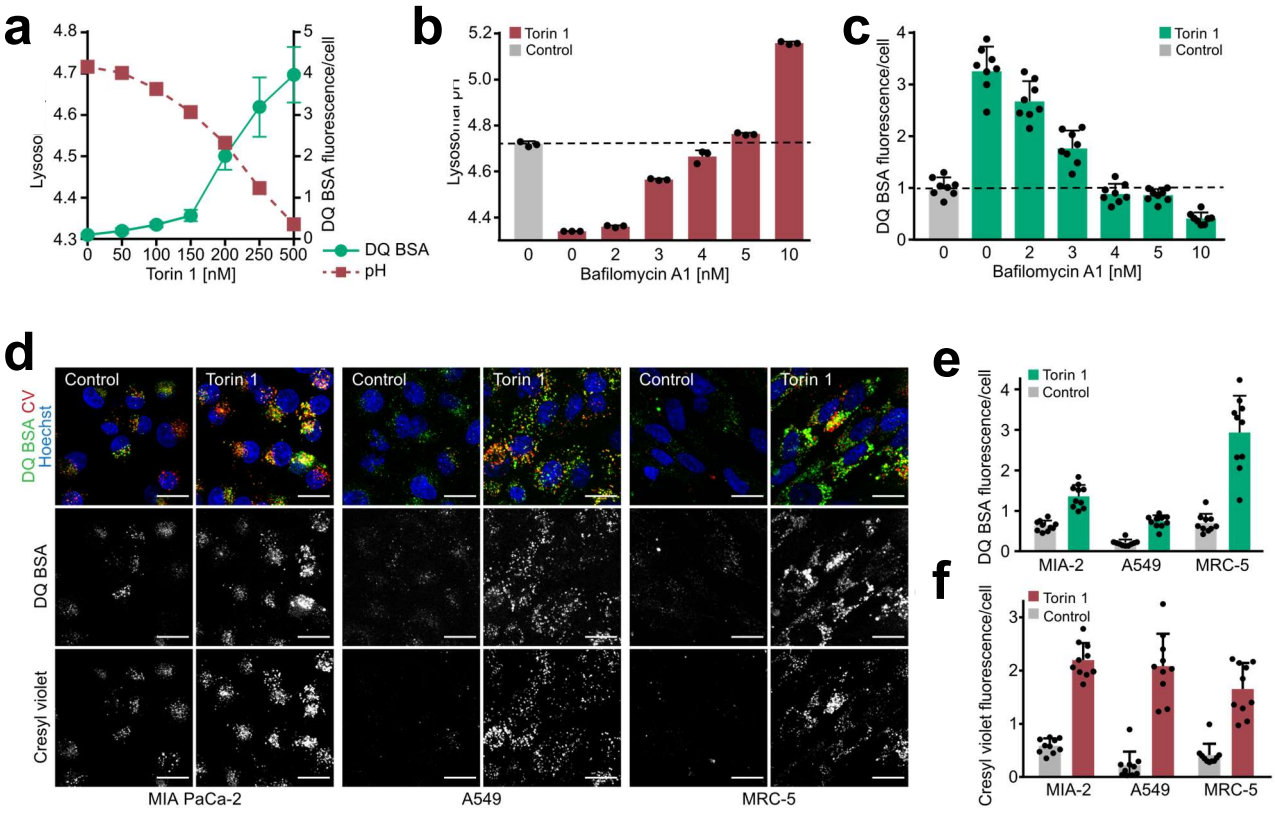

Figure 9. mTORC1-mediated drop in lysosomal pH increases the extracellular protein degradation in the lysosome in human cell lines. a. Quantification of lysosomal pH by lysosensor and DQ BSA in MEFs pre-loaded with lysosensor or DQ BSA for 4 hours, chased for 4 hours and treated with increasing concentration of torin 1 as indicated. Measurements were conducted separately under identical conditions. **b.** Quantification of lysosomal pH by lysosensor in MEFs pre-loaded with lysosensor for 4 hours, chased for 4 hours, treated with DMSO (control) or torin 1 (400 nM) and increasing concentration of bafilomycin A1 as indicated. The dashed line indicates mean lysosomal pH of control cells. **c.** Quantification of lysosomal pre-loaded DQ BSA in MEFs pre-loaded with DQ BSA for 4 hours, chased for 4 hours, treated with DMSO (control) or torin 1 (400 nM) and increasing concentration of bafilomycin A1 as indicated. The dashed line indicates mean DQ BSA fluorescence of control cells. **d.** Confocal microscopy images of human cancer cell lines (MIA PaCa-2, A549) or human fibroblasts (MRC-5) pre-loaded with DQ BSA, incubated with cresyl violet and treated with DMSO (control) or torin 1 (400 nM) for 3 hours. Scale bars = 20 μm. **e.** Quantification of DQ BSA fluorescent per cell in MIA PaCa-2, A549, and MRC-5 treated as in d. **f.** Quantification of cresyl violet fluorescent per cell in MIA PaCa-2, A549, and MRC-5 treated as in d.

Mean ±SD of one biologically independent replicate out of 3 is plotted (≥ 10 fields of view).

4.5 mTORC1 inactivation leads to increased V-ATPase assembly at the lysosome.

4.5.1 The V-ATPase V_1 domain is enriched at cellular membranes upon mTORC1 inhibition.

The lysosomal membrane contains V-ATPase, a proton pump that acidifies the lumen of lysosomes by transporting protons across the membrane. To test if V-ATPases play a role downstream of mTORC1 in regulating lysosomal pH, I quantified mTORC1-dependent changes in V-ATPases assembly on membranes. For this purpose, I tested the recruitment of the soluble V_1 domain to membranes by organelle fractionation. MEFs were incubated overnight with 10 kDa dextran followed by 4 hours of chase in fresh medium so that the probe accumulated in the lysosomes. Then, through high-speed centrifugation (18.000 g) dextran-weighted lysosomes were pelleted in the membrane fraction. mTORC1 was inhibited either with torin 1 or through amino acid starvation for 1 hour (-aa). In addition, cells were re-stimulated with amino acids for 30 minutes after 1 hour of starvation (+aa), to acutely re-activate mTORC1. The samples were then analysed by western blotting and levels of several V-ATPase subunits were quantified. Upon torin 1 treatment, the V_1 domain subunits V1A and V1E1 were increased in the membrane fraction. Conversely, during amino acid restimulation, the subunits V1A and V1E1 were decreased in the membrane fraction (**Figure 10a, b**). The V_o domain subunit Vod1 did not display any consistent changes upon mTORC1 inhibition. These data suggest that upon mTORC1 inhibition, the peripheral V_1 domain of the V-ATPase is recruited from the cytosol to membranes where the V_o domain constitutively resides. Amino acid readdition rapidly decreased the level of membrane-associated V_1 domains, indicating that V_1 membrane recruitment is reversible and depends on the activation status of mTORC1.

4.5.2 mTORC1 regulates V_1 domain movement between the lysosome and cytoplasm.

To study the dynamics of V-ATPase assembly at the lysosome in live cell, Nora Siefert established a cell line in our laboratory in which the V_1 and V_o domains were tagged with two different fluorescent proteins. For the V_1 domain, V1B2 was tagged with mNeonGreen. To better analyse V-ATPase assembly, the V_o domain was tagged by expressing Voa3-mScarlet (**Figure 10c**). Using those reagents, I looked at the movement of the V_1 and V_o domains simultaneously by confocal microscopy. The Voa subunit is responsible for the localization of the V-ATPase complex to different organelles. Thus, I first evaluated the localization of the Voa3 subunit to confirm its lysosomal localization. Voa3-mScarlet was expressed in MEFs in

which Lamp1, a common lysosomal marker, was endogenously tagged with mNeonGreen. Voa3-mScarlet colocalised with Lamp1-mNeonGreen, with a Manders' correlation coefficient (MCC) higher than 0.95, regardless of the activity status of mTORC1 (**Figure 10d, e**). Thus, Voa3-mScarlet can be used to follow lysosomal V-ATPase. Then, I analysed directly V-ATPase assembly at the lysosome by confocal live imaging.

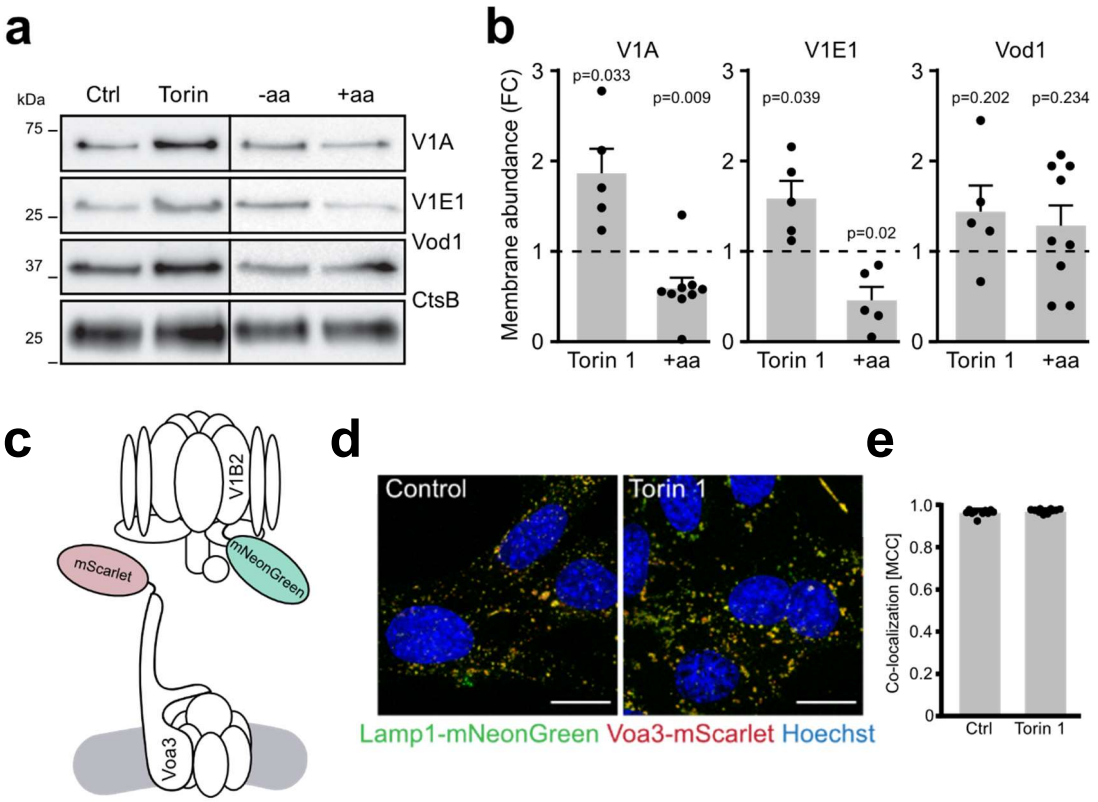

Figure 10. V_1 domain is recruited on membrane upon mTORC1 inactivation. a. Western blot of membrane fractions enriched in dextran-loaded lysosomes from MEFs treated with DMSO (control) or torin 1 (400 nM) for 1 hour, or starved from all amino acids for 1 hour (-aa) followed by 30 minutes of amino acids restimulation (+aa). **b.** Quantification of V-ATPase subunit levels in membrane fractions as detected in a. Normalised ratio torin 1/DMSO and +aa/-aa are plotted as means ± s.e.m. for 5 biologically independent experiments for V1A, V1E1, Vod1 + torin 1 and V1E1 +aa or 9 biologically independent experiments for V1A and Vod1 +aa. Dashed lines indicate protein abundance in the DMSO/−aa groups. **c.** Schematic of V_1 and V_o domain tagging strategy for live imaging. V1B2 was tagged with mNeonGreen to label the V_1 domain, and Voa3 was tagged with mScarlet to label the V_o domain. **d.** Confocal microscopy images of MEFs expressing LAMP1 endogenously tagged with mNeonGreen and ectopically expressing Voa3-mScarlet treated with DMSO (control) or torin 1 (400 nM) for 1 hour. Scale bars = 20 µm. **e.** Manders correlation coefficient (MCC) for co-localization of Voa3-mScarlet with Lamp1-mNeonGreen. Mean ±SD of one biologically independent replicate is plotted (≥10 fields of view).

At basal conditions where mTORC1 is active, V1B2-mNeonGreen was mainly diffuse in the cytoplasm without clear lysosomal localisation. After 1 hour of torin 1 addition, a substantial fraction of V1B2-mNeonGreen localised to vesicles that appeared to be lysosomes (**Figure 11a**). In contrast, after 30 minutes of torin 1 treatment, a substantial fraction of V_1 domain was localised to Voa3-mScarlet-positive lysosomes (**Figure 11b**). The accumulation of the V1B2-mNeonGreen strongly increased over time on the Voa3-mScarlet-positive vesicles (**Figure 11c**). To analyse the recruitment of V_1 domain to individual lysosomes, I quantified V1B2-mNeonGreen intensity per lysosome, defined as Voa3-mScarlet-positive vesicles. V1B2-mNeonGreen recruitment was globally increased on all lysosomes upon 1 hour of torin 1 treatment (**Figure 11d**). Analysis of V_1 domain subunit levels in membrane fractions suggested that lysosomal V_1 recruitment is a reversible mechanism controlled by mTORC1. Thus, I analysed the reversible disassembly of the V-ATPase upon mTORC1 activation by live imaging. MEFs co-expressing V1B2-mNeonGreen and Voa3-mScarlet were amino acid starved for 1 hour, then cells were restimulated with amino acids and V_1 movement was followed over time by confocal microscopy. After 15 minutes of amino acid readdition, a substantial fraction of V1B2-mNeonGreen was released from lysosomes (**Figure 11e**). Overall, mTORC1 inhibition induces reversible recruitment of the V_1 domain to lysosomes. The interaction between V_1 and V_o generates active V-ATPases, thus inducing lysosomal lumen acidification. Therefore, I investigated the interrelation of V_1 lysosomal movement and lysosomal acidification upon mTORC1 inhibition. I followed MEFs expressing V1B2-mNeonGreen incubated with cresyl violet upon torin 1 treatment over time. After 1 hour of torin 1 treatment V1B2-mNeonGreen moved to lysosomes, which became cresyl violet positive within a similar timespan (**Figure 11f**). Rapamycin treatment did not change the cytoplasmic localization of V1B2-NeonGreen, consistent with previous data (**Figure 12a**). To confirm V_1 domain localization at the lysosome upon mTORC1 inhibition, V_1 movement was analysed by tagging another subunit with a different fluorophore, V1A-eGFP. V1A-eGFP moved to vesicles positive for cresyl violet after 1 hour of torin 1 treatment (**Figure 12b**). Moreover, to test if V_1 movement upon mTORC1 inhibition is preserved in a different cell line, V1B2-mNeonGreen was expressed in a lung carcinoma cell line, A549. V1B2-mNeonGreen moved to cresyl violet positive vesicles upon mTORC1 inhibition in A549 cells (**Figure 12c**).

These data further corroborate that mTORC1 regulates V-ATPase assembly at the lysosome. When mTORC1 is inactive, the V_1 domain is localised to the lysosomal membrane. When mTORC1 gets activated, the V_1 domain does not localise at the lysosome and moves back to

the cytoplasm. Upon mTORC1 inhibition the V_1 recruitment at the lysosome leads to the formation of a functional proton pump decreasing the lysosomal pH.

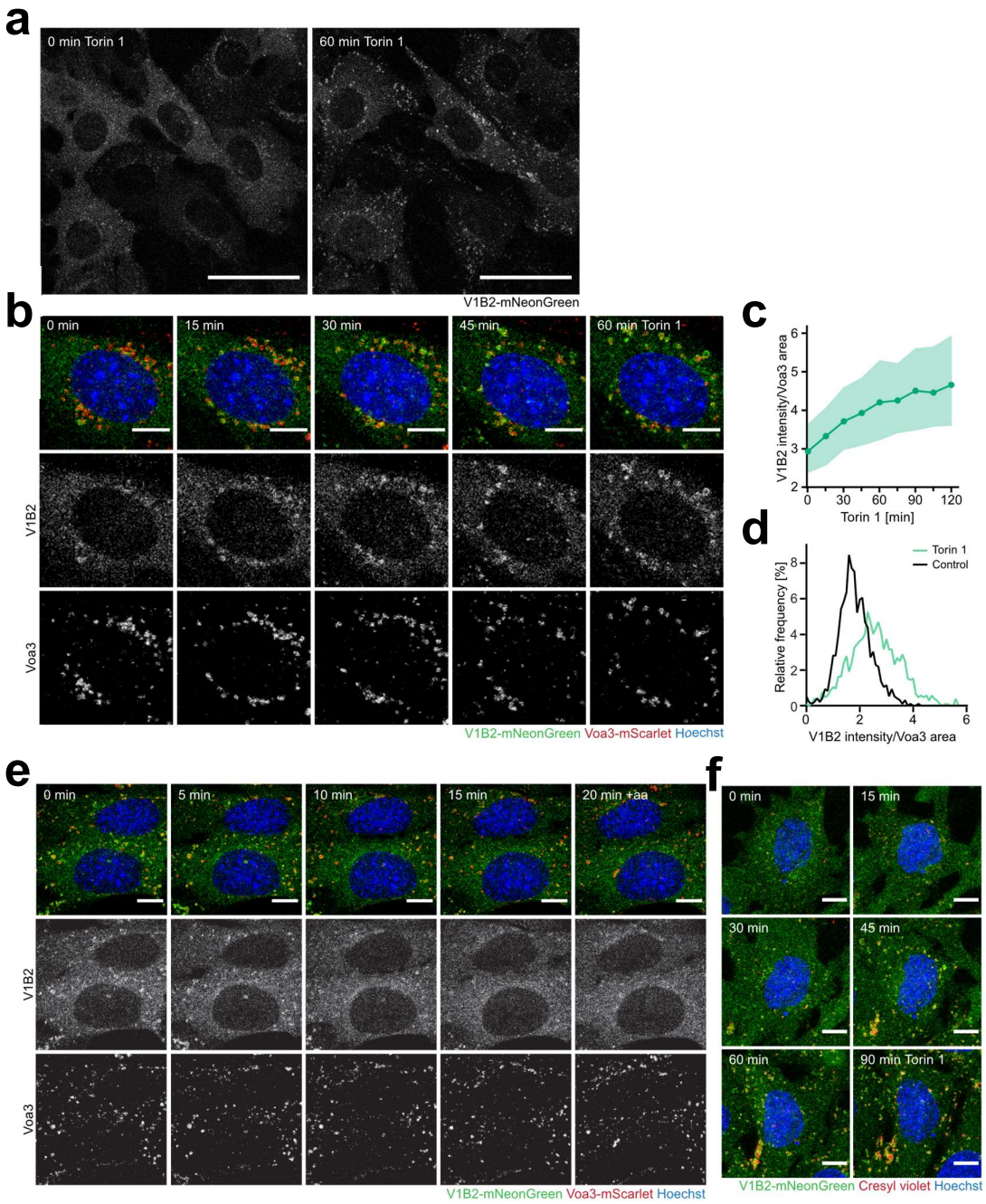

Figure 11. mTORC1 inhibition induces movement of the V_1 domain to the lysosomal V_o domain. a. Confocal microscopy images of MEFs expressing V1B2-NeonGreen before and after 1 hour of torin 1 (400 nM) treatment. Scale bars = 50 µm. One biologically independent replicate out of 5 is shown. **b.** Confocal microscopy images of MEFs co-expressing V1B2-mNeonGreen and Voa3-mScarlet followed over time after torin 1 (400 nM) addiction. Scale bars = 10 µm. One biologically independent replicate out of 5 is shown. **c.** Quantification of V1B2-NeonGreen intensity on the Voa3-mScarlet area over time as in b. **d.** Relative distribution of lysosomes V1B2-NeonGreen-positive before or after 1 hour of torin 1 (400 nM) treatment as in b. Lysosomes are defined as Voa3-mScarlet-positive vesicles. **e.** Confocal microscopy images of MEFs co-expressing V1B2-mNeonGreen and Voa3-mScarlet

amino acid starved for 1 hour followed over time upon amino acid re-addiction. Scale bars = 10 µm. One biologically independent replicate out of 3 is shown. **f.** Confocal microscopy images of MEFs expressing V1B2-mNeonGreen incubated with cresyl violet (1 µM) and followed over time after torin 1 (400 nM) addition. One biologically independent replicate out of 3 is shown.

4.5.3 DXML1/2 are required for V-ATPase assembly upon mTORC1 inactivation.

Several proteins have been implied in V-ATPase assembly in yeast and mammals, such as RILP and DXML1/2 complex. I decided to use the newly developed V-ATPase assembly live imaging assay to further assess the relevance of RILP and DXML1/2 in V-ATPase regulation upon mTORC1 inhibition. RILP and DXML1/2 were shown to be important for lysosomal acidification but a direct connection to V-ATPase assembly was never proven in mammals.

The Rab7 effector, RILP, has been reported to promote endosomal recruitment and stability of the V-ATPase V1G1 subunit[68]. Genetic ablation of RILP did not decrease V-ATPase assembly and cresyl violet intensity in response to torin 1 treatment (**Figure 12d**). DMXL1/2, appear to be functionally related to the yeast V-ATPase assembly factor, the RAVE complex[63]. In contrast to RILP, the double knockout of DMXL1/2 strongly decreased V_1 lysosomal recruitment both at basal conditions and in torin 1-treated cells (**Figure 12d**). In addition, the double knockout of DMXL1/2 suppressed the mTORC1-dependent increase in cresyl violet signal. In conclusion, this result indicates that RILP is dispensable for mTORC1-regulated V-ATPase assembly whereas DMXL1/2 has a crucial role in V-ATPase assembly both in basal conditions and upon mTORC1 inactivation.

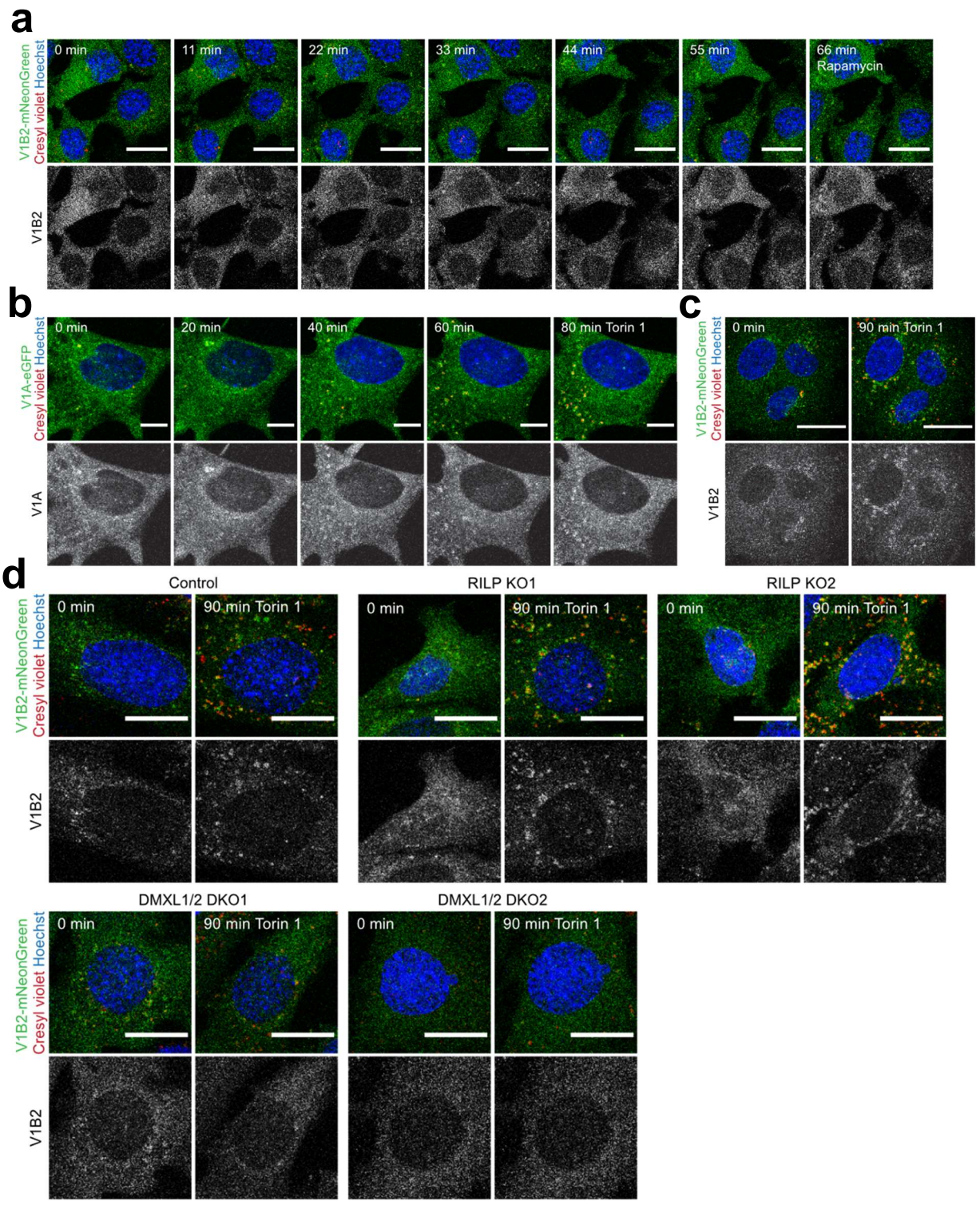
a
V1B2-mNeonGreen
Cresyl violet Hoechst
0 min
11 min
22 min
33 min
44 min
55 min
66 min
Rapamycin
V1B2
b
V1A-eGFP
Cresyl violet Hoechst
0 min
20 min
40 min
60 min
80 min Torin 1
V1A
c
V1B2-mNeonGreen
Cresyl violet Hoechst
0 min
90 min Torin 1
V1B2
d
Control
RILP KO1
RILP KO2
V1B2-mNeonGreen
Cresyl violet Hoechst
0 min
90 min Torin 1
V1B2
DMXL1/2 DKO1
DMXL1/2 DKO2

Figure 12. Rapamycin does not increase V-ATPase assembly while DMXL1/2 are essential for V-ATPase assembly. a. Confocal microscopy images of MEFs expressing V1B2-NeonGreen, incubated with cresyl violet and followed over time after torin 1 (400 nM) addiction. Scale bars = 20 µm. **b.** Confocal microscopy images of MEFs expressing V1A-eGFP incubated with cresyl violet and followed over time after torin 1 (400 nM) addiction. Scale bars = 10 µm. **c.** Confocal microscopy images of A549 lung cancer cell line expressing V1B2-mNeonGreen incubated with cresyl violet before and after 90 minutes of torin 1 (400 nM) treatment. Scale bars = 20 µm. **d.** Confocal microscopy images of MEFs expressing doxycycline-inducible Cas9 transduce with sgRNA targeting non-coding chromosome regions (Ctrl) or RILP (KO) or DXML1/2 double-knockout (DKO) expressing V1B2-mNeonGreen incubated with cresyl violet before and after 90 minutes of torin 1 (400 nM) treatment. Scale bars = 20 µm. One biologically independent replicate out of 3 is shown.

One biologically independent replicate out of 3 is shown.

4.6 The chaperonin TRiC associates with the V_1 domain in the cytoplasm in an mTORC1-dependent manner.

4.6.1 TRiC is co-immunoprecipitated by the V_1 domain but not by the V_o domain.

To identify candidate proteins involved in mTORC1-regulated V-ATPase assembly, I generated interactomes of the V_1 and V_o domains using co-immunoprecipitation (Co-IP) coupled with proteomics. The proteomic measurements were performed by Dominic Helm, and the data analysis was performed by Martin Schneider in the DKFZ proteomic core facility. Nora Siefert generated lentiviral constructs expressing V1B2 and Voa3 tagged with HA and Flag, respectively. She generated the MEFs cell lines expressing the constructs, which were used by me to pull down the two V-ATPase domains separately. MEFs cell lines expressing an empty vector or Flag-Voa3 or HA-V1B2 were cultured for three passages in media containing amino acid isotopes. Arginine (13C6) and lysine (D4) were used as medium isotopes, arginine (13C6, 15N4) and lysine (D9) were used as heavy isotopes. Biological replicates were generated on 4 consecutive days, and isotope labelling was swapped among conditions to avoid any technical bias. After immunoprecipitation of the affinity-tagged V-ATPase subunit, samples were analysed by liquid chromatography–mass spectrometry coupled with SILAC to identify interacting proteins, MEFs expressing empty vector were used as control. Flag-Voa3 coimmunoprecipitated almost all other V-ATPases subunits and lysosomal known V-ATPase interactors, like ragulator (Lamtor) and Tmem55b (**Figure 13a**)[48,102]. Moreover, Flag-Voa3 coimmunoprecipitated Atp6ap1, Tmem199, and Ccdc115, which are important specifically for V_o domain assembly in the endoplasmic reticulum[103,104]. HA-V1B2 coimmunoprecipitated most of the V-ATPase subunits as well as ragulator and Tmem55b, which interact with the V-ATPase at the lysosome (**Figure 13b**). HA-V1B2 did not coimmunoprecipitate Atp6ap1, Ccdc115, and

Tmem199, consistent with their role in the endoplasmic reticulum. Finally, I detected interactions between both Flag-Voa3 and HA-V1B2 with flotillin-1 (Flot1) and flotillin-2 (Flot2), two membrane-scaffolding proteins, which were not previously described as V-ATPase interactors. Moreover, HA-V1B2 coimmunoprecipitated Cct1-8. Cct1-8 interaction is specific for the V_1 domain; since V_o did not coimmunoprecipitate Cct1-8 (**Figure 13c, d**). Cct1-8 are the subunits of the cytoplasmic chaperonin tailless complex polypeptide 1 ring complex (TRiC). TRiC is an essential chaperonin found in eukaryotes that promote protein folding. It is constituted of 8 different subunits (CCT1-8) which formed a unique ring-shaped structure[105]. This data suggests that the V_1 domain can either interact with TRiC in the cytoplasm or with the V_o domain at the lysosomal membrane.

4.6.2 The interaction of V_1 and TRiC is responsive to mTORC1 activity.

In order to understand if mTORC1 might regulate V_o or V_1 interactions with other proteins, MEFs were starved for 1 hour of amino acids (-aa) to inhibit mTORC1 or starved for 1 hour with subsequent readdition of amino acids for 30 minutes (+aa) to reactivate mTORC1. Then, V_o and V_1 domains were immunoprecipitated and analysed with mass spectrometry as previously described (section 4.6.1), and enriched and depleted proteins from the two conditions were compared. For Flag-Voa3, no major changes in the interaction with ER or lysosomal proteins could be detected upon amino acid starvation (**Figure 13e**). Consistent with increased V-ATPase assembly, amino acid starvation increased the interaction of Voa3 with the subunits of the V_1 domain. Upon amino acid starvation, as detected also for Flag-Voa3, HA-V1B2 was able to coimmunoprecipitate mainly V_o subunits and lysosomal proteins (**Figure 13f**). In contrast, upon mTORC1 reactivation, the V_1 domain decreased the interaction with lysosomal proteins and increased the interaction with TRiC subunits. To validate these results, MEFs expressing tagged TRiC subunits, Cct1-Flag or Cct2-Flag, were generated and used to reciprocally coimmunoprecipitate the TRiC-V_1 complex. The subunits HA-V1B2 and V1A of the V_1 domain were coimmunoprecipitated with Cct1/2-Flag and could be detected by western blot (**Figure 13g**). Moreover, upon amino acids restimulation an increased interaction between TRiC and the V_1 domain subunits, HA-V1B2 and V1A, was observed, validating the proteomic data.

Overall, these data demonstrate that mTORC1 inhibits V-ATPase assembly. The V_1 domain mainly interacts with cytosolic TRiC when mTORC1 is active. Upon mTORC1 inhibition, the V_1 domain moves to lysosomes, where it interacts with the V_o domain. Finally, the results suggest

that V_1-V_o and V_1-TRiC interactions are mutually exclusive since I observed reciprocal changes in the interaction of V_1 with V_o and TRiC depending on mTORC1 activity.

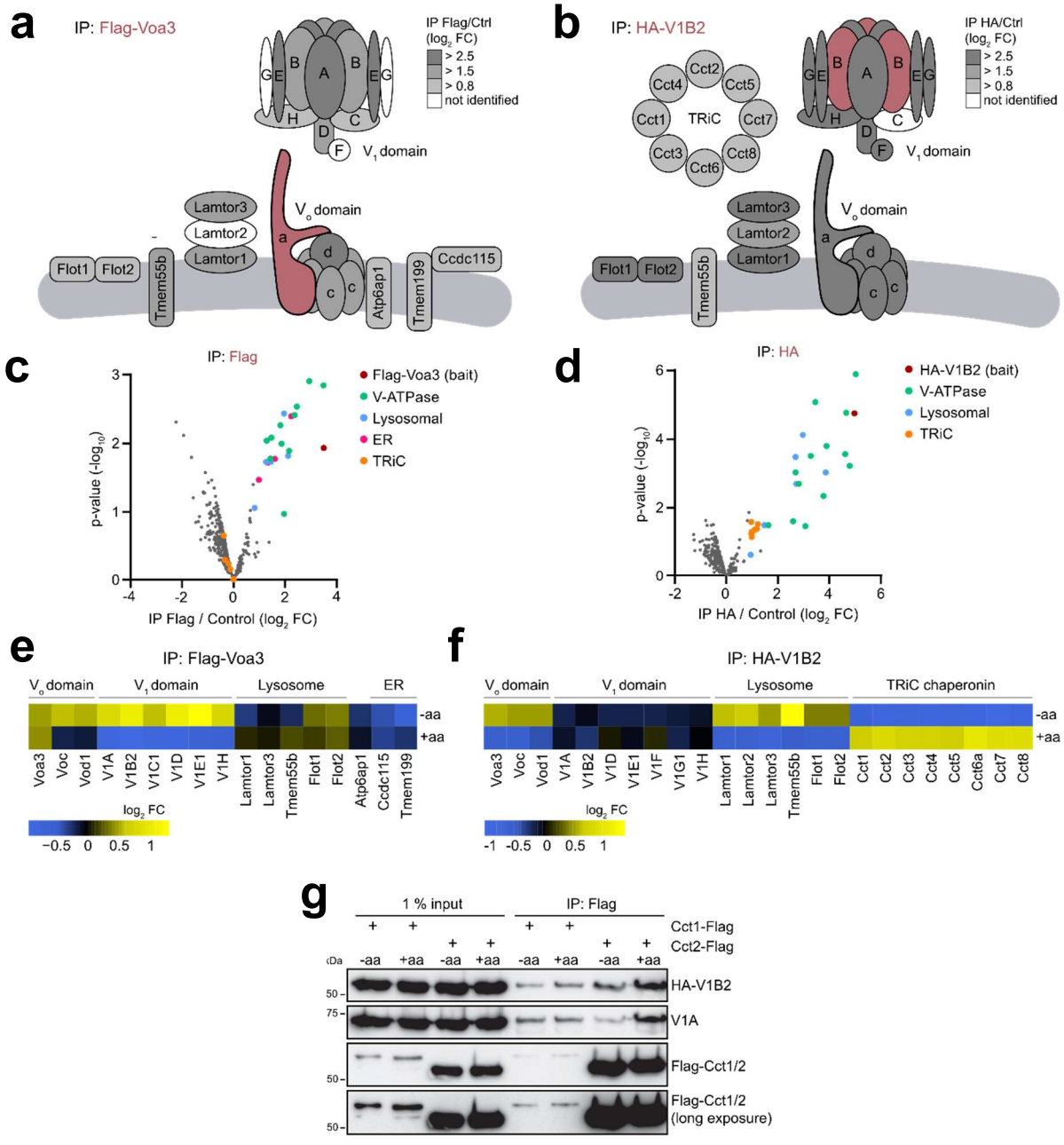

Figure 13. The V_1 domain associates with cytoplasmic TRiC when mTORC1 is active. a. Flag-Voa3 Co-IP coupled with liquid chromatography-mass spectrometry; the interactors are shown in the cartoon. Grayscale display the fold change (log_2FC) compared to control (Ctrl, no Tagged Voa3). 4 biologically independent experiments. **b.** HA-V1B2 Co-IP coupled with liquid chromatography-mass spectrometry, the interactors are showed in the

cartoon, grayscale displays the fold change (log_2FC) compared to control (Ctrl, no Tagged V1B2). 4 biologically independent experiments. **c.** Co-IP coupled with liquid chromatography-mass spectrometry from MEFs expressing Flag-Voa3. The fold change (log_2FC) compared to control (Ctrl, no Tagged Voa3) is plotted. 4 biologically independent experiments. **d.** Co-IP coupled with liquid chromatography-mass spectrometry from MEFs expressing HA-V1B2. The fold change (log_2FC) compared to control (Ctrl, no Tagged V1B2) is plotted. 4 biologically independent experiments. **e.** Heatmap showing the level of interaction between identified proteins and Flag-Voa3 in the SILAC-CoIP for 1 hour of amino acid starvation versus full media (-aa), or for 1 hour of amino acid starvation followed by 30 minutes of amino acid restimulation versus 1 hour of amino acid starvation (+aa). **f.** Heatmap showing the level of interaction between identified proteins and HA-V1B2 in the SILAC-CoIP for 1 hour of amino acid starvation versus full media (-aa), or for 1 hour of amino acid starvation followed by 30 minutes of amino acid restimulation versus 1 hour of amino acid starvation (+aa). **g.** Cct1-Flag and Cct2-Flag Co-IP analysed by western blotting. MEFs were starved from all amino acids for 1 hour (-aa) followed by 30 minutes of amino acid restimulation (+aa).

4.7 Loss of TRiC destabilises V_1 and impairs lysosomal acidification and protein catabolism.

4.7.1 Loss of TRiC decreases V_1 domain levels.

To understand the role of TRiC in V-ATPase assembly, constitutive and doxycycline-inducible knockouts for the TRiC subunits Cct1 and Cct2 were generated, using CRISPR/Cas9. MEFs expressing doxycycline-inducible Cas9 were transduced with an sgRNA for Cct1 or an sgRNA for Cct2. Knockout cells were generated by treating MEFs for 3 days with doxycycline. Untreated cells were used as control. Western blotting showed an almost complete loss of the levels of Cct1, while Cct2 levels showed a partial reduction. However, Cct2 reduction also decreased Cct1 levels (**Figure 14a**). The abundance of V-ATPase subunits was analysed in Cct1 and Cct2 knockouts by western blot. Loss of Cct1 or Cct2 led to a strong decrease in the levels of V1A and V1E1, whereas the levels of the Vod1 subunit were not affected (**Figure 14b**). To use an orthogonal approach, I used confocal imaging to analyse the level of V1B2-mNeonGreen upon genetic ablation of Cct1 and Cct2. Consistent with the western blotting results, a strong decrease in the levels of V1B2-mNeonGreen in MEFs depleted for Cct1 and Cct2 was observed (**Figure 14c, d**). To rule out the possibility that TRiC is essential for the proper folding of mNeonGreen, Cct1 was ablated in MEFs endogenously tagged with Lamp1-mNeonGreen using two different sgRNAs. However, no difference in mNeonGreen intensity was detected in Cct1 knockout cells compared to control cells (**Figure 14e, f**). The results suggest that V_1 subunits get destabilised if their cytoplasmic binding partner, TRiC, is absent.

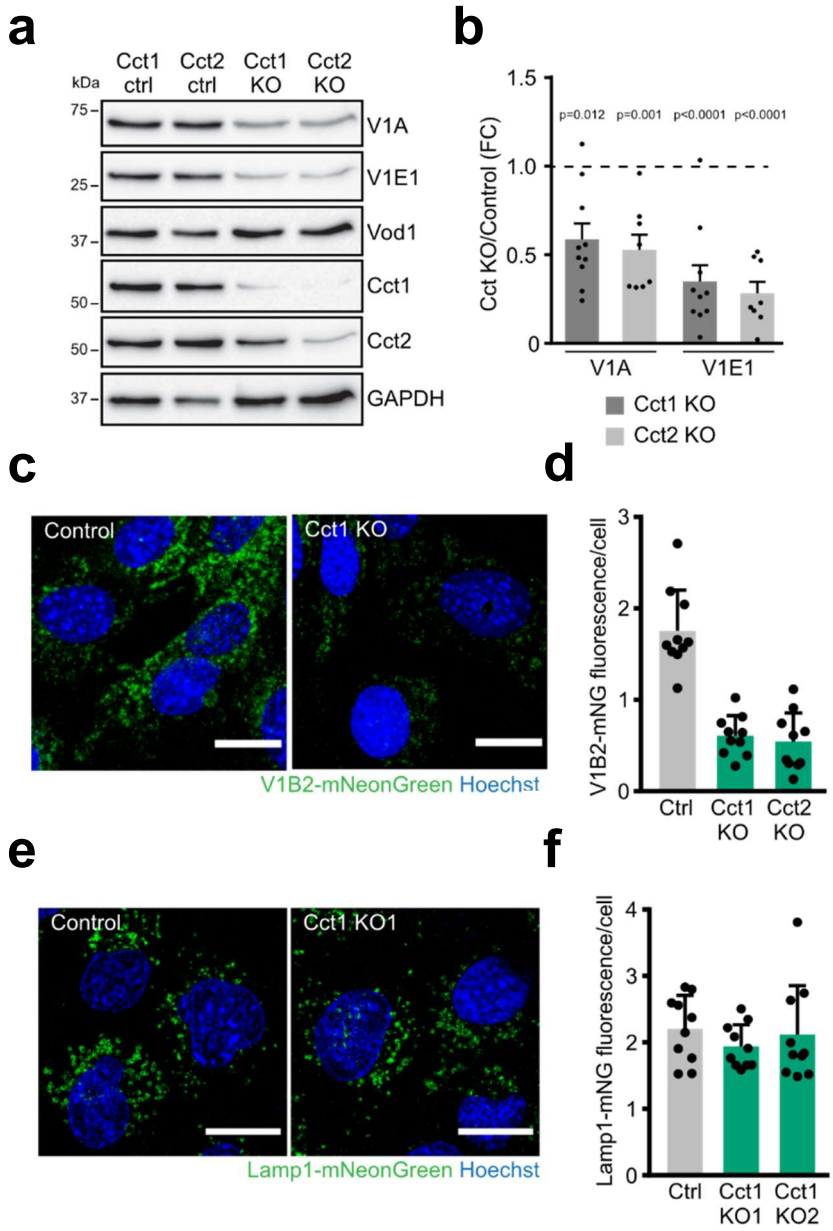

Figure 14. TRiC loss decreased V_1 subunit abundance. a. Western blot of MEFs expressing doxycycline-inducible Cas9 transduce with sgRNA targeting Cct1 and Cct2 untreated (ctrl) or treated (KO) with doxycycline (400 ng/mL) for 3 days before the start of the experiment. **b.** Quantification of V-ATPase subunits level in whole cell lysates as detected in a. Normalised ratio means for Cct KO/ctrl are plotted ±s.e.m. for 8 biologically independent experiments for Cct1 and 10 biologically independent experiments for Cct2. Dashed lines indicate protein abundance in the control groups. **c.** Confocal microscopy images of MEFs control or Cct1 KO expressing V1B2-mNeonGreen imaged in basal conditions. Scale bars = 20 µm. **d.** Quantification of V1B2-mNeonGreen fluorescent per cell in MEFs treated as in c for control, Cct1 or Cct2 KO. Mean ±SD of one biologically independent replicate out of 3 is plotted (≥10 fields of view). **e.** Confocal microscopy images of MEFs control or Cct1 KO endogenously expressing Lamp1-mNeonGreen imaged in basal conditions. Scale bars = 20 µm. **f.** Quantification of the Lamp1-mNeonGreen fluorescent per cell in MEFs treated as in c for control, Cct1 or Cct2 KO. Mean ±SD of one biologically independent replicate out of 3 is plotted (≥10 fields of view).

4.7.2 Loss of TRiC suppresses lysosomal acidification and catabolism.

In order to understand if TRiC loss affects lysosomal acidification, V-ATPase activity and lysosomal acidification were tested. To this end, I took advantage of the pH-dependent properties of the fluorophore FITC. FITC fluorescence is pH-sensitive and quenched in the acidic environment of lysosomes. Therefore, FITC can be used to assess lysosomal pH. Control or Cct2 knockout MEFs were incubated overnight with 10 kDa FITC-dextran. Then, cells were washed and chased with fresh medium for 4 hours. Thereby, FITC-dextran accumulated in lysosomes. FITC intensity was then analysed by confocal imaging. Cct2 knockout had increased FITC signal per cell in basal conditions. Torin 1 treatment did not decrease FITC signal to the same extent as in wild-type MEFs (**Figure 15a, b**). Thus, in the absence of TRiC, lysosomes are less acidic and less responsive to mTORC1 inhibition.

I then analysed directly V-ATPase activity, once again taking advantage of the pH-dependent fluorescent property of FITC. As above, lysosomes were loaded overnight with 10 kDa FITC-dextran. Then, MEFs were chased for 4 hours. During the chase period, MEFs were treated with torin 1 for 1 hour to maximize V-ATPase assembly. MEFs were also treated for 30 minutes with bafilomycin A1 to inhibit V-ATPase activity and neutralise the lysosomal pH. Just before imaging, bafilomycin A1 was removed and the resulting FITC quenching due to V-ATPase re-activation was followed over time by confocal imaging. Control lysosomes rapidly quenched FITC signal. By contrast, in inducible Cct1 and Cct2 knockouts FITC fluorescence was quenched much more slowly and to a lesser degree (**Figure 15c, d**).

Less acidic lysosomes might have decreased proteolytic activity. To test this, DQ BSA degradation was overseen in MEFs. TRiC knockouts were not able to upregulate DQ BSA degradation upon mTORC1 inhibition (**Figure 15e, f**). In order to prove that suppression in lysosome acidification and DQ BSA degradation is mediated by loss of the TRiC complex, I performed rescue experiments with TRiC knockout cells. MEFs depleted of Cct1 or Cct2 were transduced with CRISPR/Cas9-resistant constructs for Cct1 or Cct2. Re-expressing Cct1 or Cct2 restored lysosomal DQ BSA degradation upon mTORC1 inhibition (**Figure 16a**).

In conclusion, in the absence of the V_1 cytosolic binding partner, TRiC, cells are not able to properly acidify the lysosomal lumen. As a consequence, they increase to a lesser extent the catabolism of endocytosed proteins upon mTORC1 inhibition.

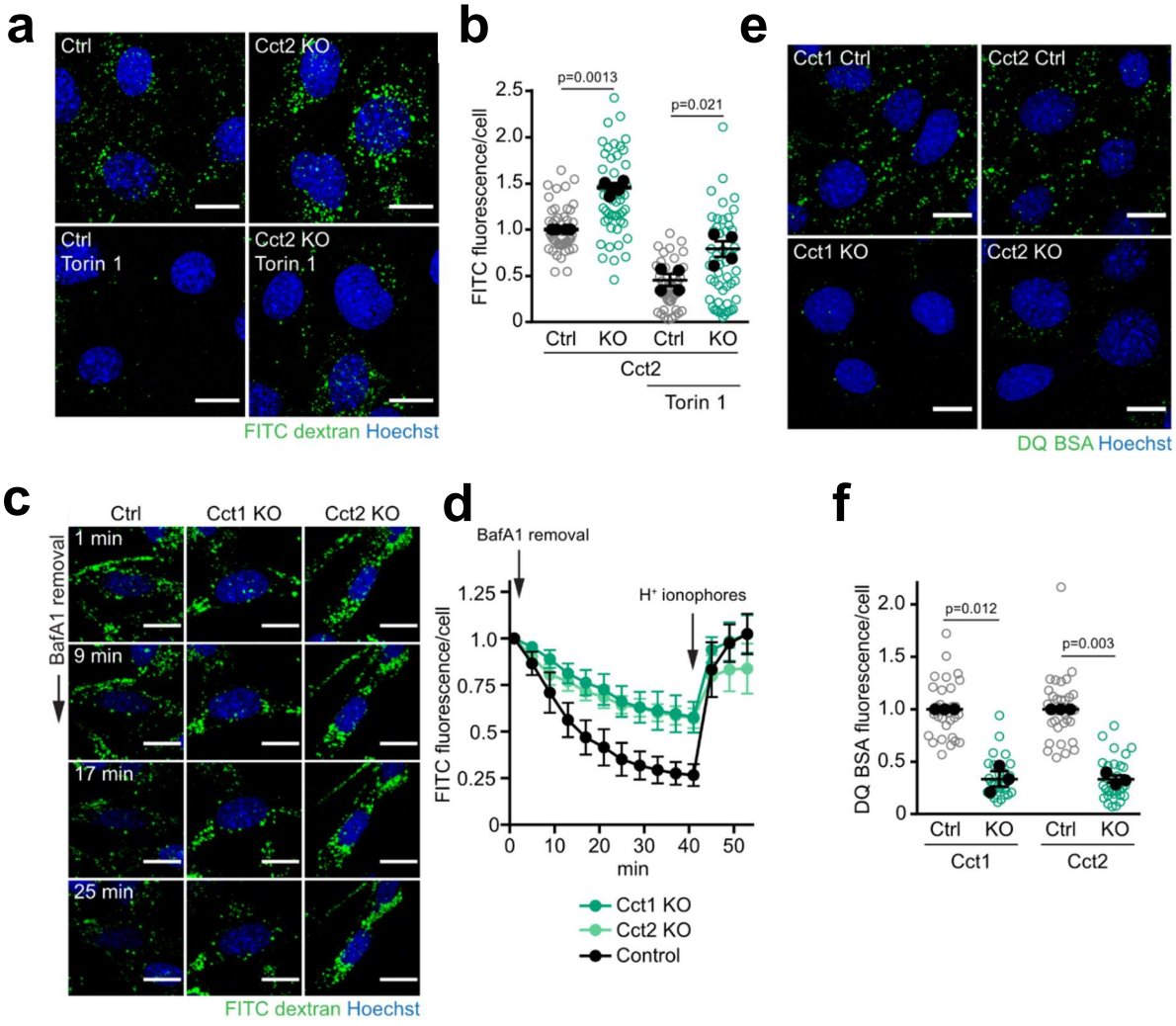

Figure 15. TRiC loss prevents mTORC1-dependent lysosomal acidification. a. Confocal microscopy images of MEFs expressing doxycycline-inducible Cas9 transduce with sgRNA targeting Cct2 untreated (ctrl) or treated (KO) with doxycycline (400 ng/mL) for 3 days before the start of the experiment. Control and KO MEFs were preloaded with 10 kDa FITC-dextran overnight, followed by chase of 3 hours and treated with DMSO (control) or torin 1 (400 nM) for 1 hour. Scale bars = 20 µm. **b.** Quantification of FITC-dextran fluorescent per cell in MEFs treated as in a. **c.** Confocal microscopy images of MEFs expressing constitutive Cas9 and sgRNA targeting non-coding chromosome regions (Ctrl), Cct1 or Cct2 (KO) preloaded with 10 kDa FITC-dextran treated with torin 1 (400 nM) and bafilomycin A1 (20 nM) for 1 hour. MEFs were imaged over time upon bafilomycin A1 removal. **d.** Quantification of FITC-dextran quenching over time as in c. **e.** Confocal microscopy images of MEFs expressing doxycycline-inducible Cas9 transduce with sgRNA targeting Cct1 or Cct2 untreated (ctrl) or treated (KO) with doxycycline (400 ng/mL) for 3 days before the start of the experiment. MEFs control, Cct1 or Cct2 KO were incubated with DQ BSA and treated with DMSO (control) or torin 1 (400 nM) for 5 hours. Scale bars = 20 µm. **f.** Quantification of DQ BSA fluorescent per cell in MEFs treated as in e.

Data are plotted as normalised replicate mean ± s.e.m. (closed circles) for 4 biologically independent experiments for b) or 3 biologically independent experiments for e) and g), and fields of view (open circles, ≥ 10 per replicate). A two-tailed unpaired t-test with Welch correction was used to calculate p-values.

4.7.3 Cct2 S260 phosphorylation is dispensable for mTORC1-mediated suppression of lysosomal protein catabolism.

Cct2 S260 is phosphorylated by S6 kinase (S6K), an mTORC1 effector[106]. To understand if this phosphosite is important to maintain basal level of cytoplasmic V_1 domain and the consequent V-ATPase assembly, Marten Wittmann in our laboratory generated phosphorylation-deficient Cct2 S260A and phosphomimetic Cct2 S260D constructs for Cct2 fused to a Myc-tag. As previously reported[106], Cct2 knockout caused a strong proliferation defect, which was rescued by re-expression of Cct2 wild type or Cct2 S260D but not Cct2 S260A (**Figure 16b**). Thus, this phosphosite is critical for cell proliferation. However, all Cct2 constructs were able to rescue the catabolism of extracellular proteins in the lysosome (**Figure 16c**). Moreover, the re-expression of the Cct2 variants completely restored the basal level of V1A and V1E1 subunits of the V-ATPase (**Figure 16d**). Finally, I used a specific S6K inhibitor, LY2584702, to test if S6K is the mTORC1 effector regulating lysosomal protein degradation. LY2584702 treatment for 6 hours completely abolished S6K activity (**Figure 17a**), but it did not induce an increase in cresyl violet or DQ BSA (**Figure 17b-d**). Thus, mTORC1 does not regulate V-ATPase assembly through Cct2 S260 phosphorylation or S6K signalling.

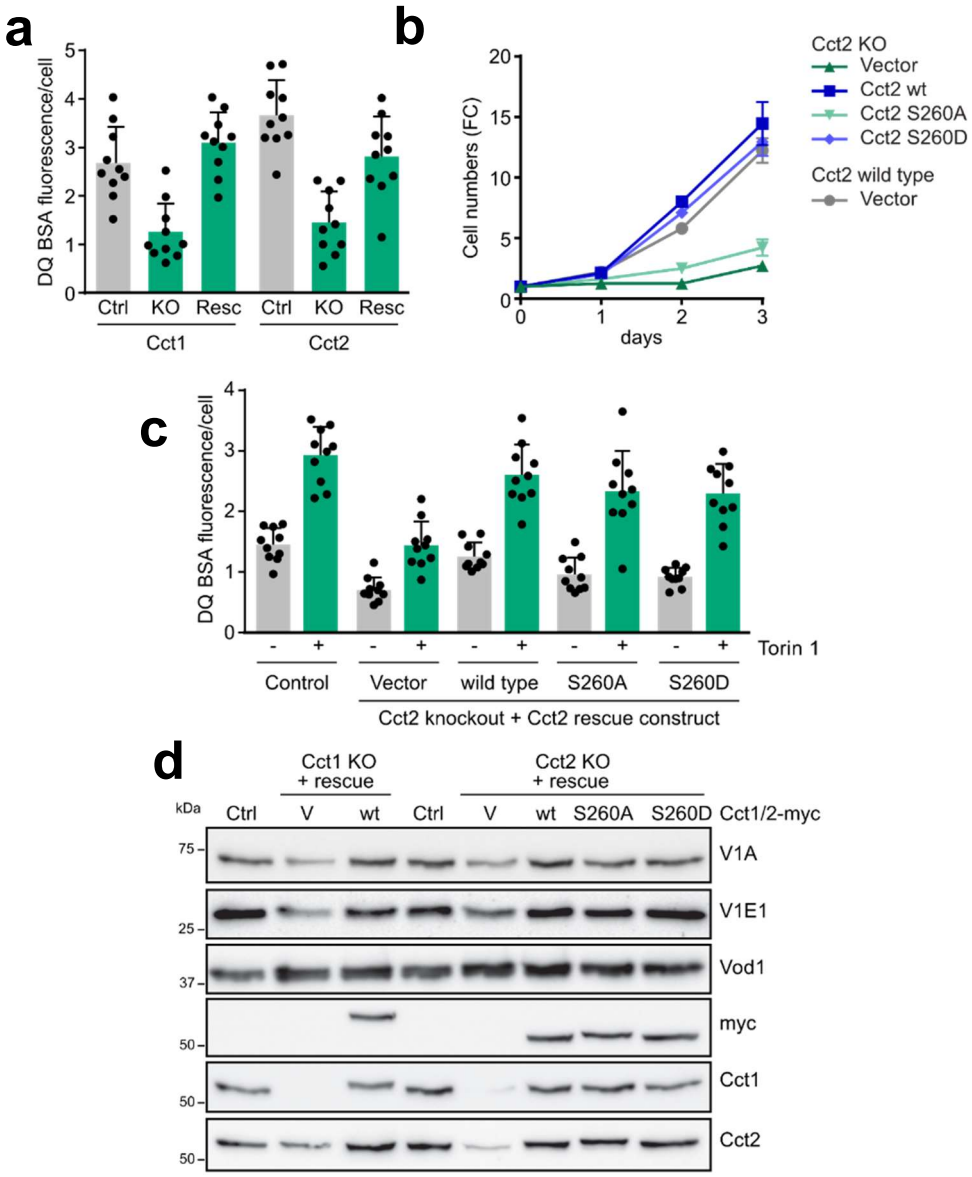

Figure 16. TRiC re-expression rescued extracellular protein catabolism and V_1 level. a. Quantification of DQ BSA fluorescent per cell in MEFs expressing doxycycline-inducible Cas9 transduce with sgRNA targeting Cct1 and Cct2 untreated (ctrl) or treated (KO) with doxycycline (400 ng/mL) for 3 days before the start of the experiment upon torin 1 (400 nM) treatment for 5 hours. Where indicated rescue construct for Cct1 or Cct2 was ectopically re-expressed (Resc.). **b.** Proliferation assay of MEFs control or Cct2 KO ectopically expressing Cct2 wild type, S260A, or S260D variants. Mean ±SD of one biologically independent replicate out of 3 is plotted (3 technical replicates). **c.** Confocal microscopy quantification of DQ BSA fluorescent per cell in MEFs control or Cct2 KO ectopically expressing Cct2 wild type, S260A or S260D variants treated with DMSO (control) or torin 1 (400 nM) for 5 hours. Mean ±SD of one biologically independent replicate out of 3 is plotted (≥10 fields of view). **d.** Western blot of whole cell lysates of control, Cct1 or Cct2 KO ectopically expressing TRiC wild type, S260A or S260D variants as indicated.

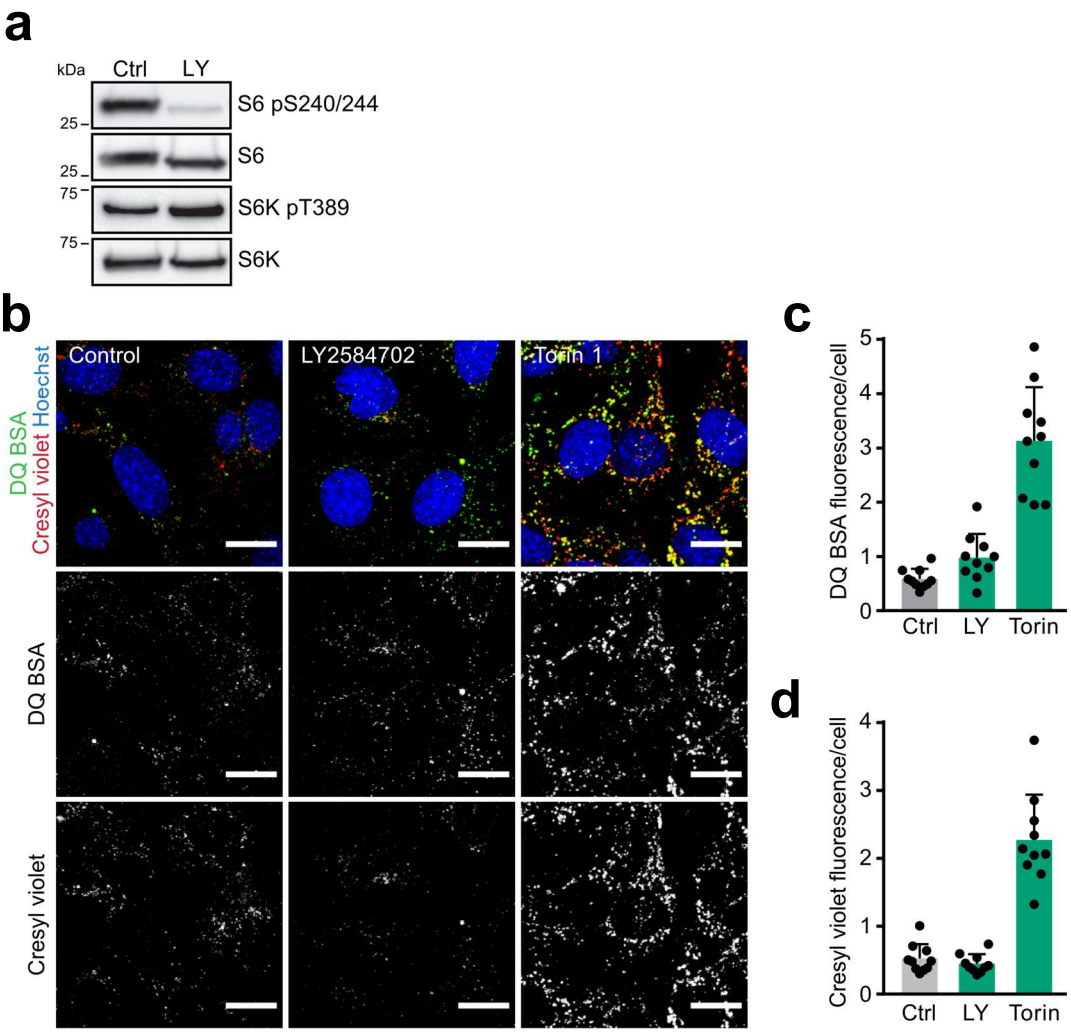

Figure 17. S6K inhibition does not increase DQ BSA degradation and lysosomal acidification. a. Western blot of MEFs upon LY2584702 (5 μM), S6K inhibitor, treatment for 5 hours. **b.** Confocal microscopy images of MEFs incubated with cresyl violet and DQ BSA and treated with DMSO (control) or LY2584702 (5 μM), torin 1 (400 nM) for 5 hours. Scale bars = 20 μm. **c.** Quantification of DQ BSA fluorescent per cell in MEFs treated as in b. **d.** Quantification of cresyl violet fluorescent per cell in MEFs treated as in b.

Mean ±SD of one biologically independent replicate out of 3 is plotted (≥10 fields of view).

4.8 mTORC1 inactivation upregulates the catabolic capacity of the cell lysosomal population.

The above data revealed that mTORC1 inactivation promotes V-ATPase assembly and lysosomal acidification. To understand the impact on lysosomal metabolism, I looked at the general population of lysosomes after torin 1 treatment. Nora Siefert generated MEFs expressing Lamp1 endogenously tagged with mNeonGreen to label lysosomes. In previous assays, I used Magic Red substrates and DQ BSA to quantify cathepsin and lysosomal protein degradation activity per lysosome, respectively. Taking advantage of MEFs endogenously expressing Lamp1-mNeonGreen I could measure cathepsin activation and DQ BSA increase per lysosome. Thereby, I would quantify the percentage of lysosomes that are catabolically activated upon mTORC1 inhibition.

As described in section 4.2, to load lysosomes with DQ BSA, MEFs were incubated with DQ BSA for 4 hours followed by 3 hours chase period with fresh medium. Lysosomal catabolism was followed by confocal imaging over time before and after torin 1 addition. The accumulation of DQ BSA was quantified over time on the Lamp1-mNeonGreen-positive vesicles. The mNeonGreen channel was used to define the overall lysosomal population. Before torin 1 treatment, DQ BSA signal did not change and only a small subset of mNeonGreen-positive lysosomes were positive for DQ BSA (**Figure 18a, b**). This, suggests that at basal conditions only a few lysosomes actively catabolize extracellular proteins. Upon torin 1 treatment DQ BSA signal increased throughout the lysosomal population, suggesting that the majority of lysosomes becomes proteolytically active.

To further understand if mTORC1 regulates lysosomal activity in a specific subset of lysosomes or if the general lysosomal population is affected cathepsin MR substrates or DQ BSA were measured by confocal imaging. The images were used to quantify the fraction of lysosomes that showed increased cathepsin MR substrate activity or DQ BSA dequenching compared to the automatic threshold applied by Fiji. The auto-threshold was used in cells treated with torin 1, which exhibit elevated lysosomal catabolic activity. Subsequently, the average auto-threshold value was applied to all conditions within the same experiment. In line with the previous data[107], in resting cells, only around 20% of lysosomes were positive for MR cathepsin B or cathepsin L substrates (**Figure 19a, b**). In contrast, after 1 hour of torin 1 treatment almost 60% of the lysosomes displayed high cathepsin B and L activity. Similarly, when lysosomes were preloaded with DQ BSA, in control cells only around 10% of lysosomes displayed high DQ BSA signal. However, upon 2 hours of torin 1 treatment, almost 80% of the lysosomal population started to degrade DQ BSA that had been accumulated in their lumen (**Figure 19c-e**). These data suggest that under basal conditions, the majority of the lysosomes have low

activity. Upon mTORC1 inhibition, however, the lysosomal population responds by increasing their proteolytic activity.

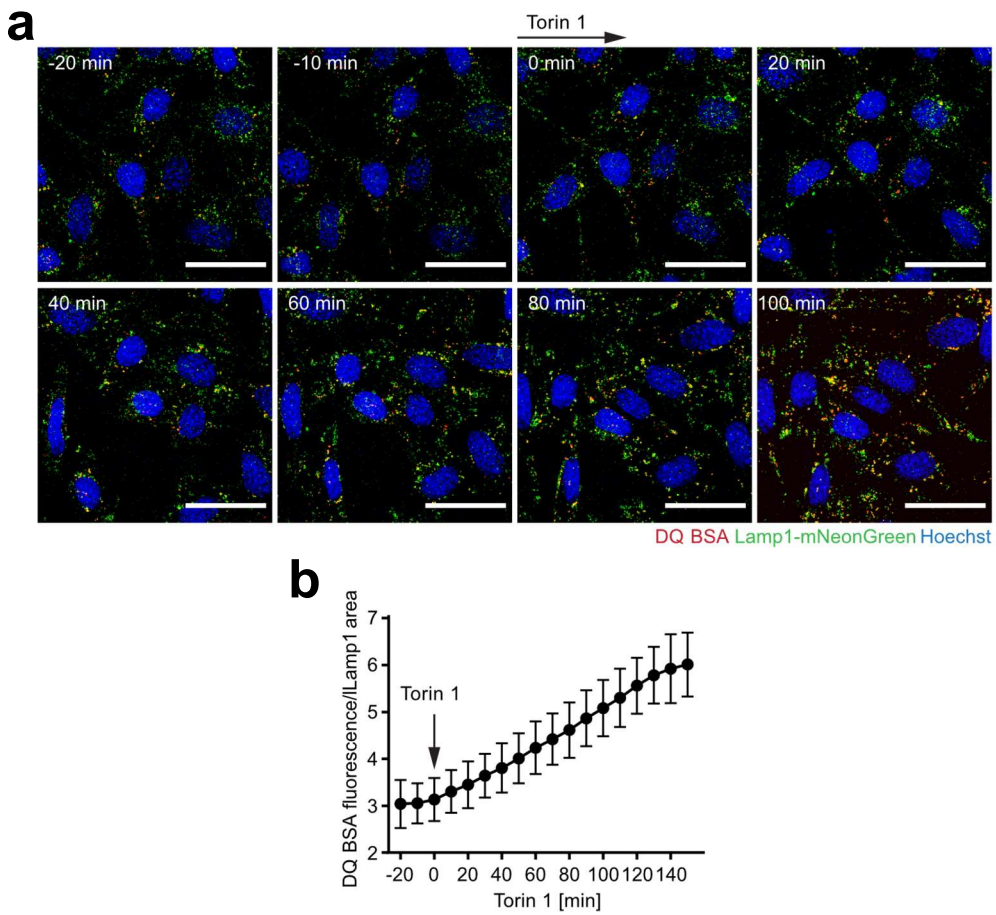

Figure 18. Lysosomes increase digestion of stored extracellular proteins upon mTORC1 inactivation. a. Confocal microscopy images of MEFs endogenously expressing Lamp1-mNeonGreen pre-loaded with DQ BSA for 4 hours, chased for 3 hours and treated with torin 1 (400 nM) at time zero and followed over time. **b.** Quantification of DQ BSA intensity on the Lamp1-mNeonGreen area over time as in a. Mean ±SD of one biologically independent replicate out of 3 is plotted (≥ 10 fields of view). Scale bars = 20 μm.

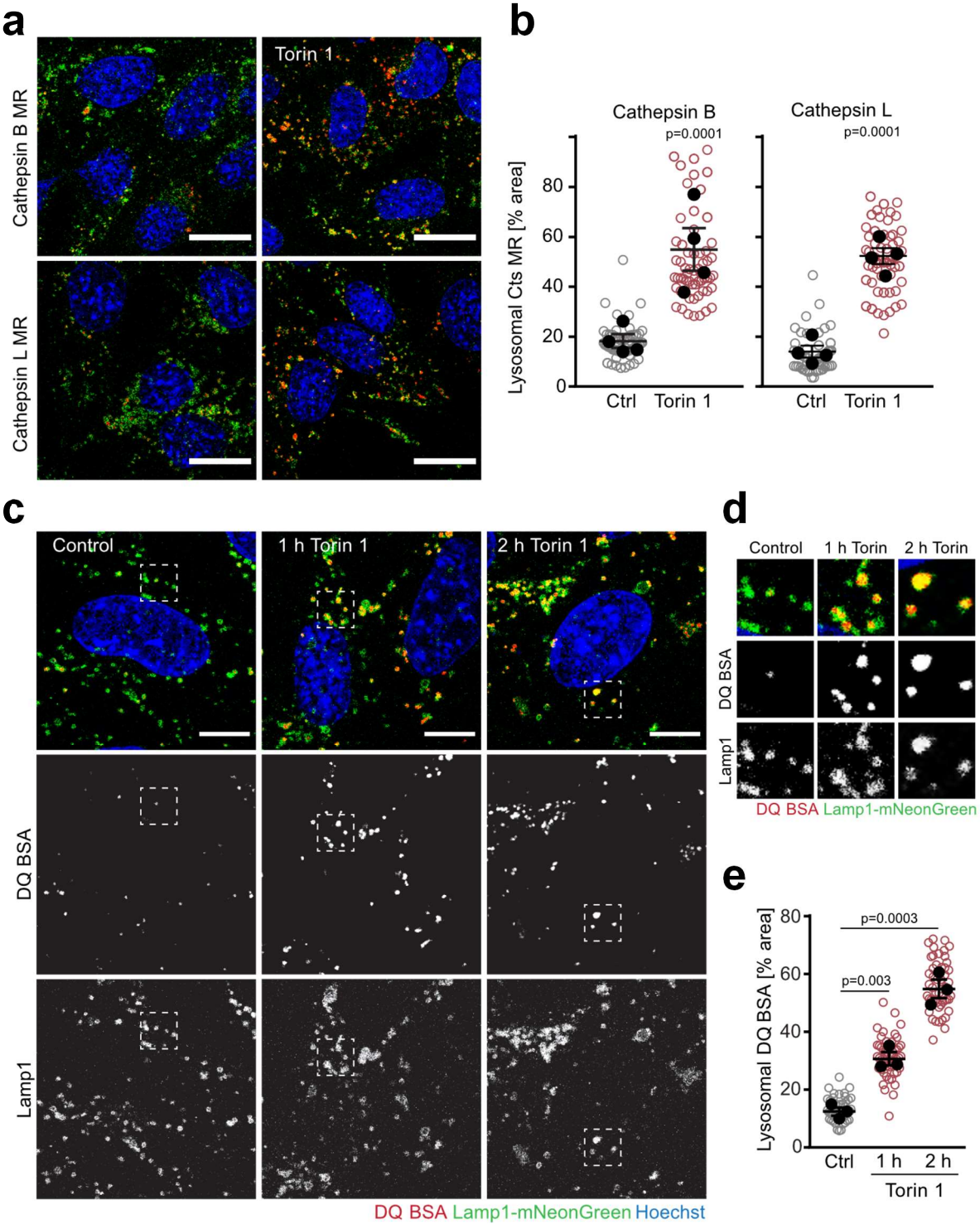
a
Cathepsin B MR
Cathepsin L MR
Torin 1
b
Cathepsin B
Cathepsin L
p=0.0001
p=0.0001
Lysosomal Cts MR [% area]
0
20
40
60
80
Ctrl
Torin 1
Ctrl
Torin 1
c
Control
1 h Torin 1
2 h Torin 1
DQ BSA
Lamp1
DQ BSA Lamp1-mNeonGreen Hoechst
d
Control
1 h Torin
2 h Torin
DQ BSA
Lamp1
DQ BSA Lamp1-mNeonGreen
e
Lysosomal DQ BSA [% area]
p=0.0003
p=0.003
0
20
40
60
80
Ctrl
1 h
2 h
Torin 1

Figure 19. Lysosomal catabolic activity is enhanced throughout the lysosomal population. a. Confocal microscopy images of MEFs endogenously expressing Lamp1-mNeonGreen incubated with cathepsin B MR or cathepsin L MR substrates for 10-12 minutes and treated with DMSO (control) or torin 1 (400 nM) for 1 hour. Scale bars = 20 μm. **b.** Percentage of lysosomes positive for cathepsin B MR or cathepsin L MR substrates as in a. Lysosomes are defined as Lamp1-mNeonGreen-positive vesicles. **c.** Confocal microscopy images of MEFs pre-loaded with DQ BSA for 4 hours, chased for 3 hours and treated with DMSO (control) or torin 1 (400 nM) for 1 or 2 hours as indicated. Scale bars = 10 μm. **d.** Magnification of areas highlighted in c. **e.** Percentage of lysosomes positive for DQ BSA as in c. Lysosomes are defined as Lamp1-mNeonGreen-positive vesicles.

Data are plotted as normalised replicate mean ± s.e.m. (closed circles) for 4 biologically independent experiments for cathepsin MR and 3 biologically independent experiments for DQ BSA, and fields of view (open circles, ≥ 10 per replicate). A two-tailed unpaired t-test with Welch correction was used to calculate p-values.

5 Discussion and conclusion

In this work, I uncover a novel function for mTORC1 in regulating lysosomal acidification and proteolysis. It was known that mTORC1 blocks lysosomal catabolism of extracellular and proteins. Indeed, mTORC1 inhibition allows cells to use extracellular albumin as an alternative nutrient source in the absence of free amino acids[5]. During my PhD, I found out the molecular mechanism of how mTORC1 regulates lysosomal catabolism of extracellular proteins. I showed that upon mTORC1 inhibition the lysosomal lumen becomes more acidic within 1 hour and found out that mTORC1 regulates V-ATPase assembly at lysosomes. When nutrients are available and mTORC1 is active, the majority of lysosomes show an elevated pH and low protease activity. The peripheral V_1 domain is mostly present in the cytoplasm stabilised by the chaperonin TRiC (**Figure 20a**). Conversely, under nutrient deprivation, mTORC1 is inactivated and the V_1 domain is recruited to the lysosome where it assembles with the V_o domain (**Figure 20b**). The functional V-ATPase can then pump protons into the lysosomal lumen decreasing lysosomal pH. As a consequence, lysosomal proteases get activated and start to digest proteins that were accumulated inside the lysosome. In the absence of nutrients, cells inactivate mTORC1 thus upregulating the lysosomal latent catabolic capacity, conceivably this mechanism allows cells to quickly adapt to changes in nutrient availability. Interestingly, this process is an alternative, faster mechanism to increase lysosomal catabolic capacity compared to the canonical mechanism of TFEB activation and the consequent increase in lysosomal mass[108].

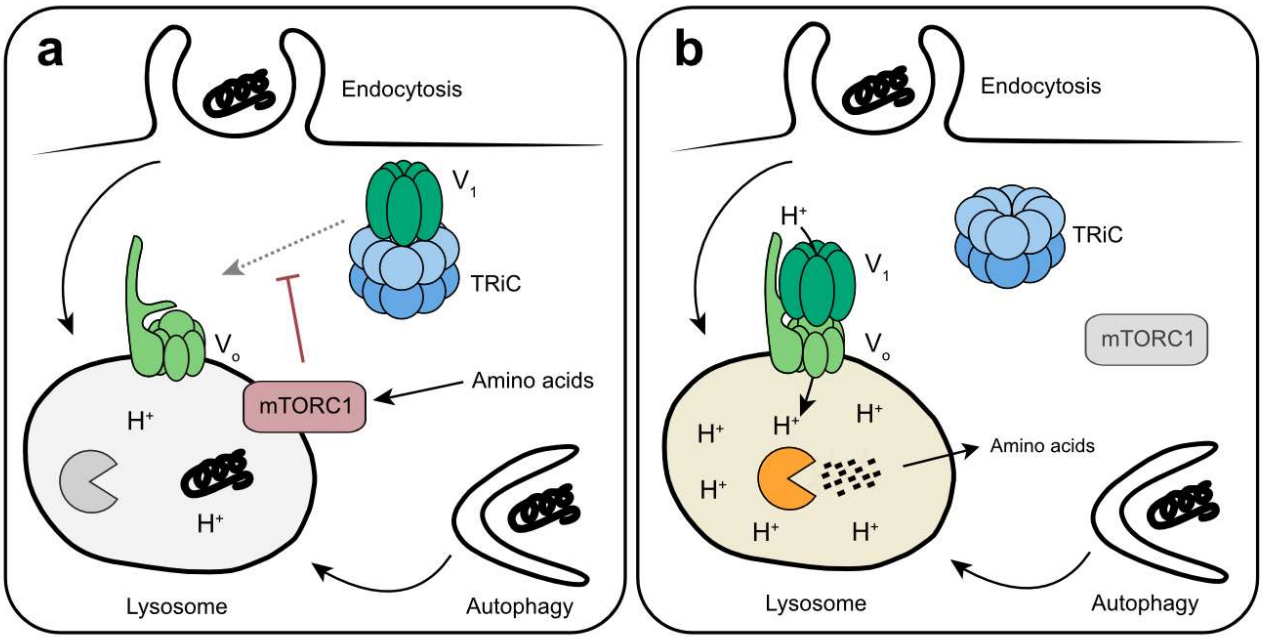

Figure 20. Graphical model for mTORC1 regulation of lysosomal catabolism. a. In nutrient-rich conditions, most V-ATPase V_1 domains reside in the cytoplasm, where they are stabilised by interaction with the chaperonin TRiC. A large fraction of lysosomes is poorly catabolically active and has an elevated pH. **b.** During amino acid starvation, mTORC1 is inactivated and the V_1 domain is recruited to the lysosomes and assembled with the V_o domain. The active proton pump acidifies the lysosomal lumen and increases protease activity and digestion of macromolecules accumulated in the lysosomal lumen.

5.1 Establishment of a novel V-ATPase assembly live imaging assay

Fractionation of the membrane and cytoplasmic fractions can disrupt the intact V-ATPase, causing detachment of the V_1 domain from the lysosomes during mechanical lysis of the cell. This can lead to an artificial increase in the amount of V_1 in the cytoplasmic fraction and result in a lower estimation of the total amount of V-ATPase assembled at the membrane. Additionally, studying V-ATPase assembly by membrane fractionation was found to be poorly reliable and difficult to reproduce. For these reasons, with the help of Nora Siefert, I developed a novel V-ATPase assembly live imaging assay. This assay allowed me to look at the live dynamics of V-ATPase assembly by analysing the movement of the V_1 domain in relation to the lysosomal V_o domain. Unlike membrane fractionation, no intermediate steps (*e.g.*, cell lysis) are involved. The live imaging assay for V-ATPase assembly was found to be more reliable and consistent when compared to membrane fractionation. Moreover, the V-ATPase enzyme is present in various membranous compartments ranging from the endoplasmic reticulum to the plasma membrane. Hence, the live imaging assay allows for the analysis of V-ATPase recruitment at specific organelles, whereas membrane fractionation does not permit the study of V-ATPase assembly at any particular organelle. This is because, although lysosomes are enriched during membrane fractionation, most membranes are precipitated, resulting in a lack of specificity in the organelles being studied. However, similar to the membrane fractionation, at basal conditions, most of the V1B2-mNeonGreen is diffused in the cytoplasm. It should be noted that V1B2-mNeonGreen is overexpressed in these cells, which could lead to artefacts due to overexpression of a single V-ATPase subunit. Endogenous tagging a subunit of the V_1 domain would allow the proper assessment of the relative amount of the cytoplasmic and lysosomal V_1 without introducing artefacts.

5.2 mTORC1 inactivation increases lysosomal protein catabolism by directly regulating lysosomal pH

mTORC1 is activated in nutrient-rich conditions to promote growth but is inhibited during starvation to allow cellular adaptation in nutrient scarcity. Thus, mTORC1 inactivation leads to an increase in cell catabolic activity, while anabolic activities are blocked[109]. mTORC1 is activated at the lysosome, a converging point of growth factor signals and nutrients, which are necessary for mTORC1 activation. Evidence suggests that amino acids inside the lysosome change the nucleotide state of Rag GTPases by promoting V-ATPase-ragulator-Rag interactions[110]. In this model, V-ATPases are essential for mTORC1 activation by amino acids, placing the V-ATPase upstream of mTORC1 activation. However, Zoncu and colleagues

showed that V_o constitutively interacts with ragulator, whereas V_1 only interacts with the V_o-ragulator complex during amino acid starvation[48]. They concluded that readdition of amino acid induces a conformational change in the V-ATPase-Ragulator complex, allowing mTORC1 recruitment and activation. We showed that amino acid starvation increases the recruitment of V_1 to the lysosome, where Ragulator resides and that V_1 recruitment upon mTORC1 inhibition causes lysosomal acidification. Taken together, these data suggest that V-ATPase is crucial for mTORC1 activation but also functions as a mTORC1 downstream effector for lysosomal pH regulation. Specifically, the V_o domain is a lysosomal anchor for ragulator-Rag, which is important for mTORC1 activation, leading to the disassembly of V_1-V_o domains and an increase in lysosomal pH [48,109–111].

5.3 Mammalian cells react to mTORC1 inactivation by globally increasing lysosomal catabolic activity

When facing nutrient deprivation, mammalian cells can upregulate the usage of alternative nutrient sources through lysosomal degradation. In the absence of nutrients, mTORC1 inactivation leads to the upregulation of catabolic pathways, such as autophagy[109,111]. Under fed conditions, mTORC1 phosphorylates ULK1, preventing its activation and the downstream cascade that leads to autophagosome formation[54]. In the presence of nutrients, a basal level of autophagy is essential for housekeeping function, eliminating non-functional organelles and protein aggregates. However, during nutrient starvation, autophagy sustains cell viability by supplying nutrients for a limited period of time[32]. In contrast, macropinocytosis supplies exogenous macromolecules to the lysosome to generate nutrients, thus supporting continuous cell proliferation under nutrient starvation[4]. Amino acid starvation also increases degradation of extracellular and intracellular protein by inducing transcriptional activation of genes involved in autophagy, macropinosome formation, and uptake of external materials[112,113]. Moreover, cells during starvation increase transcriptional expression of lysosomal genes. Specifically, TFEB activates the transcription of many essential lysosomal genes, thus inducing lysosomal biogenesis, and enhancing the overall lysosomal degradative potential. Upon mTORC1 inhibition, TFEB translocates to the nucleus where it promotes the expression of lysosomal hydrolases, lysosomal membrane proteins, and components of the V-ATPase complex[34,55,108].

The present study suggests that proteins accumulated in the lysosomes are only inefficiently degraded in nutrient-replete conditions. Rather, only few lysosomes are actively degrading their protein contents, whereas the majority of the lysosomes, even those containing extracellular materials, display low catabolic activity. However, nutrient starvation increases

lysosomal catabolic activity through V-ATPase assembly and the consequent acidification of the lysosomal lumen. The increase in degradation of extracellular and intracellular proteins produces a pool of free amino acids and might trigger mTORC1 reactivation. Thus, increased lysosomal degradation may act as a negative feedback loop to terminate lysosomal acidification and degradation restoring lysosomal homeostasis[28,114]. It was observed that various cell types have a large population of lysosomes that, despite containing mature acid hydrolases, has pH values higher than 6 and display little catabolic activity[107,115]. It has been proposed that this population of lysosomes could be used as ready-to-use storage organelles for degradative enzymes[107].

The present work suggests that inactive lysosomes may function as ready-to-use storage organelles for extracellular proteins becoming proteolytically active upon nutrient scarcity and the resulting mTORC1 inactivation. Conceivably, this is an alternative mechanism that allows cells to rapidly adapt to nutrient starvation by inducing nutrient generation through lysosomal protein catabolism[108]. In this way, cells can rapidly increase the latent lysosomal catabolic capacity and adapt to nutrient fluctuation in the extracellular environment. The acute activation of lysosomal digestive activity, mediated by V-ATPase assembly, and a long-term increase in lysosome number, mediated by TFEB activation, conceivably allows adjusting cellular catabolic capacity over different time scales.

5.4 Amino acid starvation induces DMXL1/2-dependent V-ATPase assembly

The major mechanism to regulate V-ATPases activity is the reversible disassembly of the V_1 and V_o domains. V-ATPases assembly has mainly been studied in yeast, where the V-ATPase V_1 and V_o domains reversibly disassemble upon glucose withdrawal[59,116]. Conceivably, this mechanism maintains stable ATP levels in the absence of glucose. Metabolic inputs can also regulate V-ATPase assembly in mammalian cells, but the underlying mechanisms are not clear. In some mammalian cell lines, V-ATPase disassembly is sensitive to glucose starvation[117]. Moreover, metabolic enzymes, like aldolase A and 1-phosphofructokinase, are essential for the stability of assembled V-ATPases. Indeed, aldolase A dissociation from the V-ATPase complex precedes V-ATPase disassembly upon glucose starvation[118,119]. Although mTORC1 regulates cell metabolism and sits on lysosomes, its role in V-ATPase regulation has not been completely understood. Long-term mTORC1 inhibition with rapamycin treatment blocks V-ATPase assembly during dendritic cell maturation[67]. Nevertheless, acute treatment with rapamycin does not have any effects on V-ATPase activity[120]. However, by inhibiting mTORC1 with mTOR kinase inhibitor or amino acids starvation, I revealed the role of mTORC1

in V-ATPase assembly. I identified the first nutrient-mediated signalling pathway to regulate V-ATPase assembly at the lysosome in mammals.

In yeast, the RAVE (Regulator of H+-ATPase of Vacuolar and Endosomal membranes) complex is essential for catalysing V-ATPases assembly. In eukaryotes, different proteins have been implicated in V-ATPase assembly. The DMXL1/2 complex has been suggested to have a similar role to the yeast RAVE[63]. Indeed, I demonstrated that DMXL1/2 is necessary for V-ATPase assembly in basal conditions and upon mTORC1 inhibition. New preliminary data from our laboratory (data not shown) suggest that although DMXL1/2 knockout does not show V-ATPase assembly, they acidify lysosomes upon mTORC1 inhibition. DMXL1/2 double-knockout shows a delayed increase in lysotracker signal upon torin 1 treatment. Further investigation is required to understand how mTORC1 is able to acidify lysosomes in the absence of assembled V-ATPase, but it might suggest that mTORC1 regulates lysosomal pH with multiple pathways, conceivably also through regulation of the counterion flux.

5.5 TRiC is important for V1 domain stabilization and V-ATPase assembly

In this project, I discovered that the V_1 domain of the V-ATPase and the cytosolic chaperonin TRiC interact in an amino acid-regulated manner. Interestingly, the V_1 domain interaction with the membrane-associated-V_o domain at the lysosome or with TRiC in the cytosol appears to be mutually exclusive. Thus, I could observe the movement of the V_1 domain between the two complexes depending on mTORC1 signalling. The loss of TRiC strongly decreases overall V_1 domain levels without changing the abundance of the V_o domain or other lysosomal proteins. This suggests that the V_1 domain in the cytoplasm is prone to degradation or aggregation if not interacting with TRiC. These observations suggest first that the interaction between V_1 and TRiC is critical to stabilise the cytoplasmic pool of V_1 domains in basal conditions, and second that maintaining a ready-to-use pool of V_1 domain is important for cells to quickly regulate lysosomal pH upon external stimuli. TRiC has been observed to be regulated by growth factors and mTORC1 signaling[106]. The mTORC1 effector S6K phosphorylates the CCT2 subunit at S260, which is required for normal cell proliferation and growth[106]. Moreover, TRiC not only functions in protein folding but can also stabilise protein complexes; *e.g.*, the m6A RNA methyltransferase complex is stabilised by TRiC in an mTORC1-dependent manner[121]. Although I could recapitulate the impact of Cct2 S260 phosphorylation on cell proliferation, neither direct S6K inhibition nor CCT2 S260 phosphomutants showed an effect on mTORC1-dependent lysosomal acidification. Furthermore, rapamycin inhibits mTORC1-dependent S6K activation but does not increase V-ATPase assembly or lysosomal acidification. Overall, these

observations suggest that the mTORC1 effector S6K is not involved in V-ATPase regulation. Conceivably, mTORC1 promotes V_1 interaction with TRiC indirectly, for example by directly or indirectly phosphorylating V_1 domain subunits, V_o domain subunits, or by regulating an assembly factor.

In this project, I discovered that TRiC is necessary to stabilise the V_1 domain in the cytoplasm, but the molecular reason why V_1 depends on TRiC remains to be determined. My experiments suggest two hypotheses. One possibility is that TRiC sequesters the V_1 domain in the cytoplasm. In this scenario, mTORC1 might phosphorylate either the V_1 domain or TRiC to promote their interaction if lysosomal pH has to be kept elevated. Once the V_1 domain and TRiC interact, V_1 cannot be recruited to the lysosome to assemble with the V_o domain. Such TRiC-mediated sequestration could be a regulatory mechanism to prevent V-ATPase assembly and lysosomal acidification. The second hypothesis is that TRiC is required for V_1 domain stabilisation. My experiments support the second hypothesis, indicating a role of TRiC in stabilising the cytoplasmic V_1 domain. While mTORC1 might directly regulate the interaction between V_1 and V_o at the lysosome, the cytoplasmic V_1 domain needs to interact with TRiC to avoid lysosomal or proteasomal degradation or aggregation. However, these two hypotheses are not mutually exclusive. mTORC1 could mediate TRiC-dependent sequestration of the V_1 domain, but at the same time TRiC-V_1 interaction could be important to maintain a pool of cytoplasmic V_1 stable. However, further investigation is required to fully understand the molecular role of TRiC in V-ATPase assembly.

5.6 mTORC1-dependent V-ATPase assembly is a potential cancer target

In vitro cancer cells experience an environment with plenty of free nutrients; thus they do not rely on catabolic pathways to generate building blocks[28]. However, poorly vascularised tumours create environments depleted in amino acids and glucose[122], and cancer cells have to rely on alternative nutrient sources, like extracellular macromolecules[28]. Cancer cells exploit the use of endocytic pathways like Ras/PI3K-drive macropinocytosis to take up macromolecules from the extracellular environment and digest them in the lysosome, liberating their nutrients content[28,123]. Previously it has been shown that mTORC1 inhibition strongly increases the lysosomal catabolism of extracellular albumin, thus promoting survival and proliferation under amino acid depletion[5]. Indeed, it has been shown that in different solid tumours, mTORC1 inhibition has only limited efficacy[124]. The regulating role of mTORC1 in V-ATPase assembly and the consequent increase in lysosomal nutrient generation may explain why cancer cells *in vivo* are resistant to mTORC1 inhibition.

Inhibition of lysosomal nutrient generation has been studied in preclinical and clinical settings as a potential treatment for cancer. For instance, chloroquine or bafilomycin A1 decrease lysosomal nutrient generation. Chloroquine has been found to inhibit the acidification of lysosomes by raising their pH, but it has a poor effect on cancer cell proliferation[125]. Bafilomycin A1 significantly suppresses cancer cell proliferation. However, bafilomycin A1 and other V-ATPase inhibitors are highly toxic for patients since V-ATPase activity is essential in healthy tissues due to pleiotropic functions at multiple organelles[126]. The present work suggests that targeting specifically V-ATPase assembly at the lysosome might be a potential cancer therapy in combination with mTORC1 inhibition. The combinatory therapy would prevent an increase in the utilization of extracellular proteins as an alternative nutrient source and mTORC1-dependent growth.

5.7 Future perspective and open questions

Overall, this project described how mTORC1 regulates lysosomal protein catabolism to rapidly adjust cellular catabolic activity in the absence of nutrients. However, several interesting questions arose from this project, which will be addressed in future projects by our lab.

First, I demonstrated that mTORC1 is upstream of V-ATPase assembly at the lysosome. However, the specific mTORC1 downstream effector remains to be defined. The present study suggests that mTORC1 might act directly on the V_1 domain, increasing V_1 affinity for TRiC or blocking interaction with the V_o domain. However, mTORC1 phosphorylation of a subunit of the V_o domain, TRiC, or assembly factors facilitating V-ATPase assembly is also possible.

Second, I showed that mTORC1 suppresses V-ATPase assembly at the lysosome. However, V-ATPases are also present in other organelles, such as Golgi, endosomes, and the plasma membrane. The V-ATPase is important for the acidification of endosomes, which results in the separation of various ligands from their receptors, *e.g.*, lysosomal cathepsin and the M6P receptor [9]. In the Golgi, the V-ATPases maintain a slightly acidic environment, which seems to be important for proper glycosylation and trafficking of several enzymes to the endolysosomal system [58]. The V-ATPase at the plasma membrane is involved in the acidification of the extracellular environment, which affects several processes such as bone resorption and renal acid-base homeostasis [127,128]. An open question is if mTORC1 drives V-ATPase assembly only at lysosomes or also in these other organelles.

Third, in this project, I discussed a novel interaction between V-ATPase and Flotillin 1/2. Flotillin 1/2 are present in different cellular organelles and they form membrane microdomains that

function as signalling platforms. Their interaction with the V-ATPase is not mTORC1 dependent, nevertheless, it would be interesting to dissect the functional relevance of the V-ATPase-flotillin interaction.

6 Reference

1. Sabatini, D.M. (2017). Twenty-five years of mTOR: Uncovering the link from nutrients to growth. Proceedings of the National Academy of Sciences *114*, 11818–11825. 10.1073/pnas.1716173114.

2. Collins, M.P., and Forgac, M. (2018). Regulation of V-ATPase Assembly in Nutrient Sensing and Function of V-ATPases in Breast Cancer Metastasis. Front Physiol *9*. 10.3389/fphys.2018.00902.

3. Efeyan, A., Comb, W.C., and Sabatini, D.M. (2015). Nutrient-sensing mechanisms and pathways. Nature *517*, 302–310. 10.1038/nature14190.

4. Palm, W. (2019). Metabolic functions of macropinocytosis. Philosophical Transactions of the Royal Society B: Biological Sciences *374*, 20180285. 10.1098/rstb.2018.0285.

5. Palm, W., and Thompson, C.B. (2017). Nutrient acquisition strategies of mammalian cells. Nature *546*, 234–242. 10.1038/nature22379.

6. Hsu, P.P., and Sabatini, D.M. (2008). Cancer Cell Metabolism: Warburg and Beyond. Cell *134*, 703–707. 10.1016/j.cell.2008.08.021.

7. Rabinowitz, J.D., and White, E. (2010). Autophagy and Metabolism. Science (1979) *330*, 1344–1348. 10.1126/science.1193497.

8. Lawrence, R.E., and Zoncu, R. (2019). The lysosome as a cellular centre for signalling, metabolism and quality control. Nat Cell Biol *21*, 133–142. 10.1038/s41556-018-0244-7.

9. Yadati, T., Houben, T., Bitorina, A., and Shiri-Sverdlov, R. (2020). The Ins and Outs of Cathepsins: Physiological Function and Role in Disease Management. Cells *9*, 1679. 10.3390/cells9071679.

10. Sanman, L.E., van der Linden, W.A., Verdoes, M., and Bogyo, M. (2016). Bifunctional Probes of Cathepsin Protease Activity and pH Reveal Alterations in Endolysosomal pH during Bacterial Infection. Cell Chem Biol *23*, 793–804. 10.1016/j.chembiol.2016.05.019.

11. Brömme, D., Bonneau, P.R., Lachance, P., Wiederanders, B., Kirschke, H., Peters, C., Thomas, D.Y., Storer, A.C., and Vernet, T. (1993). Functional expression of human cathepsin S in Saccharomyces cerevisiae. Purification and characterization of the recombinant enzyme. Journal of Biological Chemistry *268*, 4832–4838. 10.1016/S0021-9258(18)53472-4.

12. Sapolsky, A.I., Howell, D.S., and Woessner, J.F. (1974). Neutral Proteases and Cathepsin D in Human Articular Cartilage. Journal of Clinical Investigation *53*, 1044–1053. 10.1172/JCI107641.

13. Naseem, R.H., Hedegard, W., Henry, T.D., Lessard, J., Sutter, K., and Katz, S.A. (2005). Plasma cathepsin D isoforms and their active metabolites increase after myocardial infarction and contribute to plasma renin activity. Basic Res Cardiol *100*, 139–146. 10.1007/s00395-004-0499-3.

14. Wyant, G.A., Abu-Remaileh, M., Wolfson, R.L., Chen, W.W., Freinkman, E., Danai, L. V., Vander Heiden, M.G., and Sabatini, D.M. (2017). mTORC1 Activator SLC38A9 Is Required to Efflux Essential Amino Acids from Lysosomes and Use Protein as a Nutrient. Cell *171*, 642-654.e12. 10.1016/j.cell.2017.09.046.

15. Abu-Remaileh, M., Wyant, G.A., Kim, C., Laqtom, N.N., Abbasi, M., Chan, S.H., Freinkman, E., and Sabatini, D.M. (2017). Lysosomal metabolomics reveals V-ATPase- and mTOR-dependent regulation of amino acid efflux from lysosomes. Science (1979) *358*, 807–813. 10.1126/science.aan6298.

16. Li, S.C., and Kane, P.M. (2009). The yeast lysosome-like vacuole: Endpoint and crossroads. Biochimica et Biophysica Acta (BBA) - Molecular Cell Research *1793*, 650–663. 10.1016/j.bbamcr.2008.08.003.

17. Doherty, G.J., and McMahon, H.T. (2009). Mechanisms of Endocytosis. Annu Rev Biochem *78*, 857–902. 10.1146/annurev.biochem.78.081307.110540.

18. Gleixner, E.M., Canaud, G., Hermle, T., Guida, M.C., Kretz, O., Helmstädter, M., Huber, T.B., Eimer, S., Terzi, F., and Simons, M. (2014). V-ATPase/mTOR Signaling Regulates Megalin-Mediated Apical Endocytosis. Cell Rep *8*, 10–19. 10.1016/j.celrep.2014.05.035.

19. Mettlen, M., Chen, P.-H., Srinivasan, S., Danuser, G., and Schmid, S.L. (2018). Regulation of Clathrin-Mediated Endocytosis. Annu Rev Biochem *87*, 871–896. 10.1146/annurev-biochem-062917-012644.

20. Edeling, M.A., Smith, C., and Owen, D. (2006). Life of a clathrin coat: insights from clathrin and AP structures. Nat Rev Mol Cell Biol *7*, 32–44. 10.1038/nrm1786.

21. Neumann, S., and Schmid, S.L. (2013). Dual Role of BAR Domain-containing Proteins in Regulating Vesicle Release Catalyzed by the GTPase, Dynamin-2. Journal of Biological Chemistry *288*, 25119–25128. 10.1074/jbc.M113.490474.

22. Finicle, B.T., Jayashankar, V., and Edinger, A.L. (2018). Nutrient scavenging in cancer. Nat Rev Cancer *18*, 619–633. 10.1038/s41568-018-0048-x.

23. Thelen, A.M., and Zoncu, R. (2017). Emerging Roles for the Lysosome in Lipid Metabolism. Trends Cell Biol *27*, 833–850. 10.1016/j.tcb.2017.07.006.

24. McMahon, H.T., and Boucrot, E. (2011). Molecular mechanism and physiological functions of clathrin-mediated endocytosis. Nat Rev Mol Cell Biol *12*, 517–533. 10.1038/nrm3151.

25. Joseph, J.G., and Liu, A.P. (2020). Mechanical Regulation of Endocytosis: New Insights and Recent Advances. Adv Biosyst *4*, 1900278. 10.1002/adbi.201900278.

26. Antonescu, C.N., McGraw, T.E., and Klip, A. (2014). Reciprocal Regulation of Endocytosis and Metabolism. Cold Spring Harb Perspect Biol *6*, a016964–a016964. 10.1101/cshperspect.a016964.

27. Palm, W. (2019). Metabolic functions of macropinocytosis. Philosophical Transactions of the Royal Society B: Biological Sciences *374*, 20180285. 10.1098/rstb.2018.0285.

28. Palm, W., Park, Y., Wright, K., Pavlova, N.N., Tuveson, D.A., and Thompson, C.B. (2015). The Utilization of Extracellular Proteins as Nutrients Is Suppressed by mTORC1. Cell *162*, 259–270. 10.1016/j.cell.2015.06.017.

29. Kamphorst, J.J., Nofal, M., Commisso, C., Hackett, S.R., Lu, W., Grabocka, E., Vander Heiden, M.G., Miller, G., Drebin, J.A., Bar-Sagi, D., et al. (2015). Human Pancreatic Cancer Tumors Are Nutrient Poor and Tumor Cells Actively Scavenge Extracellular Protein. Cancer Res *75*, 544–553. 10.1158/0008-5472.CAN-14-2211.

30. van der Vusse, G.J. (2009). Albumin as Fatty Acid Transporter. Drug Metab Pharmacokinet *24*, 300–307. 10.2133/dmpk.24.300.

31. Henson, P.M., Bratton, D.L., and Fadok, V.A. (2001). Apoptotic cell removal. Current Biology *11*, R795–R805. 10.1016/S0960-9822(01)00474-2.

32. Mathew, R., Karantza-Wadsworth, V., and White, E. (2007). Role of autophagy in cancer. Nat Rev Cancer *7*, 961–967. 10.1038/nrc2254.

33. Nelson, D.A., Tan, T.-T., Rabson, A.B., Anderson, D., Degenhardt, K., and White, E. (2004). Hypoxia and defective apoptosis drive genomic instability and tumorigenesis. Genes Dev *18*, 2095–2107. 10.1101/gad.1204904.

34. Peña-Llopis, S., Vega-Rubin-de-Celis, S., Schwartz, J.C., Wolff, N.C., Tran, T.A.T., Zou, L., Xie, X.-J., Corey, D.R., and Brugarolas, J. (2011). Regulation of TFEB and V-ATPases by mTORC1. EMBO J *30*, 3242–3258. 10.1038/emboj.2011.257.

35. Hara, K., Maruki, Y., Long, X., Yoshino, K., Oshiro, N., Hidayat, S., Tokunaga, C., Avruch, J., and Yonezawa, K. (2002). Raptor, a Binding Partner of Target of Rapamycin (TOR), Mediates TOR Action. Cell *110*, 177–189. 10.1016/S0092-8674(02)00833-4.

36. Kim, D.-H., Sarbassov, D.D., Ali, S.M., King, J.E., Latek, R.R., Erdjument-Bromage, H., Tempst, P., and Sabatini, D.M. (2002). mTOR Interacts with Raptor to Form a Nutrient-Sensitive Complex that Signals to the Cell Growth Machinery. Cell *110*, 163–175. 10.1016/S0092-8674(02)00808-5.

37. Guertin, D.A., Stevens, D.M., Thoreen, C.C., Burds, A.A., Kalaany, N.Y., Moffat, J., Brown, M., Fitzgerald, K.J., and Sabatini, D.M. (2006). Ablation in Mice of the mTORC Components raptor, rictor, or mLST8 Reveals that mTORC2 Is Required for Signaling to Akt-FOXO and PKCα, but Not S6K1. Dev Cell *11*, 859–871. 10.1016/j.devcel.2006.10.007.

38. Saxton, R.A., and Sabatini, D.M. (2017). mTOR Signaling in Growth, Metabolism, and Disease. Cell *168*, 960–976. 10.1016/j.cell.2017.02.004.

39. Peterson, T.R., Laplante, M., Thoreen, C.C., Sancak, Y., Kang, S.A., Kuehl, W.M., Gray, N.S., and Sabatini, D.M. (2009). DEPTOR Is an mTOR Inhibitor Frequently Overexpressed in Multiple Myeloma Cells and Required for Their Survival. Cell *137*, 873–886. 10.1016/j.cell.2009.03.046.

40. Tee, A.R., Fingar, D.C., Manning, B.D., Kwiatkowski, D.J., Cantley, L.C., and Blenis, J. (2002). Tuberous sclerosis complex-1 and -2 gene products function together to inhibit mammalian target of rapamycin (mTOR)-mediated downstream signaling. Proceedings of the National Academy of Sciences *99*, 13571–13576. 10.1073/pnas.202476899.

41. Carracedo, A., Ma, L., Teruya-Feldstein, J., Rojo, F., Salmena, L., Alimonti, A., Egia, A., Sasaki, A.T., Thomas, G., Kozma, S.C., et al. (2008). Inhibition of mTORC1 leads to MAPK pathway activation through a PI3K-dependent feedback loop in human cancer. Journal of Clinical Investigation. 10.1172/JCI34739.

42. Gwinn, D.M., Shackelford, D.B., Egan, D.F., Mihaylova, M.M., Mery, A., Vasquez, D.S., Turk, B.E., and Shaw, R.J. (2008). AMPK Phosphorylation of Raptor Mediates a Metabolic Checkpoint. Mol Cell *30*, 214–226. 10.1016/j.molcel.2008.03.003.

43. Brugarolas, J., Lei, K., Hurley, R.L., Manning, B.D., Reiling, J.H., Hafen, E., Witters, L.A., Ellisen, L.W., and Kaelin, W.G. (2004). Regulation of mTOR function in response to hypoxia by REDD1 and the TSC1/TSC2 tumor suppressor complex. Genes Dev *18*, 2893–2904. 10.1101/gad.1256804.

44. Kim, E., Goraksha-Hicks, P., Li, L., Neufeld, T.P., and Guan, K.-L. (2008). Regulation of TORC1 by Rag GTPases in nutrient response. Nat Cell Biol *10*, 935–945. 10.1038/ncb1753.

45. Sancak, Y., Bar-Peled, L., Zoncu, R., Markhard, A.L., Nada, S., and Sabatini, D.M. (2010). Ragulator-Rag Complex Targets mTORC1 to the Lysosomal Surface and Is Necessary for Its Activation by Amino Acids. Cell *141*, 290–303. 10.1016/j.cell.2010.02.024.

46. Bar-Peled, L., Chantranupong, L., Cherniack, A.D., Chen, W.W., Ottina, K.A., Grabiner, B.C., Spear, E.D., Carter, S.L., Meyerson, M., and Sabatini, D.M. (2013). A Tumor Suppressor Complex with GAP Activity for the Rag GTPases That Signal Amino Acid Sufficiency to mTORC1. Science (1979) *340*, 1100–1106. 10.1126/science.1232044.

47. Gu, X., Orozco, J.M., Saxton, R.A., Condon, K.J., Liu, G.Y., Krawczyk, P.A., Scaria, S.M., Harper, J.W., Gygi, S.P., and Sabatini, D.M. (2017). SAMTOR is an S-adenosylmethionine sensor for the mTORC1 pathway. Science (1979) *358*, 813–818. 10.1126/science.aao3265.

48. Zoncu, R., Bar-Peled, L., Efeyan, A., Wang, S., Sancak, Y., and Sabatini, D.M. (2011). mTORC1 senses lysosomal amino acids through an inside-out mechanism that requires the vacuolar H(+)-ATPase. Science (1979) *334*, 678–683. 10.1126/science.1207056.

49. Cockman, E., Anderson, P., and Ivanov, P. (2020). TOP mRNPs: Molecular Mechanisms and Principles of Regulation. Biomolecules *10*, 969. 10.3390/biom10070969.

50. Porstmann, T., Santos, C.R., Griffiths, B., Cully, M., Wu, M., Leevers, S., Griffiths, J.R., Chung, Y.-L., and Schulze, A. (2008). SREBP Activity Is Regulated by mTORC1 and Contributes to Akt-Dependent Cell Growth. Cell Metab *8*, 224–236. 10.1016/j.cmet.2008.07.007.

51. Peterson, T.R., Sengupta, S.S., Harris, T.E., Carmack, A.E., Kang, S.A., Balderas, E., Guertin, D.A., Madden, K.L., Carpenter, A.E., Finck, B.N., et al. (2011). mTOR Complex 1 Regulates Lipin 1 Localization to Control the SREBP Pathway. Cell *146*, 408–420. 10.1016/j.cell.2011.06.034.

52. Düvel, K., Yecies, J.L., Menon, S., Raman, P., Lipovsky, A.I., Souza, A.L., Triantafellow, E., Ma, Q., Gorski, R., Cleaver, S., et al. (2010). Activation of a Metabolic Gene Regulatory Network Downstream of mTOR Complex 1. Mol Cell *39*, 171–183. 10.1016/j.molcel.2010.06.022.

53. Cunningham, J.T., Rodgers, J.T., Arlow, D.H., Vazquez, F., Mootha, V.K., and Puigserver, P. (2007). mTOR controls mitochondrial oxidative function through a YY1–PGC-1α transcriptional complex. Nature *450*, 736–740. 10.1038/nature06322.

54. Kim, J., Kundu, M., Viollet, B., and Guan, K.-L. (2011). AMPK and mTOR regulate autophagy through direct phosphorylation of Ulk1. Nat Cell Biol *13*, 132–141. 10.1038/ncb2152.

55. Settembre, C., Zoncu, R., Medina, D.L., Vetrini, F., Erdin, S., Erdin, S., Huynh, T., Ferron, M., Karsenty, G., Vellard, M.C., et al. (2012). A lysosome-to-nucleus signalling mechanism senses and regulates the lysosome via mTOR and TFEB. EMBO J *31*, 1095–1108. 10.1038/emboj.2012.32.

56. Yu, L., McPhee, C.K., Zheng, L., Mardones, G.A., Rong, Y., Peng, J., Mi, N., Zhao, Y., Liu, Z., Wan, F., et al. (2010). Termination of autophagy and reformation of lysosomes regulated by mTOR. Nature *465*, 942–946. 10.1038/nature09076.

57. Collins, M.P., Stransky, L.A., and Forgac, M. (2020). AKT Ser/Thr kinase increases V-ATPase–dependent lysosomal acidification in response to amino acid starvation in mammalian cells. Journal of Biological Chemistry *295*, 9433–9444. 10.1074/jbc.RA120.013223.

58. Rivinoja, A., Pujol, F.M., Hassinen, A., and Kellokumpu, S. (2012). Golgi pH, its regulation and roles in human disease. Ann Med *44*, 542–554. 10.3109/07853890.2011.579150.

59. Forgac, M. (2007). Vacuolar ATPases: rotary proton pumps in physiology and pathophysiology. Nat Rev Mol Cell Biol *8*, 917–929. 10.1038/nrm2272.

60. McGuire, C.M., and Forgac, M. (2018). Glucose starvation increases V-ATPase assembly and activity in mammalian cells through AMP kinase and phosphatidylinositide 3-kinase/Akt signaling. Journal of Biological Chemistry *293*, 9113–9123. 10.1074/jbc.RA117.001327.

61. Kane, P.M. (2006). The Where, When, and How of Organelle Acidification by the Yeast Vacuolar H^+-ATPase. Microbiology and Molecular Biology Reviews *70*, 177–191. 10.1128/MMBR.70.1.177-191.2006.

62. Bond, S., and Forgac, M. (2008). The Ras/cAMP/Protein Kinase A Pathway Regulates Glucose-dependent Assembly of the Vacuolar (H+)-ATPase in Yeast. Journal of Biological Chemistry *283*, 36513–36521. 10.1074/jbc.M805232200.

63. Jaskolka, M.C., Winkley, S.R., and Kane, P.M. (2021). RAVE and Rabconnectin-3 Complexes as Signal Dependent Regulators of Organelle Acidification. Front Cell Dev Biol *9*. 10.3389/fcell.2021.698190.

64. Jaskolka, M.C., and Kane, P.M. (2020). Interaction between the yeast RAVE complex and Vph1-containing Vo sectors is a central glucose-sensitive interaction required for V-ATPase reassembly. Journal of Biological Chemistry *295*, 2259–2269. 10.1074/jbc.RA119.011522.

65. Stransky, L.A., and Forgac, M. (2015). Amino Acid Availability Modulates Vacuolar H+-ATPase Assembly. Journal of Biological Chemistry *290*, 27360–27369. 10.1074/jbc.M115.659128.

66. Trombetta, E.S., and Parodi, A.J. (2003). Quality Control and Protein Folding in the Secretory Pathway. Annu Rev Cell Dev Biol *19*, 649–676. 10.1146/annurev.cellbio.19.110701.153949.

67. Liberman, R., Bond, S., Shainheit, M.G., Stadecker, M.J., and Forgac, M. (2014). Regulated Assembly of Vacuolar ATPase Is Increased during Cluster Disruption-induced Maturation of Dendritic Cells through a Phosphatidylinositol 3-Kinase/mTOR-dependent Pathway. Journal of Biological Chemistry *289*, 1355–1363. 10.1074/jbc.M113.524561.

68. De Luca, M., Cogli, L., Progida, C., Nisi, V., Pascolutti, R., Sigismund, S., Di Fiore, P.P., and Bucci, C. (2014). The Rab-interacting lysosomal protein (RILP) regulates vacuolar ATPase acting on the V1G1 subunit. J Cell Sci. 10.1242/jcs.142604.

69. Dell'Antone, P. (1979). Evidence for an ATP-driven "proton pump" in rat liver lysosomes by basic dyes uptake. Biochem Biophys Res Commun *86*, 180–189. 10.1016/0006-291X(79)90398-X.

70. Mindell, J.A. (2012). Lysosomal Acidification Mechanisms. Annu Rev Physiol *74*, 69–86. 10.1146/annurev-physiol-012110-142317.

71. Kendall, R.L., and Holian, A. (2021). The role of lysosomal ion channels in lysosome dysfunction. Inhal Toxicol *33*, 41–54. 10.1080/08958378.2021.1876188.

72. Scott, C.C., and Gruenberg, J. (2011). Ion flux and the function of endosomes and lysosomes: pH is just the start. BioEssays *33*, 103–110. 10.1002/bies.201000108.

73. Shen, D., Wang, X., Li, X., Zhang, X., Yao, Z., Dibble, S., Dong, X., Yu, T., Lieberman, A.P., Showalter, H.D., et al. (2012). Lipid storage disorders block lysosomal trafficking by inhibiting a TRP channel and lysosomal calcium release. Nat Commun *3*, 731. 10.1038/ncomms1735.

74. Scotto Rosato, A., Montefusco, S., Soldati, C., Di Paola, S., Capuozzo, A., Monfregola, J., Polishchuk, E., Amabile, A., Grimm, C., Lombardo, A., et al. (2019). TRPML1 links lysosomal calcium to autophagosome biogenesis through the activation of the CaMKKβ/VPS34 pathway. Nat Commun *10*, 5630. 10.1038/s41467-019-13572-w.

75. Calcraft, P.J., Ruas, M., Pan, Z., Cheng, X., Arredouani, A., Hao, X., Tang, J., Rietdorf, K., Teboul, L., Chuang, K.-T., et al. (2009). NAADP mobilizes calcium from acidic organelles through two-pore channels. Nature *459*, 596–600. 10.1038/nature08030.

76. Lin, P.-H., Duann, P., Komazaki, S., Park, K.H., Li, H., Sun, M., Sermersheim, M., Gumpper, K., Parrington, J., Galione, A., et al. (2015). Lysosomal Two-pore Channel Subtype 2 (TPC2) Regulates Skeletal Muscle Autophagic Signaling. Journal of Biological Chemistry *290*, 3377–3389. 10.1074/jbc.M114.608471.

77. Jinn, S., Drolet, R.E., Cramer, P.E., Wong, A.H.-K., Toolan, D.M., Gretzula, C.A., Voleti, B., Vassileva, G., Disa, J., Tadin-Strapps, M., et al. (2017). TMEM175 deficiency impairs lysosomal and mitochondrial function and increases α-synuclein aggregation. Proceedings of the National Academy of Sciences *114*, 2389–2394. 10.1073/pnas.1616332114.

78. Ballabio, A., and Gieselmann, V. (2009). Lysosomal disorders: From storage to cellular damage. Biochimica et Biophysica Acta (BBA) - Molecular Cell Research *1793*, 684–696. 10.1016/j.bbamcr.2008.12.001.

79. Ruckenstuhl, C., Netzberger, C., Entfellner, I., Carmona-Gutierrez, D., Kickenweiz, T., Stekovic, S., Gleixner, C., Schmid, C., Klug, L., Sorgo, A.G., et al. (2014). Lifespan Extension by Methionine Restriction Requires Autophagy-Dependent Vacuolar Acidification. PLoS Genet *10*, e1004347. 10.1371/journal.pgen.1004347.

80. Stephan, J., Franke, J., and Ehrenhofer-Murray, A.E. (2013). Chemical genetic screen in fission yeast reveals roles for vacuolar acidification, mitochondrial fission, and cellular GMP levels in lifespan extension. Aging Cell *12*, 574–583. 10.1111/acel.12077.

81. Nixon, R.A. (2020). The aging lysosome: An essential catalyst for late-onset neurodegenerative diseases. Biochimica et Biophysica Acta (BBA) - Proteins and Proteomics *1868*, 140443. 10.1016/j.bbapap.2020.140443.

82. Nixon, R.A. (2013). The role of autophagy in neurodegenerative disease. Nat Med *19*, 983–997. 10.1038/nm.3232.

83. Al-Bari, Md.A.A. (2017). Targeting endosomal acidification by chloroquine analogs as a promising strategy for the treatment of emerging viral diseases. Pharmacol Res Perspect *5*, e00293. 10.1002/prp2.293.

84. Marzi, A., Reinheckel, T., and Feldmann, H. (2012). Cathepsin B & L Are Not Required for Ebola Virus Replication. PLoS Negl Trop Dis *6*, e1923. 10.1371/journal.pntd.0001923.

85. Commisso, C., Davidson, S.M., Soydaner-Azeloglu, R.G., Parker, S.J., Kamphorst, J.J., Hackett, S., Grabocka, E., Nofal, M., Drebin, J.A., Thompson, C.B., et al. (2013). Macropinocytosis of protein is an amino acid supply route in Ras-transformed cells. Nature *497*, 633–637. 10.1038/nature12138.

86. Cheong, H., Wu, J., Gonzales, L.K., Guttentag, S.H., Thompson, C.B., and Lindsten, T. (2014). Analysis of a lung defect in autophagy-deficient mouse strains. Autophagy *10*, 45–56. 10.4161/auto.26505.

87. de Almeida, M., Hinterndorfer, M., Brunner, H., Grishkovskaya, I., Singh, K., Schleiffer, A., Jude, J., Deswal, S., Kalis, R., Vunjak, M., et al. (2021). AKIRIN2 controls the nuclear import of proteasomes in vertebrates. Nature *599*, 491–496. 10.1038/s41586-021-04035-8.

88. Schindelin, J., Arganda-Carreras, I., Frise, E., Kaynig, V., Longair, M., Pietzsch, T., Preibisch, S., Rueden, C., Saalfeld, S., Schmid, B., et al. (2012). Fiji: an open-source platform for biological-image analysis. Nat Methods *9*, 676–682. 10.1038/nmeth.2019.

89. Tyanova, S., Temu, T., and Cox, J. (2016). The MaxQuant computational platform for mass spectrometry-based shotgun proteomics. Nat Protoc *11*, 2301–2319. 10.1038/nprot.2016.136.

90. Ritchie, M.E., Phipson, B., Wu, D., Hu, Y., Law, C.W., Shi, W., and Smyth, G.K. (2015). limma powers differential expression analyses for RNA-sequencing and microarray studies. Nucleic Acids Res *43*, e47–e47. 10.1093/nar/gkv007.

91. Fueller, J., Herbst, K., Meurer, M., Gubicza, K., Kurtulmus, B., Knopf, J.D., Kirrmaier, D., Buchmuller, B.C., Pereira, G., Lemberg, M.K., et al. (2020). CRISPR-Cas12a–assisted PCR tagging of mammalian genes. Journal of Cell Biology *219*. 10.1083/jcb.201910210.

92. Cox, J., Hein, M.Y., Luber, C.A., Paron, I., Nagaraj, N., and Mann, M. (2014). Accurate Proteome-wide Label-free Quantification by Delayed Normalization and Maximal Peptide Ratio Extraction, Termed MaxLFQ. Molecular & Cellular Proteomics *13*, 2513–2526. 10.1074/mcp.M113.031591.

93. Cox, J., Matic, I., Hilger, M., Nagaraj, N., Selbach, M., Olsen, J. V, and Mann, M. (2009). A practical guide to the MaxQuant computational platform for SILAC-based quantitative proteomics. Nat Protoc *4*, 698–705. 10.1038/nprot.2009.36.

94. Bolstad, B.M., Irizarry, R.A., Åstrand, M., and Speed, T.P. (2003). A comparison of normalization methods for high density oligonucleotide array data based on variance and bias. Bioinformatics *19*, 185–193. 10.1093/bioinformatics/19.2.185.

95. Tyanova, S., and Cox, J. (2018). Perseus: A Bioinformatics Platform for Integrative Analysis of Proteomics Data in Cancer Research. In, pp. 133–148. 10.1007/978-1-4939-7493-1_7.

96. Benjamini, Y., and Hochberg, Y. (1995). Controlling the False Discovery Rate: A Practical and Powerful Approach to Multiple Testing. Journal of the Royal Statistical Society: Series B (Methodological) *57*, 289–300. 10.1111/j.2517-6161.1995.tb02031.x.

97. Reis, R.C.M., Sorgine, M.H.F., and Coelho-Sampaio, T. (1998). A novel methodology for the investigation of intracellular proteolytic processing in intact cells. Eur J Cell Biol *75*, 192–197. 10.1016/S0171-9335(98)80061-7.

98. Creasy, B.M., Hartmann, C.B., White, F.K.H., and McCoy, K.L. (2007). New assay using fluorogenic substrates and immunofluorescence staining to measure cysteine cathepsin activity in live cell subpopulations. Cytometry Part A *71A*, 114–123. 10.1002/cyto.a.20365.

99. Ward, O.P. (2011). Proteases. In Comprehensive Biotechnology (Elsevier), pp. 571–582. 10.1016/B978-0-08-088504-9.00222-1.

100. Hofer, F., Kraml, J., Kahler, U., Kamenik, A.S., and Liedl, K.R. (2020). Catalytic Site pKa Values of Aspartic, Cysteine, and Serine Proteases: Constant pH MD Simulations. J Chem Inf Model *60*, 3030–3042. 10.1021/acs.jcim.0c00190.

101. Ostrowski, P.P., Fairn, G.D., Grinstein, S., and Johnson, D.E. (2016). Cresyl violet: a superior fluorescent lysosomal marker. Traffic *17*, 1313–1321. 10.1111/tra.12447.

102. Hashimoto, Y., Shirane, M., and Nakayama, K.I. (2018). TMEM55B contributes to lysosomal homeostasis and amino acid-induced mTORC1 activation. Genes to Cells *23*, 418–434. 10.1111/gtc.12583.

103. Miles, A.L., Burr, S.P., Grice, G.L., and Nathan, J.A. (2017). The vacuolar-ATPase complex and assembly factors, TMEM199 and CCDC115, control HIF1α prolyl hydroxylation by regulating cellular iron levels. Elife *6*. 10.7554/eLife.22693.

104. Wang, L., Wu, D., Robinson, C. V., Wu, H., and Fu, T.-M. (2020). Structures of a Complete Human V-ATPase Reveal Mechanisms of Its Assembly. Mol Cell *80*, 501-511.e3. 10.1016/j.molcel.2020.09.029.

105. Yam, A.Y., Xia, Y., Lin, H.-T.J., Burlingame, A., Gerstein, M., and Frydman, J. (2008). Defining the TRiC/CCT interactome links chaperonin function to stabilization of newly made proteins with complex topologies. Nat Struct Mol Biol *15*, 1255–1262. 10.1038/nsmb.1515.

106. Abe, Y., Yoon, S.-O., Kubota, K., Mendoza, M.C., Gygi, S.P., and Blenis, J. (2009). p90 Ribosomal S6 Kinase and p70 Ribosomal S6 Kinase Link Phosphorylation of the Eukaryotic Chaperonin Containing TCP-1 to Growth Factor, Insulin, and Nutrient Signaling. Journal of Biological Chemistry *284*, 14939–14948. 10.1074/jbc.M900097200.

107. Bright, N.A., Davis, L.J., and Luzio, J.P. (2016). Endolysosomes Are the Principal Intracellular Sites of Acid Hydrolase Activity. Current Biology *26*, 2233–2245. 10.1016/j.cub.2016.06.046.

108. Martina, J.A., Chen, Y., Gucek, M., and Puertollano, R. (2012). MTORC1 functions as a transcriptional regulator of autophagy by preventing nuclear transport of TFEB. Autophagy *8*, 903–914. 10.4161/auto.19653.

109. Saxton, R.A., and Sabatini, D.M. (2017). mTOR Signaling in Growth, Metabolism, and Disease. Cell *168*, 960–976. 10.1016/j.cell.2017.02.004.

110. Bar-Peled, L., Schweitzer, L.D., Zoncu, R., and Sabatini, D.M. (2012). Ragulator Is a GEF for the Rag GTPases that Signal Amino Acid Levels to mTORC1. Cell *150*, 1196–1208. 10.1016/j.cell.2012.07.032.

111. González, A., and Hall, M.N. (2017). Nutrient sensing and TOR signaling in yeast and mammals. EMBO J *36*, 397–408. 10.15252/embj.201696010.

112. Zhang, Y., Recouvreux, M.V., Jung, M., Galenkamp, K.M.O., Li, Y., Zagnitko, O., Scott, D.A., Lowy, A.M., and Commisso, C. (2021). Macropinocytosis in Cancer-Associated

Fibroblasts Is Dependent on CaMKK2/ARHGEF2 Signaling and Functions to Support Tumor and Stromal Cell Fitness. Cancer Discov *11*, 1808–1825. 10.1158/2159-8290.CD-20-0119.

113. King, B., Araki, J., Palm, W., and Thompson, C.B. (2020). Yap/Taz promote the scavenging of extracellular nutrients through macropinocytosis. Genes Dev *34*, 1345–1358. 10.1101/gad.340661.120.

114. Yu, L., McPhee, C.K., Zheng, L., Mardones, G.A., Rong, Y., Peng, J., Mi, N., Zhao, Y., Liu, Z., Wan, F., et al. (2010). Termination of autophagy and reformation of lysosomes regulated by mTOR. Nature *465*, 942–946. 10.1038/nature09076.

115. Butor, C., Griffiths, G., Aronson, N.N., and Varki, A. (1995). Co-localization of hydrolytic enzymes with widely disparate pH optima: implications for the regulation of lysosomal pH. J Cell Sci *108*, 2213–2219. 10.1242/jcs.108.6.2213.

116. Xu, T., and Forgac, M. (2001). Microtubules Are Involved in Glucose-dependent Dissociation of the Yeast Vacuolar [H+]-ATPase in Vivo. Journal of Biological Chemistry *276*, 24855–24861. 10.1074/jbc.M100637200.

117. Sautin, Y.Y., Lu, M., Gaugler, A., Zhang, L., and Gluck, S.L. (2005). Phosphatidylinositol 3-Kinase-Mediated Effects of Glucose on Vacuolar H+-ATPase Assembly, Translocation, and Acidification of Intracellular Compartments in Renal Epithelial Cells. Mol Cell Biol *25*, 575–589. 10.1128/MCB.25.2.575-589.2005.

118. Merkulova, M., Hurtado-Lorenzo, A., Hosokawa, H., Zhuang, Z., Brown, D., Ausiello, D.A., and Marshansky, V. (2011). Aldolase directly interacts with ARNO and modulates cell morphology and acidic vesicle distribution. American Journal of Physiology-Cell Physiology *300*, C1442–C1455. 10.1152/ajpcell.00076.2010.

119. Lu, M., Ammar, D., Ives, H., Albrecht, F., and Gluck, S.L. (2007). Physical Interaction between Aldolase and Vacuolar H+-ATPase Is Essential for the Assembly and Activity of the Proton Pump. Journal of Biological Chemistry *282*, 24495–24503. 10.1074/jbc.M702598200.

120. Collins, M.P., Stransky, L.A., and Forgac, M. (2020). AKT Ser/Thr kinase increases V-ATPase–dependent lysosomal acidification in response to amino acid starvation in mammalian cells. Journal of Biological Chemistry *295*, 9433–9444. 10.1074/jbc.RA120.013223.

121. Tang, H.-W., Weng, J.-H., Lee, W.X., Hu, Y., Gu, L., Cho, S., Lee, G., Binari, R., Li, C., Cheng, M.E., et al. (2021). mTORC1-chaperonin CCT signaling regulates m6A RNA methylation to suppress autophagy. Proceedings of the National Academy of Sciences *118*. 10.1073/pnas.2021945118.

122. Kamphorst, J.J., Nofal, M., Commisso, C., Hackett, S.R., Lu, W., Grabocka, E., Vander Heiden, M.G., Miller, G., Drebin, J.A., Bar-Sagi, D., et al. (2015). Human Pancreatic Cancer Tumors Are Nutrient Poor and Tumor Cells Actively Scavenge Extracellular Protein. Cancer Res *75*, 544–553. 10.1158/0008-5472.CAN-14-2211.

123. Palm, W., Araki, J., King, B., DeMatteo, R.G., and Thompson, C.B. (2017). Critical role for PI3-kinase in regulating the use of proteins as an amino acid source. Proceedings of the National Academy of Sciences *114*. 10.1073/pnas.1712726114.

124. Faes, S., Demartines, N., and Dormond, O. (2017). Resistance to mTORC1 Inhibitors in Cancer Therapy: From Kinase Mutations to Intratumoral Heterogeneity of Kinase Activity. Oxid Med Cell Longev *2017*, 1–10. 10.1155/2017/1726078.

125. Verbaanderd, C., Maes, H., Schaaf, M.B., Sukhatme, V.P., Pantziarka, P., Sukhatme, V., Agostinis, P., and Bouche, G. (2017). Repurposing Drugs in Oncology (ReDO)—chloroquine and hydroxychloroquine as anti-cancer agents. Ecancermedicalscience *11*. 10.3332/ecancer.2017.781.

126. Huss, M., and Wieczorek, H. (2009). Inhibitors of V-ATPases: old and new players. Journal of Experimental Biology *212*, 341–346. 10.1242/jeb.024067.

127. Oka, T., Murata, Y., Namba, M., Yoshimizu, T., Toyomura, T., Yamamoto, A., Sun-Wada, G.-H., Hamasaki, N., Wada, Y., and Futai, M. (2001). a4, a Unique Kidney-specific Isoform of Mouse Vacuolar H+-ATPase Subunit a. Journal of Biological Chemistry *276*, 40050–40054. 10.1074/jbc.M106488200.

128. Toyomura, T., Murata, Y., Yamamoto, A., Oka, T., Sun-Wada, G.-H., Wada, Y., and Futai, M. (2003). From lysosomes to the plasma membrane: localization of vacuolar-type H+ -ATPase with the a3 isoform during osteoclast differentiation. Journal of Biological Chemistry *278*, 22023–22030. 10.1074/jbc.M302436200.